The University Of Sheffield.

Non-linear observer based control of magnetic levitation systems

Thesis submitted to the University of Sheffield for the degree of Doctor of Philosophy

by

Abdollha M. A. Benomair

Department of Automatic Control and Systems Engineering
The University of Sheffield
Mappin Street,
Sheffield, S1 3JD
United Kingdom

December 2017

Abstract

Active magnetic levitation AML systems have been widely used in magnetic levitation vehicles, wind turbine, medical applications, micro robot actuation and turbo-machinery. Contactless support of objects continues to be a fantasy for several centuries. The utilization of magnetic forces seems to be the ideal solution in many situations to such a goal. Using magnetic forces to support an object without any mechanical contact is constrained by the laws of magnetism. Earnshaw's theorem states that when the inverse-square-law forces govern several charged particles, they can never be within a stable equilibrium. The interaction between ferromagnetic objects and electromagnets of either the active or passive type, is associated with an unstable nature. This unstable behaviour can be represented by highly non-linear differential equations. In the literature many researches are based on linearised models around a specific nominal operating point then linear controller is utilized to control the system. The associated problem with the linear control technique is that the system only be adequately controlled in a small region around the equilibrium point but the variation of operating regions in such non-linear system is wide following a major disturbance. In this research, two kinds of non-linear observer-based excitation controller are proposed for Maglev to ensure the stability of non-linear system in the presence of large disturbance and over larger operation regions. A combination of full-order Non-linear high-gain observer (NHGO) with LQR-feedback linearisation is considered as first proposal . Second proposed controller is based on the Lyapunov stability theorems, and a further non-linear full-order observer-based controller via a non-linear fuzzy sliding mode controller is developed for Maglev system. The proposed control approaches are tested and validated through simulated exercises of a magnetic levitation system. Comparative assessments of the approaches are presented and discussed through the thesis.

Acknowledgement

All praise be to Allah, the Most Merciful and Beneficent. There is no God but Allah and Prophet Muhammad (Peace be upon him) is the Messenger of Allah. With His wills and gracious, I have successfully completed my thesis. First of all, I wish to express my gratitude to my supervisor Dr. Osman Tokhi for the trust, chance, support, guidance, patient, encouragement during my studies, as well as my friends'. Also to Dr HL Wei, thanks for your willingness to accept me to be one of your students. Special thanks to technical team, Ben Taylor, Paul Webster, Mubarak Nurani, Craig Bacon and Darren Fox .

I gratefully acknowledge the Libyan of High Education, The University of Sebha and Automatic Control and System Engineering of University of Sheffield (ACSE-UoS) for sponsoring my studies.

I would like to express my deepest gratitude to my family especially to my wife "Fatema", sons and daughters, to whom I am indebted for the devotion to our family wellness and education, my sister and brother-in-law, Aisha Benomair and Mohamed Busifi and also to my others sisters-brothers. Also to both of my nieces and nephews. Thanks for always making me happy.

I am thankful to all colleagues who supported me during my doctoral studies. Especially, to Saad, Sapto, Shwan, Ahmad Nor, Abdullah Al-Meshal, Fareg, Mohd Ruzaini, Ahmad Zahidi, Normaniha Ghani, Asnor, Daniella, Ghasaq, Norafizah, Omar, Hadi, Nafri, Hyreil, Ahmad, Siti, Abdullah and Bukhari.

Contents

List of Figures

List of Tables

Acronyms

AML	Active magnetic levitation
AMBs	Active magnetic bearing systems
EDS	Electrodynamic suspension
EMS	Electromagnetic suspension system
EHGO	Extended high gain observer
fis	Fuzzy inference system (Mamdani)
FLC	Fuzzy logic control
FSMC	Fuzzy sliding mode controller
FSMO	Fuzzy sliding mode observer
HEMS	Hybrid Electromagnetic suspension
HGO	High-gain observer
IAE	Integral absolute error
ISDA	Improved spiral Dynamic Algorithm
ISE	Integral squared error
IWO	invasive weeds optimization algorithm
$\mathbf{H}_\infty$	H infinity
LQi	Linear quadratic integral
LQR	Linear quadratic regulator
LTI	linear time invariant
LVAD	Left ventricular assist device
Maglev	Magnetic levitation system
MIMO	Multi input multi output
MSE	Mean square error

NHGO Non-linear high-gain observer

PID Proportional integral and derivative

PSO Particle swarm optimization

PM Permanent magnets

SDA Spiral Dynamic Algorithm

SIMO Single input multi output

SISO Single input single output

SCM Superconducting magnets

SMC Sliding mode control

SMO Sliding mode observer

VAWT Vertical axis wind turbine

VSC Variable Structure Control

VTOL Vertical take-off and landing

PSO Particle swarm optimization

IWO Invasive weed optimization

Chapter 1

Introduction

1.1 Introduction

Active magnetic levitation AML systems have been widely used in medical applications (Allaire et al., 1996), turbo-machinery (Field and Iannello, 1998), magnetic levitation vehicles (Jang et al., 2011), micro robot actuation (Hagiwara et al., 2012) and wind turbine (Aravind et al., 2012). Contactless support of objects continues to be a fantasy for several centuries. The utilization of magnetic forces seems to be the ideal solution in many situations to such a goal. Using magnetic forces to support an object without any mechanical contact is constrained by the laws of magnetism. Earnshaw's theorem (Bleuler et al., 2009) states that when the inverse-square-law forces govern several charged particles, they can never be within a stable equilibrium. The interaction between ferromagnetic objects and electromagnets of either the active or passive type, is associated with an unstable nature (Bassani, 2011).

This unstable behaviour can be represented by highly non-linear differential equations. In the literature many researches are based on linearised models around a specific nominal operating point then linear controller is utilized to control the system. The associated problem with the linear control technique is that the system can be only be adequately controlled in a small region around the equilibrium point but the variation of operating regions in such non-linear system are wide following major disturbance (Mahmud et al., 2012). Furthermore, linear controllers provide large actuation and zero tracking error cannot be guaranteed in the in presence of disturbance, Kelly 1998 (in Yu and Li (2014)). Thus,

non-linear control is considered as a better choice to ensure the stability of non-linear systems in the presence of large disturbance and over larger operating regions (Lahdhiri and Alouani, 1995; Mahmud et al., 2012).

In the design of any optimal controller, whether it is linear or non-linear, it is essential that all state variables of the system are available, whether measured all (which in many cases not applicable) or estimated. State estimation can resolve the difficulties associated with unmeasured states.

This research focus on the design of two kinds of non-linear observer-based excitation controller for magnetic levitation system. To implement this control in practical setting, the states of the Maglev system are observed using a dynamic estimator rather than measuring them.

1.2 Research problem statement

Most of controlled systems, in one aspect or another, are non-linear, with non-linear dynamics due to saturation of actuators, non-linearity of sensors or systems governed by non-linear differential equations. Although linear control tools may work well in many non-linear systems, but in some cases non-linear effects need to be taken in consideration to stabilize the system. Furthermore, considering the non-linear aspect may significantly enhance the performance and improve the overall robustness.

Magnetic levitation systems (Maglevs) are known to have reduced maintenance costs and reduced power consumption. Since a Maglev system is highly non-linear unstable system, an optimized non-linear observer-based control is proposed to tackle the non-linearity problem and to improve system robustness to disturbances and to ensure that the system works in a wider operation range.

1.3 Research aims and objectives

The research will focus to resolve the difficulty of stabilizing an unstable high non-linear Maglev system. The research work undertaken in this thesis aims to reduce the gap between the most recent advances in control theory and the corresponding engineering applications to Maglevs. In this respect, research undertakes developments in non-linear state feedback and observer based control of Maglevs.

The objectives of this research can be divided into several items as follows:

- To design and develop non-linear high-gain observer and fuzzy sliding mode observer to estimate the system states to be used in optimal states feedback control.
- To research and design a non-linear controller for a highly non-linear unstable Maglev system by implementing non-linear full-order observer-based controller via LQR-feedback linearisation.
- To apply and improve the robustness of non-linear full-order observer-based controller via LQR-feedback linearisation against parameters mismatch by utilizing integral action.
- To research and design a non-linear controller by implementing non-linear full-order observer-based controller via a non-linear fuzzy sliding mode controller.
- To apply Spiral Dynamic Algorithm (SDA) as an optimization algorithm to solve single objective optimization problem for control parameters to achieve better system performance.

1.4 Research methodology

At the beginning, an intensive literature review has been conducted. The idea behind doing this is to explore the latest developments within the scope of the research for acquiring

better and understanding of existing techniques. This includes studying magnetic levitation systems and their applications, superficial understanding of non-linear observer-based methods and any related previous works undertaken.

Secondly, model the behaviour of the unstable magnetic levitation system which can be represented by highly non-linear differential equations. Design non-linear observer that can help to obtain best estimation of the unmeasured states, so that all system states will be available to design a robust controller to overcome the non-linearity of the magnetic levitation system.

Thirdly, design and simulate a base controller technique that treats a non-linear system in a limited range as a linear system without linearising the model of the system directly. The observer-based non-linear controller will be tuned and tested on several single objective optimization test functions using two kinds of optimization algorithm.

During the forth phase of the research, based on Lyapunov stability criteria another non-linear controller is designed. This design involves a continuous control law to derive the states trajectories of non-linear plants to well-chosen surface and discontinuous control law with high speed switching control to maintain all state trajectories on the surface all the time.

The last phase will constitute performance evaluation of the proposed algorithm. Best combination of the non-linear controller and observer in light of intensive comparative is expected to emerge.

1.5 Contributions and publications of the thesis

Magnetic levitation system is inherently unstable and non-linear in nature. In this research, two kinds of non-linear observer-based excitation controller are proposed for Maglev to ensure its stability in the presence of large disturbance and over larger operation regions. A combination of full-order Non-linear high-gain observer (NHGO) with LQR-feedback linearisation is considered as a first contribution of this research. Second contribution is based on the Lyapunov stability theorems, as another non-linear full-order observer-based

controller via a non-linear fuzzy sliding mode control.

Publications arising form this research that are in print are listed below. There are further publications not listed that are in preparation for submission.

- A.M. Benomair and Tokhi, M.O. (2016), "Nonlinear full-order observer-based controller design for active magnetic levitation via LQR-feedback linearisation", Int. J. Modelling, Identification and Control, Vol. 26, No. 1,pp.59–67.

- A. M. Benomair and M. O. Tokhi, "Control of single axis magnetic levitation system using fuzzy logic control", 2015 Science and Information Conference (SAI), London, 2015, pp. 514-518.

- A. M. Benomair, F. A. Bashir and M. O. Tokhi, "Optimal control based LQR-feedback linearisation for magnetic levitation using improved spiral dynamic algorithm", 2015 20th International Conference on Methods and Models in Automation and Robotics (MMAR), Miedzyzdroje, 2015, pp. 558-562.

- A. M. Benomair, A. R. Firdaus and M. O. Tokhi, "Fuzzy sliding control with non-linear observer for magnetic levitation systems", 2016 24th Mediterranean Conference on Control and Automation (MED), Athens, 2016, pp. 256-261.

- F. Bashir, H. L. Wei and A. Benomair, "Model selection to enhance prediction performance in the presence of missing data", 2015 20th International Conference on Methods and Models in Automation and Robotics (MMAR), Miedzyzdroje, 2015, pp. 846-850.

1.6 Thesis organisation

The thesis is organized in a way to show the significant steps that reflect the research and development of designing non-linear controllers for non-linear Maglev system as well as implementing full-order non-linear observers and their platform of testing and validation methods. A brief summary of overall thesis is given as follows:

Chapter One: Deliberates a description of the research background, problem statement of this research , the aims and objectives and contributions of this research.

Chapter Two : Introduces a literature review about two types of non-linear controllers, along with brief overview of Magnetic Levitation systems and non-linear observer.

Chapter Three: Describes the dynamic model of non-linear Maglevs and introduces non-linear high gain observer and fuzzy sliding mode observer as an observer to estimate the full states.

Chapter Four: Explores and investigates with computer simulations the design of full state feedback control to solve the regulation problem and introduces some techniques of tracking control design, discusses how integral action would help to improve the robustness of the proposed controller.

Chapter Five: Introduces sliding mode control (SMC) approach and investigates fuzzy sliding mode control with computer simulations and comparison of SMC using boundary layer versus fuzzy type one.

Chapter Six: Deliberates the Spiral Dynamic Algorithm (SDA) to solve the optimization problem of the tuning parameters of the proposed controllers and compares the results those of invasive weeds another optimization algorithm (IWO).

Chapter Seven: Main conclusions drawn from the work and recommendations for further work are presented in this chapter.

1.7 Summary

Research background and the research problem statement has been instituted in this chapter. The research aim and objectives have been stated and the research methodology has been formulated and contribution to knowledge arising from this research has been highlighted.

Chapter 2

Literature Review

2.1 Introduction

This chapter is divided to into three main sections. The first section discusses control systems in general, then it focuses on non-linear controllers; two non-linear control types are briefly discussed. The magnetic levitation system and some of its applications are reviewed in the second section. The third section highlights the principle of non-linear observer and review of literature on full-order observer in different applications.

2.2 Non-linear control

Feedback control is a method where the output of the controlled system is fed-back to the input in order to make the system output follow a desired reference signal. Thus the behaviour of the controlled system is modified or changed by comparing the feedback system output to the desired reference to make the output tracking as close as possible to the reference. According to the chart shown in Figure 2.1, the control system using feedback can be classified into two main branches, namely output feedback and state feedback control. For Single Input Single Output (SISO) systems, output feedback control uses the available measured output (part of system dynamics) as a feedback signal to control the system which can be represented using transfer function (see Figure 2.2). Examples of possible methods are given in the chart but in this work the output feedback control type is not considered.

The second type of feedback control is state feedback in which the dynamics of the system can be represented by states (see Figure 2.3), where r represents the reference, x_m is the scaled input, $\hat{x}$ represents the estimated states, u is the control efforts which is a summation of feedforward and feedback control signals u_{ff} and u_{fb} respectively and y is the system output. A state may be regarded as type of accumulation of past information of the system behaviour or say information storage (Kalman et al., 1969). This type of control is based on the assumption of that all the system states are measured or at least can be estimated using any type of observer/estimator. Having system dynamics in state-space representation, state feedback control can be classified into two categories:

Linear control that applies to systems made of linear / linearised system; in these systems, the output of the system is proportional to system input and they obey the superposition principle. In state-space, system with these properties can be represented by linear differential equations with parameters which do not change over time, a major subclass can be called as linear time invariant (LTI) which can be represented in the form of

$$\begin{aligned} \dot{x}(t) &= A\,x(t) + B\,u(t) \\ y(t) &= C\,x(t) + D\,u(t) \end{aligned} \tag{2.1}$$

where $x(.)$, $u(.)$ and $y(.)$ are state, input and output vectors respectively, $A(.)$, $B(.)$, $C(.)$ and $D(.)$ are state, input, output and feedforward matrices of the system. Some linear control techniques can be implemented to control this type of system such as LQR, pole-placement, $\mathbf{H}_\infty$ and adaptive control.

Non-linear control can be used to a wider range of systems that do not obey the superposition principle. These systems can be represented by non-linear differential equations of the form

$$\begin{aligned} \dot{x} &= f(x) + g(x)\,u \\ y &= h(x) \end{aligned} \tag{2.2}$$

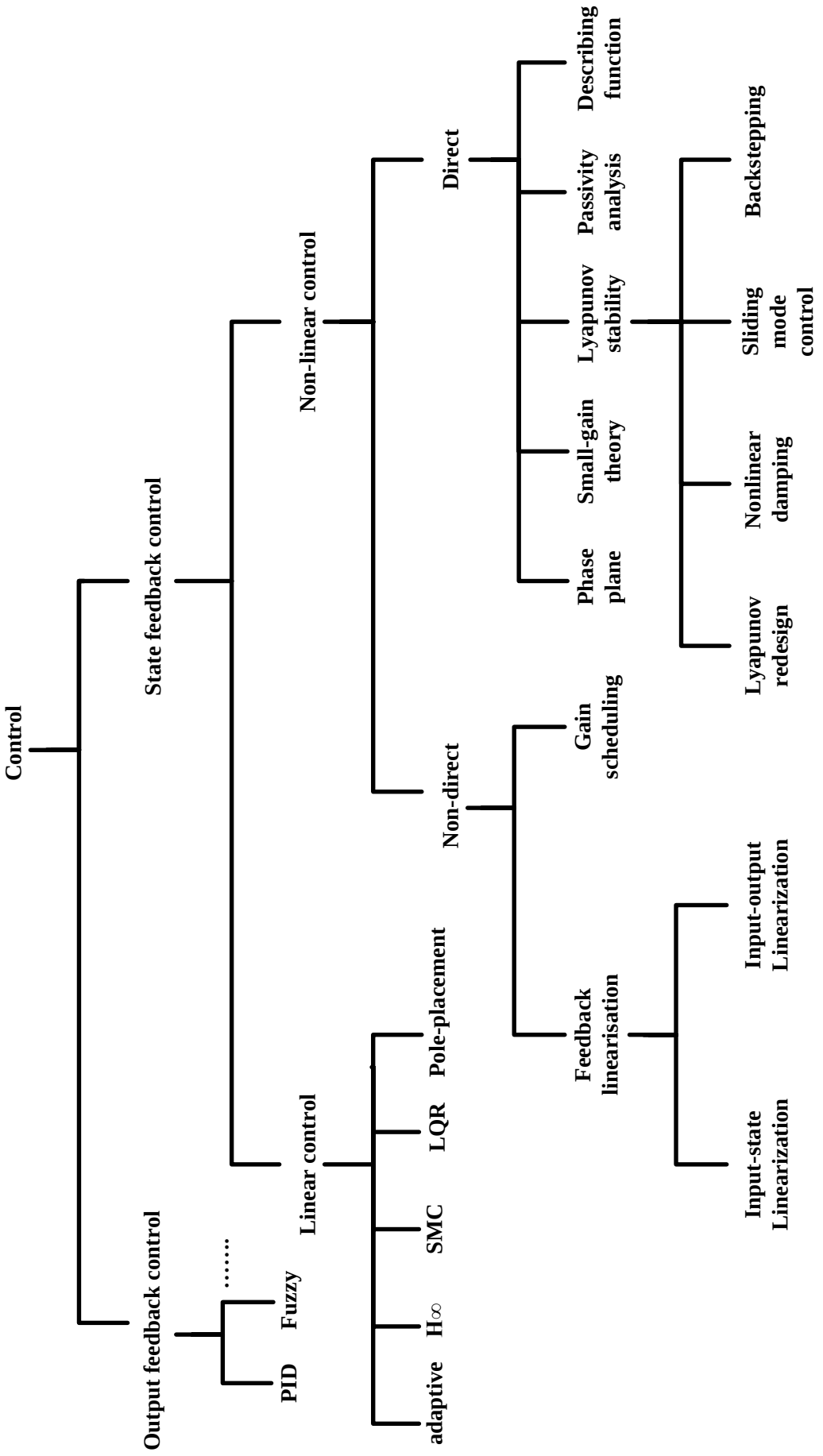

Figure 2.1: Control Systems

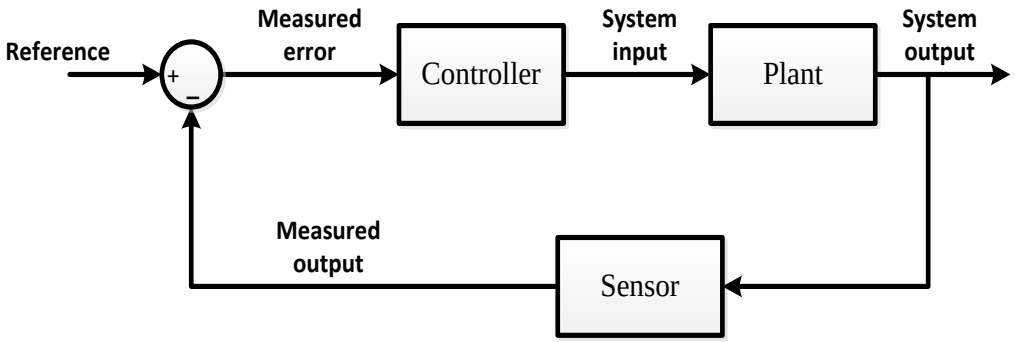

Figure 2.2: Feedback control system block diagram

where $x \in \mathbb{R}^{n \times n}$ is the state vector; $u \in \mathbb{R}^{m \times m}$ is the control vector; $y \in \mathbb{R}$ is the system output vector; $f(x)$ and $g(x)$ are n-dimensional vector fields in the state space representation and $h(x)$ is the differentiable vector field of x. A non-linear system can be controlled using direct non-linear control technique, meaning that there is no need to linearised the system i.e. the system model is represented by non-linear differential equations, using mathematical techniques that have been developed to handle even uncommon categories of non-linear systems including limit cycle theory, describing function and Poincaré maps. Some of non-linear control techniques are illustrated in the chart, e.g. small-gain theory and passivity analysis. However, in this work sliding mode control (SMC) is of the interest using non-linear control based on Lyapunov stability. More details of SMC are provided in the next section.

An alternative method of implementing non-linear control is to use an indirect method, i.e. instead of linearising the mathematical model of the system directly using a linearisation method, linearisation can be done using output or state feedback as a system input to

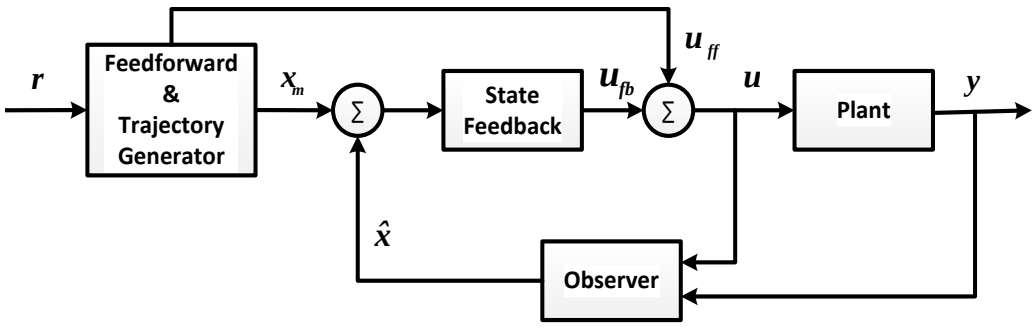

Figure 2.3: State feedback control system block diagram

cancel the non-linearity in the system, and this can be achieved using either input-output linearisation or input-state linearisation. However, this does not mean that if the plant is linear then a non-linear control techniques cannot be used, as in many cases non-linear control can be best option for its attractive features such as faster speed, better precision or reduced energy which can eventually justify the more difficult design procedure of non-linear control.

2.2.1 Feedback linearisation control

Feedback linearisation as mentioned previously is considered as a non-linear control method in which non-linear system is indirectly linearised, where linearisation is achieved by exact feedback and exact state transformations rather than linearising the system dynamics directly using linear approximation, Tylor series or Jacobian transformation.

Feedback linearisation is to employ a non-linear control law so that the controlled system combined with non-linear control behaves linear and controllable in the closed-loop. As shown in Figure 2.4, feedback linearisation is implemented using two control loops, the inner control loop is referred to as non-linear linearising control law, while the outer control loop is to control the resultant linear system achieved by the inner loop control (Erbatur et al., 1994).

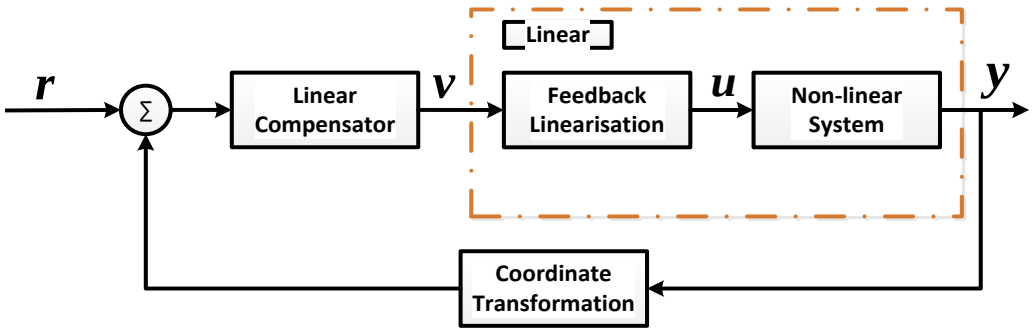

Figure 2.4: Feedback linearisation control block diagram

There are two types of feedback linearisation, input-output linearisation in which input-output map is completely linearised, yet the state equations might be partially linearised. Another type of feedback linearisation is input-state linearisation or referred to by some as full-state linearisation where the state equation is completely linearised.

In input-output linearisation, the method of linearising input-output map can be briefly explained by writing the state and output equations in the form of

$$\begin{aligned} \dot{x}(t) &= f(x,u) \\ \dot{x}(t) &= g(y,v) \end{aligned} \tag{2.3}$$

where $\dot{x}$ is the dynamic change of the system, x, u and y represent the states, input and outputs of the system receptively and v is the control synthesis or the input to the linearised system. State equation is said to be related to output equation if there is a diffeomorphism as

$$T : \rightarrow R^{n+1} \rightarrow \rightarrow R^{n+1} \tag{2.4}$$

such that $T_1(x,u) = y_1$,$T_2(x,u) = y_2$, ... and $T_{n+1}(x,u) = v$. Thus the feedback equivalent to the system can be represented in terms of state equation as

$$\begin{pmatrix} \dot{y_1} \\ \dot{y_2} \\ \vdots \\ \dot{y_n} \end{pmatrix} = \begin{pmatrix} y_1 \\ y_2 \\ \vdots \\ y_n \end{pmatrix} + \begin{pmatrix} 0 \\ 0 \\ \vdots \\ 1 \end{pmatrix} v \tag{2.5}$$

which is considered as linear, time-invariant and controllable single input system.

In this work, input-state linearisation is implemented as non-linear control to control Maglev system, more details of which are provided in chapter 4.

2.2.2 Sliding mode control

One of the earliest attempts to use variable structure control with sliding mode control was successfully managed to stabilize a linear second order system in phase form in The Soviet union by Emelyanov (Emelyanov, 1967, 1970). Since then, many studies have considered sliding mode control whether in the the control theory or on controlling various systems in many applications, including linear (Emelyanov and Taran, 1963) and non-linear systems (Hung et al., 1993), analogue and discrete systems (Gao et al., 1995), SISO (Young, 1977) and MIMO systems (Young, 1978), infinite- dimensional and large-scale system and stochastic systems(Hung et al., 1993). The use of sliding mode control has been extended to the other control functions apart from stabilization. These include construction of state observer, and driving the system states towards the sliding manifold as regularization technique.

In optimal control, a typical task is to design a control law to map current states of the controlled system at time t to the system input u, so the system dynamics can be stabilized around the origin where all the states converge to zero. Thus, whatever point the system begins away from the origin, the control law ensures that it comes back to it. Thus if the difference between the system output and desirable tracked reference is represented by state vector x, then the control action needs to return the state that belongs to this vector to zero, so the system output will track the reference. In sliding mode control, the desirable behaviour of the controller system is constrained to a reduced-order subspace out of its configuration space. This subspace is referred to as sliding surface, that is because feedback of the closed-loop confines the trajectories to this sliding surface and slide along it.

Sliding mode control design involves two steps

- Design sliding mode surface such that system trajectories exhibit required performance when confined to this surface, where system tracks the desirable reference.
- Design feedback gains to drive the system states to this surface and maintain them around it.

The robustness of the sliding mode control is referred to the control law of the kind that is not contentious, i.e. utilizing switching function in its law can drive the sliding trajectories to sliding mode in finite time. Defining switching function as a function of the distance away from the manifold, i.e. $\sigma(x)$, SMC control law would fluctuate form one state to another depending on the sign of the distance. Once the trajectories approach the surface, where $\sigma(x) = 0$, they will slide along it and move towards the origin, $x = 0$.

The use of switching function results in non-decaying high- frequency oscillation with small amplitude that appears in the neighbourhood of the sliding surface (see Figure 2.5). This high-frequency switching is known as "chattering phenomena". This chattering can be considered as un-modelled fast dynamics in the control system which ideally means the device is switching at infinite frequency. From practical point of view this is unwanted for many reasons:

- Chattering results in law accuracy in the control (Mehta and Bandyopadhyay, 2015).
- A high switching in the controlled system would cause fatigue.
- Chattering in electronic circuits means energy losses as heat and more electric power consumption.
- Overall this results in reduced serviceable life of the device.

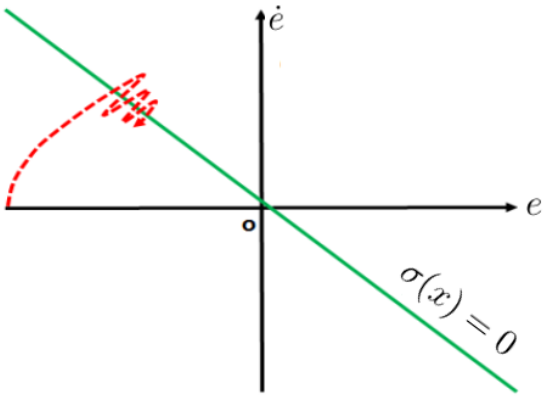

Figure 2.5: SMC chattering phenomena

Many approaches have been proposed to reduce the chattering. The first approach introduced is the use of a continuous approximation to replace the switching function in the discontinuous control (Kwatny and Siu, 1987). However, this at the end will sacrifice the robustness of sliding mode control (Young and Drakunov, 1992). Then few years later, a method was introduced to replace the switching function $sgn(\sigma(x,t))$ by saturation function $sat(\sigma(x,t))$, in which the thickness of the boundary layer around the switching surface is vary to take advantage of the system bandwidth. However, making boundary layers vary for some systems can result in large boundary width (Kachroo and Tomizuka, 1996). Further improvident can be done by decaying the boundary layer region (Sun et al., 2016) when the states reach/lie the sliding surface $(\sigma(x) = 0)$ in order to remove the chattering. In this method the thickness of the boundary layer will be lead to zero and eventually converge to zero around the origin (see Figure 2.6) where the system trajectories are maintained around the surface till all system states converge to zero at origin that is where $e_{ss} = 0$.

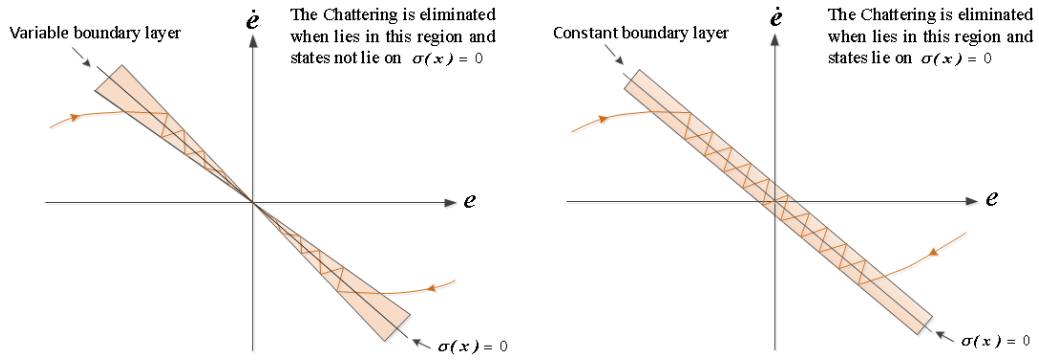

Figure 2.6: Variable boundary layer vs. constant boundary layer

Another method proposed to overcome the chattering problem is high-order sliding mode control (Benallegue et al., 2008; Bethoux et al., 2003; Goel and Swarup, 2016). This method, it makes selection of high-order sliding mode surface in terms of a set of continuous function of $s, \dot{s}, ..., s^{(r-1)}$ and the set

$$S^r = [x|s(x,t) = \dot{s} = ... = s^{(r-1)} = 0]$$

assuming the system with relative degree to r to sliding variable $s(x,t)$, S^r is the r^{th} order

sliding mode. The robustness of this high-order sliding mode control is ensured and the convergence time is chosen in advance. However, eliminating a chattering problem is only valid for low-order systems, as for high-order systems this would involve high-order differentiation which increases the noise-sensitivity (Levant, 2003). An alternative approach is to replace the sign function for higher relative degrees to so-called super twisting sliding mode control. The control law of the super-twisting sliding mode controller to eliminate the chattering for the system with unknown bounded perturbation can be described as

$$u = -K_1\sqrt{|\sigma|}\, sign(\sigma) + v \tag{2.6}$$

where u in the sliding control action, σ is the sliding surface and v is the integration of $\dot{v}$ that is given by

$$\dot{v} = -K_2\, sign(\sigma) \tag{2.7}$$

where K_1 and K_2 are the tuning gain for the modified controller.

A computational intelligence approach is another method for the engineering problems associated with sliding mode control "chattering elimination", where a fuzzy tuning scheme is used to replace the switching function $sgn(\sigma(t))$ in discontinuous control and the equivalent control stays the same as in classic sliding control. The asymptotic convergence of this strategy is proven using Lyapunov stability theory for many applications such as joint control of a hydraulically actuated mini-excavator considered by Ha et al. (2001). Although some robustness limitation might be associated with fuzzy sliding mode control using fixed fuzzy in presence of uncertainties for some application. However, for many applications high computational load associated with adaptive fuzzy sliding mode controllers is not appreciated (Hassrizal and Rossiter, 2016).

2.3 Magnetic levitation system

Magnetic levitation systems (Maglevs) provide a contribution in the industry by which systems have reduced the electricity consumption, have risen the power efficiency and reducing the cost of the maintenance. The common applications of Maglev are Power Generation (e.g. wind mill), Medical Device (such as Magnetically Suspended Artificial Heart Pump) and Maglev train. The subsequent subsections will show some uses of Maglevs.

2.3.1 Maglev trains

In recent years, population has grown not only in big cities but also in urban areas. Nowadays, it is very difficult to build new highways or airports close to larger cities. Moreover, the vast majority of current transportation utilize oil which means increment in the level of collateral environment impacts. It is an obvious requirement for quicker, cleaner and non-oil methods for transportation. Maglev trains is being one of the innovations which is centre of attention of various organisations and nations.

While conventional train gets guidance and support from the conventional rail and uses its rotary motor for propulsion, the Maglev train is supported and guided electromagnetically, magnetic levitation, and it uses a linear motor to get its propulsion force. Mainly there are three types of magnetic levitation. That is

- Electromagnetic suspension (EMS): This kind of levitation depends on the attraction force between electromagnets and the guide-way. EMS is inherently unstable which makes air-gap control and maintaining it uniform challenging. However, EMS is capable to levitate the train at low and zero speed. EMS is integrated in Korean UTM, Japanese HSST and German Transrapid.

- Electrodynamic suspension (EDS): In this technique there are two sets of magnet, one set is attached to the vehicle whereas the other is located on the guide-way. Magnetic repulsive force is used in this methodology rather than attraction force. The repulsive force between the attached magnets to the train and the magnetic field

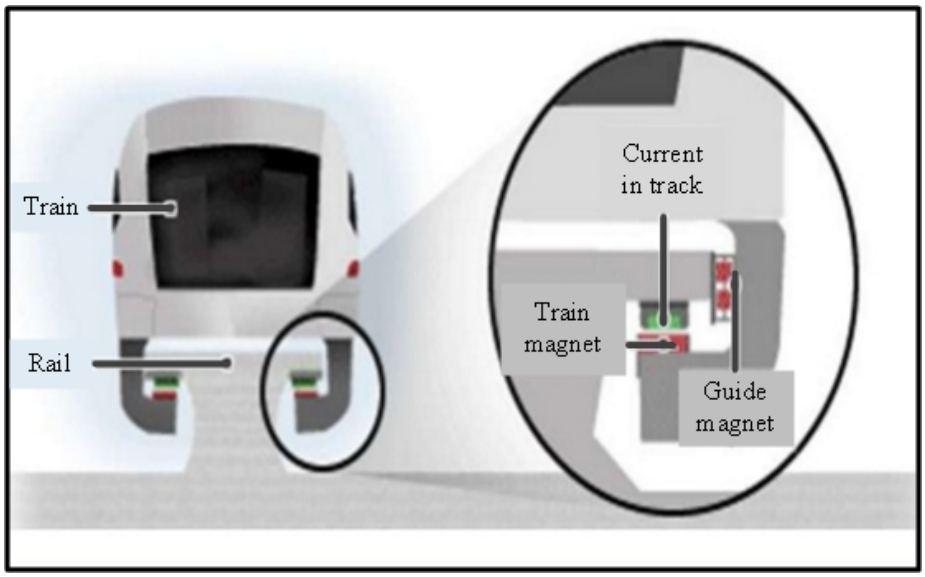

Figure 2.7: EMS Maglev train Srivastava (2016)

levitates the train, the magnetic field is generated by the induced currents throughout the conducting sheet located on the guide way. EDS is magnetically stable so there is no need for control, and it is more reliable in case of load variation and highly recommended for high-speed operation. Two types of magnets can be used in EDS the permanent magnets (PM) or the superconducting magnets (SCM).

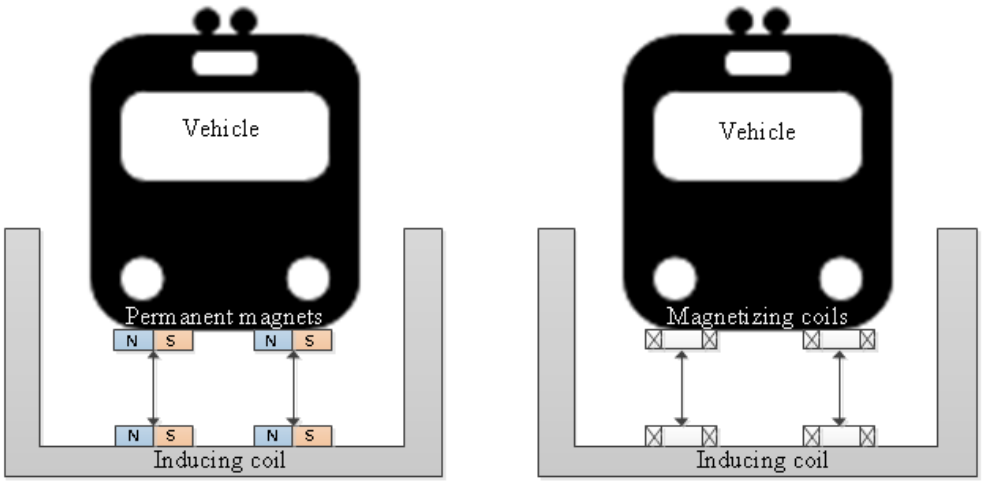

Figure 2.8: EDS Maglev train

- Hybrid Electromagnetic suspension (HEMS): Beside electromagnets, permanent magnets are utilized in this type of suspension to lessen the electric power consumption, as the magnetic field formed by the permanent magnets is able to levitate the

vehicle in a certain steady- state air-gap and electric power consumption is almost zero for the electromagnets.

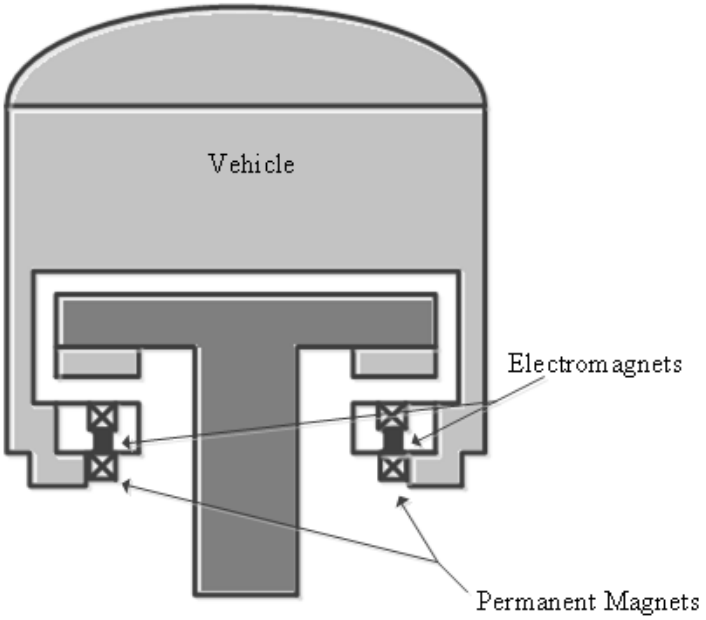

Figure 2.9: HEMS Maglev Train

2.3.2 Active magnetic bearings

The limitations associated with other contactless levitation approaches such as high rotor speeds, damping and vibration control can be efficiently overcome by using active magnetic bearings. The electronic hardware of the active magnetic bearing can be categorized into control system with its associated sensor system and the actuator system. The purpose of using such electronic hardware is to detect the position of the rotor and react on position displacements with a controlled positioning actuator action. The active magnetic bearing system has two radial planes (x,y) and an axial axis z of possible movement of the rotor as shown in Figure 2.10.

A contactless position sensor steadily detects the deviation between desired position and actual position (considered as a position error) of the rotor and feedbacks this information into a controller. These electromagnets exert electromagnetic forces of repelling effect which stabilise the rotor motion around the equilibrium point.

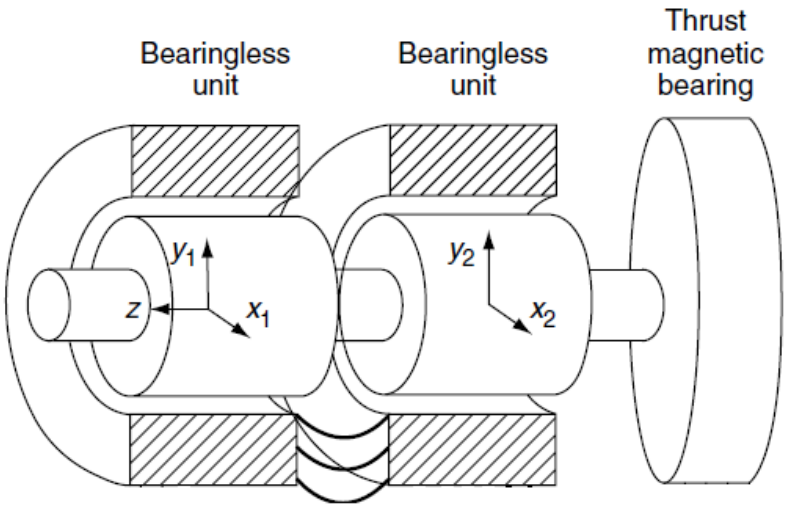

Figure 2.10: Active magnetic bearing (Bleuler et al., 2009)

Different control techniques implemented on active magnetic bearing systems (AMBs) are included in the literature. Halas (2001) investigated a proportional, integral and derivative (PID) controller in simulation studies. The simulation was carried out on non-rotating levitated objects. Another useful theoretical discussion has been reported by Bleuler et al. (2009) where PID controller has been used as part of a closed loop control technique for active magnetic bearings. The study shows that a conventional linear PID controller should be able to control a nonlinear active magnetic bearing system. Further studies using other control techniques have also been conducted. These include adaptive control (Knospe et al., 1995), robust active / robust fuzzy control (Gosiewski and Mystkowski, 2008; Hong and Langari, 2000), multi-variable feedback control (Cole et al., 2002) and fuzzy logic control (Liebert, 1995).

A number of these control techniques are based on linear system theory therefore requiring linearization of active magnetic around the operation point. Non-linear control as reported by Liebert (1995) is more complicated compared to linear control design. The basic task of both conventional bearings and active magnetic bearings is almost the same. However, there is a significant difference in the physical construction and the method of operation of these active magnetic bearings used in many specialized applications such as the following:

- Vacuum and clean room, due to contactless nature of active magnetic bearing in

such environment there is no need for lubricants, and they are inherently clean and suitable for vacuum environments (Bleuler et al., 2009).

- In medical application as the artificial heart, the use of magnetic levitation in left ventricular assist device (LVAD) is being researched (Chen et al., 2002)
- Due to low vibration and contamination of active magnetic bearing, used in high-speed precision machine spindles, semiconductor manufacturing and in turbo-machinery (for achievable high speed rotations) (Bleuler et al., 2009), (Clark et al., 2004).
- In aerospace for energy storage flywheels (Bleuler et al., 2009)

The significant use of active magnetic bearing is in Renewable Energy (due to the rising cost of energy coupled with harmful environmental effects of electric power production) like wind power generation. Vertical wind turbines equipped with AMBs can be started with wind velocity of just around 1.5m/s. Several researchers have discussed one of the important parts in the Horizontal Axis wind turbine that is direct drive generator (Polinder et al., 2006; Shrestha et al., 2017, 2008, 2010). Some have explored possibilities to reduce the weight of the heaviest part in the wind turbine, direct drive generator. It has been suggested that using a hybrid solution "combination of mechanical bearing and magnetic bearings" can significantly reduce the weight of the direct drive machine. Moreover, hybrid concept provides flexibility on the axial direction and the ease of control with each other. Zhang et al. (2012a) have presented a horizontal axis wind generator with an active axial bearing and two passive redial bearings (permanent magnet), where a comparison between the conventional and variable universe fuzzy PID strategies to control the axial position of the rotor (one degree of freedom) has been presented. The results show preferable static and dynamic performance of the variable universe fuzzy PID controller.

Rosales et al. (2013) have compared two small wind turbines, one with a ball bearing and the other with magnetic bearings. The results show that there is a boost in power by 7.2 and 33.2 percent with the Maglev wind turbine under a wind speed of 8 and 4 m/s respectively. Moreover, the start-run time is just about 8.96 s quicker for wind turbine using magnetic bearing for wind speed of 4m/s. This time becomes significant considering

the interval of time that takes gusts of wind. It further concludes that Maglev small wind turbine operates employing a speed of just under 3 m/s.

Kumbernuss et al. (2012) give full description of a Vertical Axis Wind Turbine (VAWT) using magnetic bearing. In past few years, the literature is mostly on levitation mechanisms. In the work of Kazadi et al. (2008) carried out research on the development of magnetic bearings to improve machine efficiency, and further maintenance problems, vibration, noise and friction. Regarding the vertical axis wind generator, there are some studies like "Maglev wind power turbine shaft wheel drive" by Chen Qiuping and Xiao Liu titled "vertical-wide Maglev wind power generator" cited in (Wu et al., 2010), and the like, which make use of permanent magnet to achieve the magnetic drive. However, the dynamic performance of a magnetic bearing depending on the permanent magnet cannot satisfy the need for small vertical turbines, as Maglev wind turbines using permanent magnet are not reliable.

Although the static performance is useful, the dynamic performance is poor, and importantly they cannot guarantee stability for the rotor. On the other hand, there are not many studies on examining active Maglev vertical wind turbines, "Although it is claimed that many Maglev wind turbine products have been developed, relevant published studies are rate", Zhang et al. (2012a) introduced magnetic levitation supporting the structure of Vertical Axis Wind Turbine (Wu et al., 2010; Zhang et al., 2012b). The authors compared conventional PID with self-adaptive integral-type sliding mode control (AISMC). The simulations show better dynamic response and robust characteristic using AISMC, and that AISMC control can limit the overshoot within 10%, shorting the response time by 0.038s and the system has better disturbance capability than the conventional PID.

2.4 Non-linear observer

Estimating a state of a dynamical system, whether it is estimated from system input or output, is known as “observing the state”, that is where the name of “observer” in the theory of systems comes from. In the early works, the principle of observer has been widely studied and proven in many linear systems, Linearised systems, in the so-called “observer-based control”. However, applying such type of linear observer to non-linear system theory has been successfully implemented by using the extended Kalman filter (Primbs, 1996).

Attempts have continued to construct a non-linear observer using tools developed from pure non-linear systems theories. One of the most highlighted results, which used Lyapunov stability theory, was presented by Thau (1973) and Kou et al. (1975). Primbs (1996) has considerably simplified both these results and has and presented with examples.

Techniques relying on Lie-algebraic approach have been introduced in non-linear observer design by converting non-linear states of the system to linear states where any applicable linear theory can be utilized. Non-linear state transformations method in non-linear observer design was primarily developed and introduced by Zeitz (1987) who has designed non-linear observer by transformation into a generalized canonical from and Keller (1987) has extended the Luenberger observer for non-linear control systems.

Baumann and Rugh (1986) introduced the method of injecting non-linear output, of single-input multi-output (SIMO) non-linear system, based on system linearisation in order to place the eigenvalues of the family of linearised closed-loop systems at specific values, so that the linearised error dynamics would have locally constant eigenvalue with respect to the closed-loop operating points. This method was illustrated in application of automatically balancing of an inverted pendulum. Figure 2.11 summarises the methodology that can be used to design a non-linear observer.

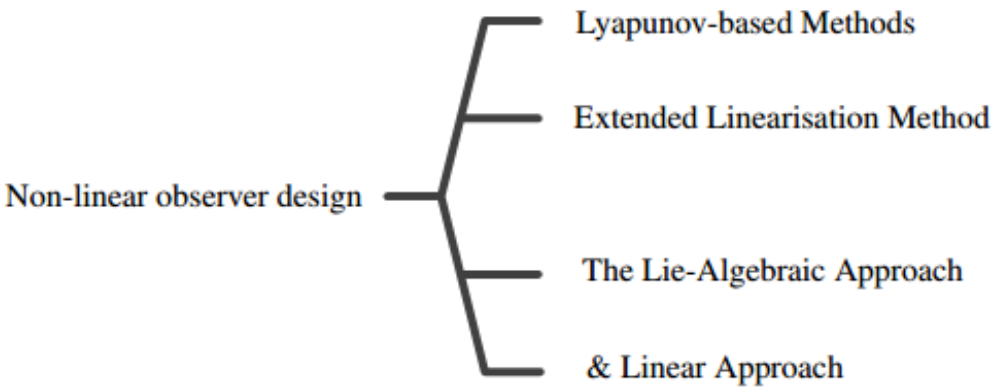

Figure 2.11: Non-linear observer design hierarchy

> " The first appearance of High Gain Observer (HGO) was in linear feedback control in 1979 in Doyle and Stein's work of LQR loop transfer recovery (Doyle and Stein, 1979). In this work, state-feedback control was designed to shape the frequency of the loop transfer function, and then the observer was brought in to recover the frequency response. Although it was not called high gain observer, but the way is worked is to tune some parameters in Riccati equation, and the parameters are actually tuned to produce high gain observer used in these days" (Khalil, 2015).

In the late of 1980's, high-gain observer was used in controlling non-linear systems (Esfandiari and Khalil, 1987; Saberi and Sannuti, 1990). Two groups of researches simultaneously developed techniques in high-gain observer for non-linear tems. These were a French group lead by Hammouri, Gauthier and a US group lead by Khalil. The French group focused on stabilising the non-linear system globally under global Lipschitz and the structure of non-linear zeros in this work was more general. However, the work done by Khalil's group was in lack of global Lipschitz conditions, i.e. the characteristic of this work doesn't require that non-linearity of the system to satisfy Lipschitz conditions, as when the observer gain is sufficiently increased that could destabilize the system, which means only semi-global results were achieved in this work with a compact set which can be made arbitrary large. The first demonstration of the presence of peaking phenomena in non-linear feedback control was in Esfandiari and Khalil's work (Khalil, 2008), where

undesirable peak would make the transient response worse and worse as the observer gain increased. It was found that the interaction of peaking phenomena with non-linearity of the system drives the system to unstable region and causes the system to have finite escape time.

The suggested seemingly simple solution to such problem was to bound the state estimation during the very beginning of the response, the peaking period, so the plant can be protected from this peaking and the estimated states remain very close to initial condition values. This period of peaking is too short compared to the time constant of the overall closed-loop dynamics, since the observer dynamics are designed to be much faster than the dynamics of the closed-loop under the state-feedback (Esfandiari and Khalil, 1992).

Another solution was proposed by Atassi and Khalil (2001) who proved that the stability of closed-loop system under state-feedback using sufficiently high observer gain was to saturate the control action instead. The idea of this saturation is realised as follows: Extended High Gain Observer (EHGO) is designed first then a compact of set of operations under state-feedback control need to be determined which means looking for a compact set of initial conditions and what a compact set of the state trajectories belong to, after this find the maximum control to be fed to the system and saturate the control just above this value. This solution proves stability and also shows how output feedback controller can recover the performance of the state feedback controller. In this work the solution of saturating the control action is used to overcome the peaking problem. Some of previous related works that use or implement High-Gain observer (linear / non-linear) are summarized in Table 2.1.

To design a robust controller to overcome the non-linearity of the magnetic levitation system as well as deal with the uncertainties in the system, all system states need to be available to the controller. Both types of robust state-feedback controller, linear and non-linear, are based on the assumption that all the state variables are measurable or all the state variables need to be converted in terms of measured variables and this is difficult in

Table 2.1: Previous works matrix for High-Gain Observer

Author	Application	Combined Controller	Model	comments
Adekanle et al. (2017)	Grid-Connected Doubly-Fed Induction Generator	Integral Backstepping Controller	linear	Robustness against resistance variation Estimate mechanical torque of the machine
Kumar et al. (2017)	Distributed Power System	Adaptive control strategy	Discrete	Experimental validation Achieve reasonable steady state accuracy
Khalil (2017)	Permanent Magnet Synchronous Motors	feedback linearisation control	Nonlinear	Experimental implementation for EHGO 20% parameters mismatch
Du et al. (2015)	Marine Dynamic Positioning System	Adaptive Output Feedback Control	linear	Robustness against environment disturbances Estimate unavailable velocities of ships
Haisheng and Jinkun (2012)	VTOL aircraft	Sliding mode control	linear	Under-actuated system Non-minimum phase system
Mahmud et al. (2012)	Interconnected power systems	Exact feedback linearisation	Non-linear	Non-linear high gain observer Observer linear gain calculated using Kalman filtering
Liu et al. (2012)	Governor of hydro-turbine generator	Feedback linearisation	linear	Parameter optimization 20% parameters mismatch
Heredia and Yu (2000)	Robot Manipulator	PD control	linear	Linear high gain observer 20% parameters mismatch
Ahsan et al. (2013)	Magnetic Levitation System	Feedback linearisation	linear	Linear extended high gian observer is used Control action has been saturated (peaking phenomena)
Katayama and Oshima (2011)	ECP Maglev SYSTEMS	Backstepping control	Discrete	Experimental works, Linear High-gain observer Continuous control design for MIMO systems
Chen and Hsiao (2011)	3-pole Active Magnetic Bearing System	Backstepping control	linear	Experimental works Nonlinear high gian observer is used
Shu and Meisinger (2011)	High-speed Maglev train	LQR control	linear	Kalman Filter Noise rejection
Yang et al. (2009)	Magnetic Levitation System	Backstepping control	linear	Experimental works Disturbance observer
Baranowski and Piatek (2008)	Magnetic Levitation System	PID control	Nonlinear	Nonlinear high gian observer vs. Reduced oreder observer Bigger operation range using NHGO
Li and Gutierrez (2008)	6-DOF Precision Maglev	MIMO sliding mode controller	linear	Non-linear velocity observer Disturbance observer

practice. The issues linked to unmeasured states could be solved through the state estimation process (Shao et al., 2015). Considering that all state variables of magnetic levitation system are available for feedback, the position of a levitated object can be measured with an appropriate sensor and current through the coil generating active magnetic field. However, the velocity measurement is a challenging task, since the only option is numerical differentiation of the position.

A linear reduced-order observer-based control scheme has been proposed by Munaro et al. (2002) to ensure local stability for perturbations in the equilibrium and estimated states. The design technique of tracking controllers using integral control reported by Munaro et al. (2001) has used linear reduced-order observer to estimate the states of the input-state linearisation design.

A non-linear full-order high-gain observer has been conducted in magnetic levitation educational ball system by Baranowski and Piatek (2008) and compared with reduced-order linear observer, where these observers are used with two different structures, namely PID with a non-linear feed-forward and a cascade linearising feedback. The results show that both observers provide much smoother control signal than those with numerical differentiation, and full-order Non-linear high gain observer provides larger operation range than the reduced-order observer. However, the control signal provided by reduced-order observer differed only in small details caused by additional disturbance, since the full-order observer used only one measurement while the reduced-order used two disturbed measurements instead of three measurements for the full-order observer.

In Mahmud et al. (2012) combined non-linear high-gain observer with exact linearisation approach and used to control interconnected power system. Full estimated states of power system were directly fed back as an input to the system to conduct the control law which in this case was not expressed in terms of all measurement variables. The methodology of designing non-linear high gain observer and the theory behind are presented and justified in their paper, and this approach is mainly adopted in this research. The novelty of this work is to design the linear gain of the high-gain observer (HGO) which is calcu-

lated from analogy of linear observer gain design, that is Kalman filter linear gain. The influence of the disturbance such as noise-sensitivity and uncertainties are not considered in their work.

Chapter 3

Dynamic Model of Magnetic Levitation System

3.1 Introduction

Active magnetic levitation (AML) systems have been widely used in medical applications (Allaire et al., 1996), turbo-machinery (Field and Iannello, 1998), magnetic levitation vehicles (Jang et al., 2011), micro robot actuation (Hagiwara et al., 2012) and wind turbine (Aravind et al., 2012). Contactless support of objects continues to be a fantasy for several centuries. The utilization of magnetic forces seems to be the ideal solution in many situations to such a goal. Using magnetic forces to support an object without any mechanical contact is constrained by the laws of magnetism. Earnshaw's theorem (Bleuler et al., 2009) states that when the inverse-square-law forces govern several charged particles, they can never be within a stable equilibrium. The interaction between ferromagnetic objects and electromagnets of either the active or passive type (Bassani, 2011) is associated with an unstable behaviour.

This unstable behaviour can be represented by highly non-linear differential equations. In the literature many researches are based on linearised models around a specific nominal operating point. In such cases, the tracking performance can rapidly deteriorate as deviation from the operating point increases. However, in order to guarantee a local asymptotic stability over larger range and ensure good tracking, it is necessary to consider a non-linear model (Al-Muthairi and Zribi, 2004; Shameli et al., 2007; Yu et al., 2010) rather

than a linearised one (Barie and Chiasson, 1996; Cho et al., 1993; Mizuno et al., 1996; Romero Acero et al., 2016; Shi and Lee, 2010; Uswarman et al., 2014; Yu and Qian, 2012).

3.2 Nonlinear dynamic model of active magnetic levitation

Figure 3.1 shows an active magnetic levitation system (AML). The Maglev system serves to keep a small steel ball in stable levitation at some steady-state operating position. An electromagnet is used to produce forces to support the ball. The electromagnetic forces are related to the electrical current passing through the electromagnet coil.

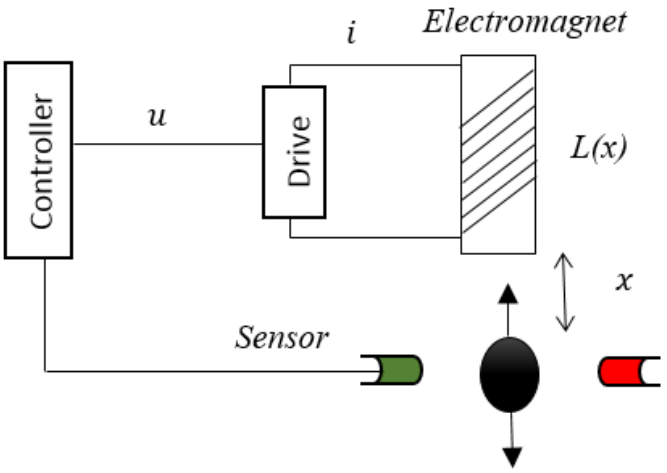

Figure 3.1: Active magnetic levitation system (AML)

Electromagnetic force produced by current can be calculated by applying Kirchhoff's voltage law to the electric system loop

$$v(t) = v_R + v_L = i\,.\,R + L\dot{i} + i\dot{L} \tag{3.1}$$

where v is applied voltage, i is coil current, R is coil resistance and $L(x)$ is coil inductance. A typical approximation according to Wong (1986) it is assumed that the inductance varies

inversely with the position of the ball;

$$L(x) = L_c + \frac{L_0 x_0}{x} \tag{3.2}$$

where x_0 is considered as an arbitrary reference position. An alternative approximation for $L(x)$ is given by Woodson and Melcher (1968) as

$$L(x) = L_c + \frac{L_0}{\left(1 + \frac{x}{a}\right)} \tag{3.3}$$

where, L_c is constant inductance of the electromagnetic coil in the absence of object, x is the position of the object, L_0 and a are system parameters. However, in this work the approximation in equation (3.2) is used because of its simplicity.

The stored magnetic energy is a function of the coil current i and the separation of the ball ferromagnetic x

$$W(i, x) = \frac{1}{2} L(x)\, i^2 \tag{3.4}$$

Since the electromagnetic force is the partial derivative of the stored magnetic energy, assuming magnetically linear material, the strength of electromagnet is given by

$$f_{em} = -\frac{\partial W}{\partial x} = -\frac{i^2}{2}\left[\frac{dL(x)}{dx}\right] \tag{3.5}$$

Considering equation (3.2)

$$f_{em} = -\frac{1}{2} L_0 x_0 \left(\frac{i}{x}\right)^2 \tag{3.6}$$

A conservation of energy argument by Barie et al. (1996) paper shows that magnetic constant of the coil is given as

$$c = \frac{1}{2} L_0 x_0 \tag{3.7}$$

Substituting for $L(x)$ from equation (3.2) into equation (3.1) and considering equation (3.7) yields

$$\frac{\partial i}{\partial t} = \frac{-R}{L}\, i + \left(\frac{2c}{L}\,\frac{i}{x^2}\right)\frac{\partial x}{\partial t} + \frac{1}{L}\, v \tag{3.8}$$

The object is suspended by balancing between the force of gravity and electromagnetic force. Applying Newton's 3rd law of motion, the dynamic form of the mechanical system can be written as follows:

Define the states $x_1 = x$ (position), $x_2 = V$ (velocity), $x_3 = i$ (current) and the system input $u = v$ (applied voltage). The non-linear state space model of AML system can be expressed as

$$\begin{bmatrix} \dot{x}_1 \\ \dot{x}_2 \\ \dot{x}_3 \end{bmatrix} = \begin{bmatrix} x_2 \\ g - \dfrac{c}{m}\left(\dfrac{x_3}{x_1}\right)^2 \\ -\dfrac{R}{L}x_3 + \dfrac{2c}{L}\left(\dfrac{x_2 x_3}{x_1^2}\right) + \dfrac{1}{L}u \end{bmatrix} \tag{3.9}$$

3.3 Non-linear observer design for magnetic levitation system

To design a robust controller to overcome the non-linearity of the magnetic levitation system as well as dealing with the uncertainties in the system, all system states need to be available to the controller. Both types of robust state-feedback controller, linear and non-linear, are based on the assumption that all the state variables are measurable or all the state variables need to be converted in terms of measured variables and this is difficult in practice. The issues linked to unmeasured states could be solved through the state estimation process (Shao et al., 2015). Considering that all state variables of magnetic levitation system are available for feedback, the position of a levitated object can be measured with an appropriate sensor and current through the coil generating active magnetic field. However, the velocity measurement is a challenging task, since the only option is numerical differentiation of the position. This requires to design an observer to estimate unmeasured system states. In this work, a non-linear high-gain observerNHGO is proposed for many reasons;

- High gain observer is reasonably simple to be designed as it does not it requires involve complicated formula nor solving complex differential equations.
- It can guarantee semi-global or even global stability for large class of high-order non-linear systems which means it can provide stability for large operation range for any arbitrarily chosen initial conditions.
- It is considerably fast, i.e. observer estimation error converges to zero within very short finite time.
- It is robust to many types of disturbances whether it external or internal including system parameters mismatch.
- In case of being used in state feedback, high gain observer can provide very similar performance compared to the performance provided by measured state feedback controller.

3.3.1 Non-linear high-gain observer design

Let, the non-linear system be represented as

$$\begin{aligned} \dot{x} &= f(x) + g(x)\,u \\ y &= h(x) \end{aligned} \tag{3.10}$$

where $x \in \mathbb{R}^{n\times n}$ is the state vector; $u \in \mathbb{R}^{m\times m}$ is the control vector; $y \in \mathbb{R}$ is the system output vector; $f(x)$ and $g(x)$ are n-dimensional vector fields in the state space representation and $h(x)$ is the differentiable vector field of x. To design an optimal controller based on state feedback for such a non-linear system; all states need to be measured or estimated. The object position can be measured by an appropriate sensor and coil current. The velocity measurement, however, is not straight forward. The difficulties associated with unmeasured states can be solved through a state estimation process.

A non-linear observer can be set up as

$$\dot{\hat{x}} = f(\hat{x}) + g(\hat{x})u + l(\hat{x})(y - h(\hat{x})) \tag{3.11}$$

where $g(\hat{x}) = \begin{bmatrix} 0 & 0 & 1/L \end{bmatrix}^T$, $h(\hat{x}) = \hat{x}_1$ and $l(x)$ is non-linear gain which can be written as

$$l(\hat{x}) = (J(\hat{x}))^{-1}G \tag{3.12}$$

Here, J is the Jacobian matrix of coordinates obtained from non-linear coordinate transformation,

$$J(\hat{x}) = \frac{\partial}{\partial x}\begin{bmatrix} h(\hat{x}) \\ \mathcal{L}_f h(\hat{x}) \\ \vdots \\ \mathcal{L}_f^{n-1} h(\hat{x}) \end{bmatrix} \tag{3.13}$$

Thus from formulation of the above equation, and the proof of associated theorem presented in Mahmud et al. (2012), the non-linear gain for the AML is obtained as

$$l(x) = \begin{bmatrix} dh(\hat{x}) \\ d\mathcal{L}_f h(\hat{x}) \\ d\mathcal{L}_f^2 h(\hat{x}) \end{bmatrix}^{-1} \begin{bmatrix} G_1 \\ G_2 \\ G_3 \end{bmatrix} \tag{3.14}$$

where $\mathcal{L}_f h(\hat{x})$ denotes a Lie derivative of $h(\hat{x})$ in the direction of vector field f and G vector is the linear gain which can be calculated using any linear observer such as Kalman filtering in Mahmud et al. (2012). Here, the row vectors $dh(\hat{x})$, $d\mathcal{L}_f h(\hat{x})$ and $d\mathcal{L}_f^2 h(\hat{x})$ must be linearly independent (observability condition) (Hedrick and Girard, 2005). After manipulations, the Jacobian matrix J can be written as follows

$$J(\hat{x}) = \begin{bmatrix} 1 & 0 & 0 \\ 0 & 1 & 0 \\ \frac{2c}{m}\frac{\hat{x}_3^2}{\hat{x}_1^3} & 0 & -\frac{2c}{m}\frac{\hat{x}_3}{\hat{x}_1^2} \end{bmatrix} \tag{3.15}$$

It can be readily shown that

$$|J(\hat{x})| = -\frac{2c}{m}\frac{\hat{x}_3}{\hat{x}_1^2} \tag{3.16}$$

hence the non-linear gain l can be written as

$$l = \begin{bmatrix} G_1 \\ G_2 \\ \frac{\hat{x}_3}{\hat{x}_1} G1 - \frac{m}{2c}\frac{\hat{x}_1^2}{\hat{x}_3} G_3 \end{bmatrix} \tag{3.17}$$

Therefore, the non-linear observer for AML system can expressed as 3.18

$$\begin{aligned} \begin{bmatrix} \dot{\hat{x}}_1 \\ \dot{\hat{x}}_2 \\ \dot{\hat{x}}_3 \end{bmatrix} &= \begin{bmatrix} \hat{x}_2 \\ g - \frac{c}{m}\left(\frac{\hat{x}_3}{\hat{x}_1}\right)^2 \\ -\frac{R}{L}\hat{x}_3 + \frac{2c}{L}\frac{\hat{x}_2\hat{x}_3}{\hat{x}_1^2} \end{bmatrix} + \begin{bmatrix} 0 \\ 0 \\ \frac{1}{L} \end{bmatrix} u \\ &+ \begin{bmatrix} G_1 \\ G_2 \\ \frac{\hat{x}_3}{\hat{x}_1} G1 - \frac{m}{2c}\frac{\hat{x}_1^2}{\hat{x}_3} G_3 \end{bmatrix} (x_1 - \hat{x}_1) \end{aligned} \tag{3.18}$$

Verification of this kind of observer is considered a difficult task as it requires that the right side of equation (3.9) should ascertain the global Lipschitz condition. For this reason this type of observer is considered only as local stable observer, which means that the estimation error dynamics of equation (3.11) should have a finite escape time (observer error converges to zero within a finite time). Thus in this work the gains 'G' were constructed in such a way, that the observer dynamics (high-gain observer 'HGO') are much faster than the system dynamics (at least five-times).

The estimated states which are obtained from the non-linear observer are used to implement the control law of the exact linearising controller (see Figure 3.2).

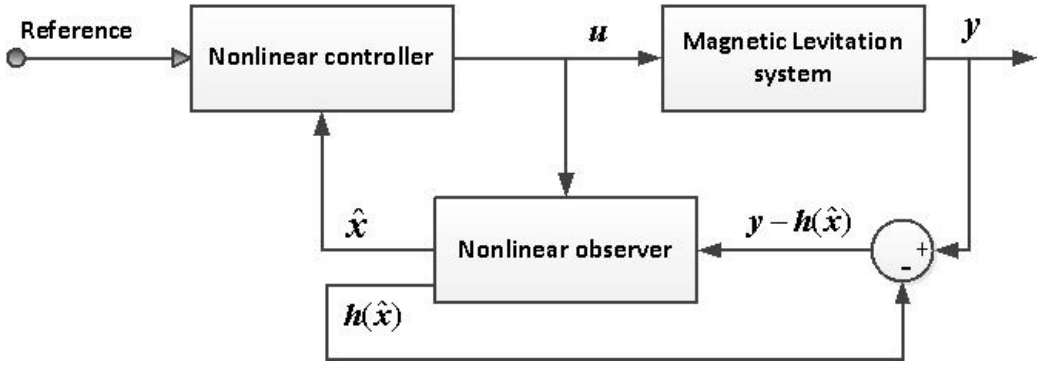

Figure 3.2: Full-order non-linear observer-based excitation

3.3.2 Implementation and results of non-linear observer

This section presents simulation results assessing the performance of Non-linear high-gain observer (NHGO). The results are split into two main parts. The first part will highlight the capability of the observer in terms of the state estimation. Then the noise rejection will be presented in the second part.

In order to chose the observer gains, the design methodology that detailed in section 3.3 will be followed. The dynamics of the non-linear observer for AML system was expressed in equation (3.18); the observer-based controller assigns the observer eigenvalues in a way that makes the observer dynamics faster than the dynamics of closed-loop system under state feedback.

The linear gain "G" of the proposed observer was calculated according to the formula that was used in (Baranowski and Piatek, 2008; Khalil and Praly, 2014) and (Khalil, 2008) in the form of

$$G = \begin{bmatrix} G_1 \\ G_2 \\ G_3 \end{bmatrix} = \begin{bmatrix} \frac{3\,a}{\epsilon} \\ \frac{3\,a^2}{\epsilon} \\ \frac{a^3}{\epsilon} \end{bmatrix} \tag{3.19}$$

where $\epsilon \in (0, 1]$ and a are parameters to be tuned. The closed-loop system under output feedback is asymptotically stable for all $\epsilon > 0$. The parameter a is recommended by (Baranowski and Piatek, 2008) to be at least 150, whereas in (Khalil and Praly, 2014) ϵ is

instead tuned within the range of [0.01- 0.01]. However, in this work ϵ was set to 0.5 and a should be at least 10 to have good noise rejection in very noisy conditions. This results in

$$G = \begin{bmatrix} 6a \\ 12a^2 \\ 8a^3 \end{bmatrix} \tag{3.20}$$

Simulations were carried out with the system parameter values shown in Table 3.1:

3.3.2.1 Estimation of system states

In this section, estimation of all system states is considered without introducing any type of measurement noise in order to enhance the transient response of the estimation error utilizing various values of a in the range of [50,150], while ϵ in equation (3.19) was set to 0.5.

Figures 3.3 - 3.5 show estimation error of estimated states (position, velocity and current) against time per second using the non-linear full-order observer-based controller for Maglev system via LQR-feedback linearisation. The simulation here compares the performance of the proposed non-linear observer for different values of a. Simulations were carried out with the following values for the system parameters: $M = 21.2 \times 10^{-3}$ kg, $C = 8.248 \times 10^{-5}\ N{\times}m/A^2$, $R = 4.2\,\Omega$, $L = 0.02$ H. Initial conditions of the non-linear Maglev model were different from the ones for the non-linear observer as they were set for non-linear model to $x_{10} = 18 \times 10^{-3}$ m for the position, the velocity was set to $x_{20} = 0$

Table 3.1: Parameters of magnetic levitation system

Symbol	Description	Value	Unit
L	Coil Inductance	200	mH
R	Coil Resistance	4.2	Ω
m	Steel Mall Mass	0.0212	Kg
c	Electromagnet Force Constant	8.248×10^{-5}	$N.(m/A)^2$

m/s and $x_{30} = \sqrt{m \times g \times 18 \times 10^{-3}}$ = 0.9039 A as initial condition for the current, and the initial conditions for the observer were [0.014, 0, 0.7030].

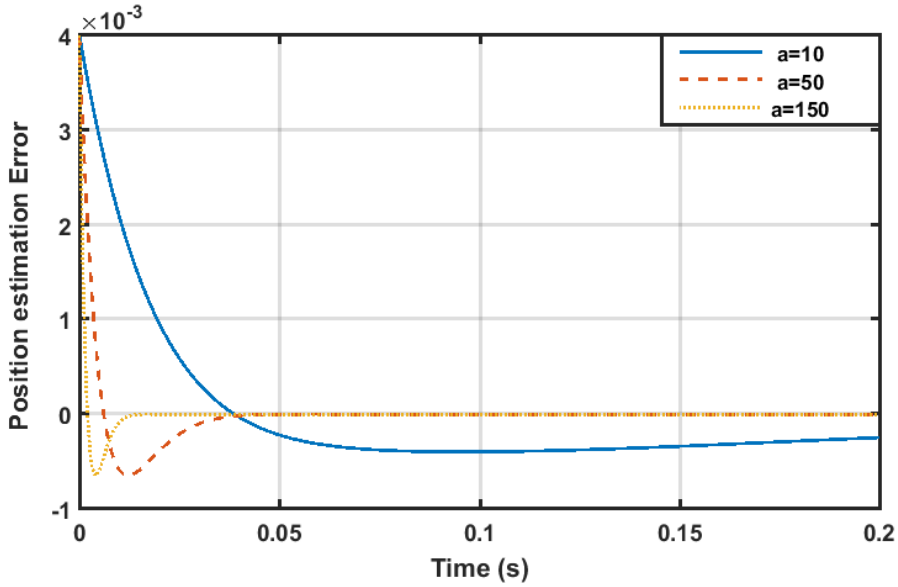

Figure 3.3: Position estimation error without noise

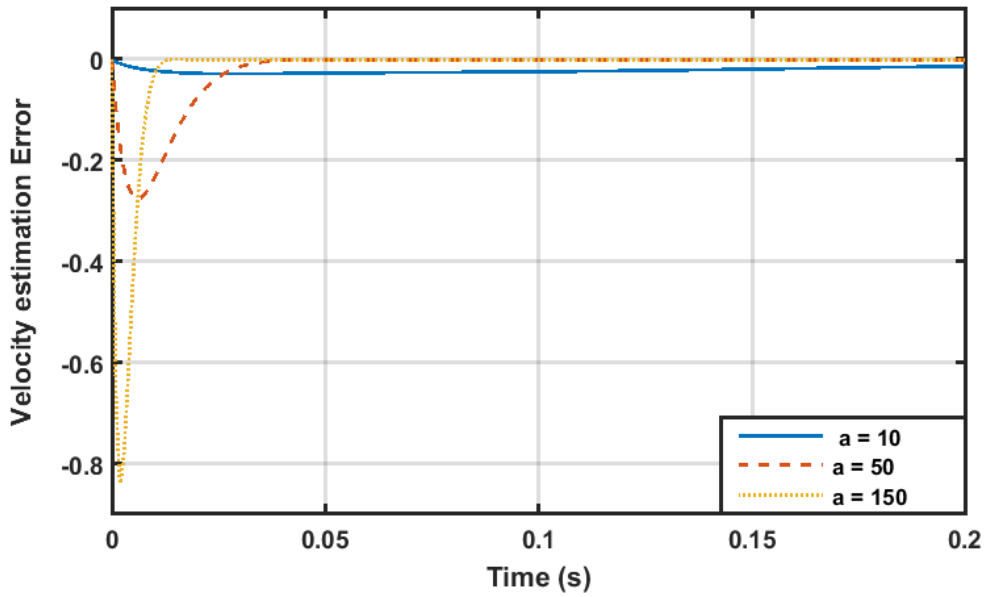

Figure 3.4: Velocity estimation error without noise

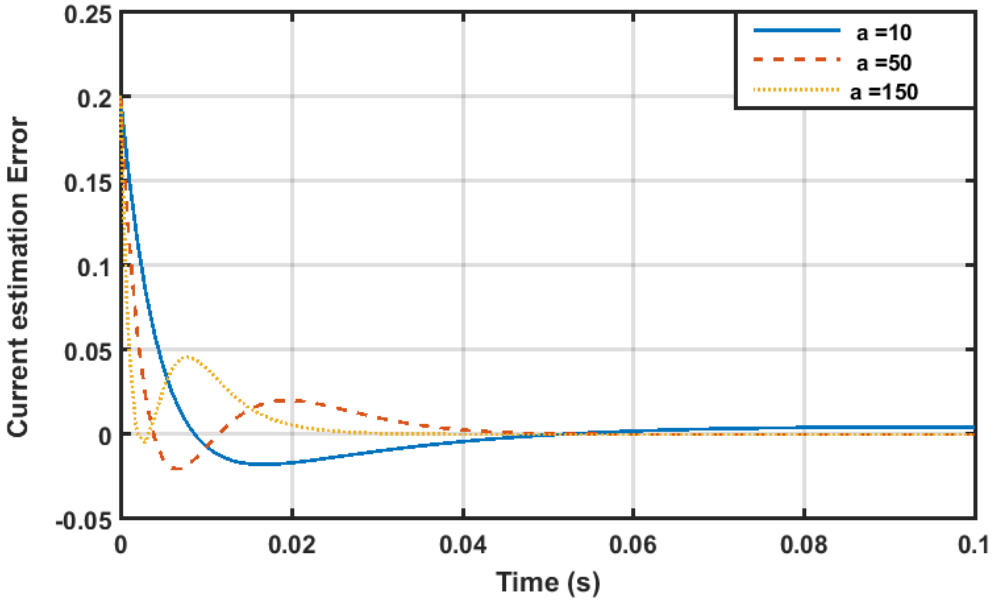

Figure 3.5: Current estimation error without noise

Figures 3.3 and 3.4 show the estimation error for all estimated states in absence of noise when the linear gain was $a = 150$ is less than the estimation error when $a = 10$ or 50. As noted, in absence of disturbance, the non-linear observer with higher linear gain performed much better, as the states estimate converged faster to the actual states.

3.3.2.2 Noise rejection

Noise, model mismatch and disturbance are other issues that must be taken into consideration in observer tuning. The maximum linear gains of the non-linear observer is to be tuned to achieve reasonable noise attenuation with adequate margins of stability. In this section, the robustness of non-linear high gain observe is tested by introducing disturbance.

Experiments were carried out to verify the robustness and stability of this algorithm (non-linear full-order observer-based controller for Maglev system via LQR-feedback linearisation). Simulation results were obtained using different tuning parameters for the observer when measurement noise was introduced; the system measurements were influenced by uncorrelated stochastic white Gaussian noise , additive output noise, with zero mean value and the same covariance of c(.) and sampling time $T_s(.)$ in second. The controller tuning parameters were fixed and the same system parameters and initial conditions

in section 3.3.2.1 were used.

Figures 3.6 to 3.8 show the estimated state $\hat{x}_1$ position state x_1 for different values of a set to 10, 50 and 150 respectively when the system input was step input of 0.015 for 2 seconds then step up to the value of 0.03 for another 2 seconds.

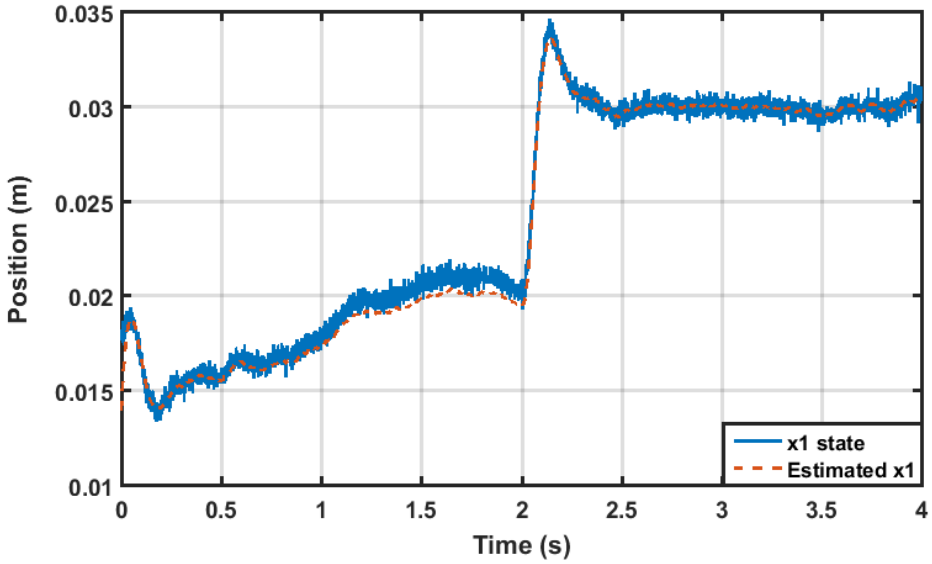

Figure 3.6: Position state versus estimated state when $a = 10$

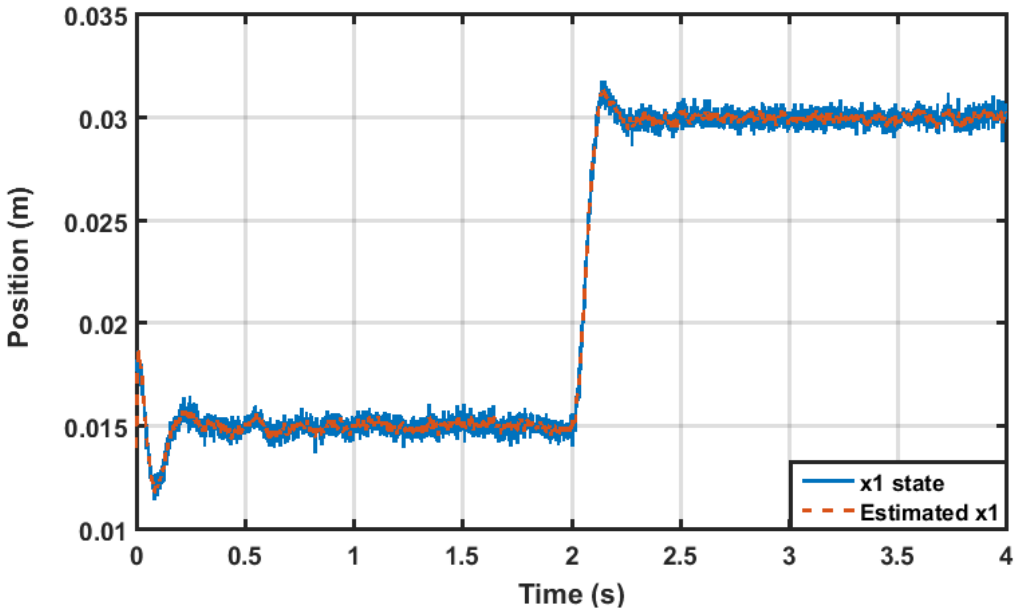

Figure 3.7: Position state versus estimated state when $a = 50$

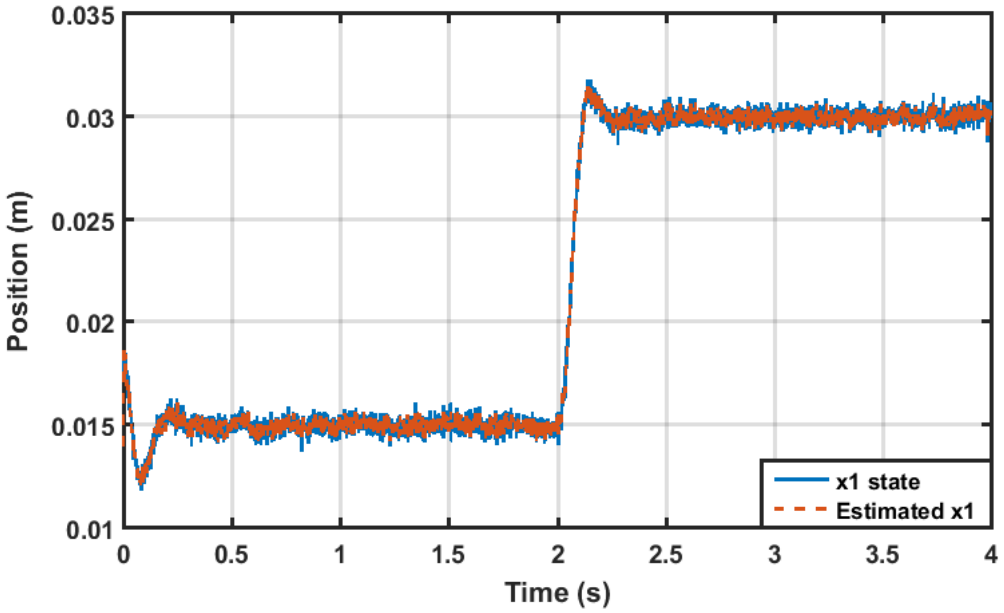

Figure 3.8: Position state versus estimated state when $a = 150$

It can be seen that the observer was more able to reject the measurement noise when a was set to 10 as the estimation went smoother than others. Moreover, the control action was much smoother using the observer with 10 as tuning value for a compared to values of 50 and 150 as shown in Figure 3.9.

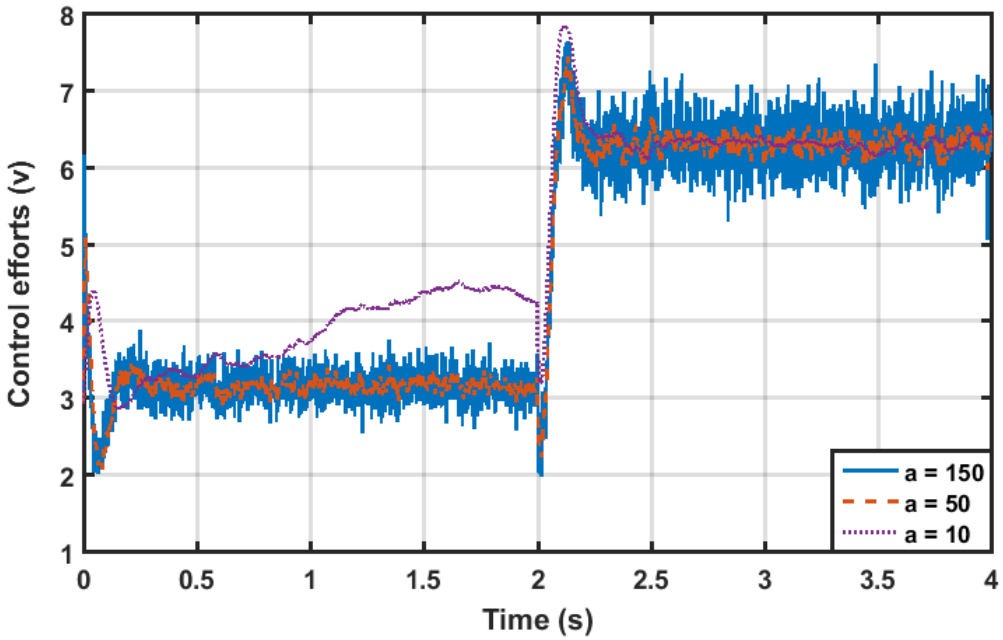

Figure 3.9: Control efforts with different observer tuning parameters

However, it can be seen that the track estimation went off the measured position state for sometime when $a = 10$ and in the case of having $a = 150$ the system tended to be more sensitive to the noise, in contrast to the observer when $a = 50$ tended to have less smooth estimation with better tracking. Mean square error (MSE) values for full estimated states (position, velocity and current) are presented in Table 3.2 using different observer gains. As noted the lowest error was likely to be provided by the observer when the linear gain was set to $a = 50$.

Table 3.2: MSE values for the estimated states using different observer tuning parameters

observer gain	MSE		
" a"	Position	Velocity	Current
10	3.05×10^{-7}	5.84×10^{-4}	5.70×10^{-5}
50	1.42×10^{-7}	3.36×10^{-4}	7.85×10^{-5}
150	1.80×10^{-7}	4.80×10^{-3}	1.58×10^{-4}

Simulation results in Figure 3.10 demonstrate the potential of having $a = 50$ to conduct the linear gain for the non-linear observer to enhance the overall system response, compared to the gain $a = 10$ and for when a getting high to 150.

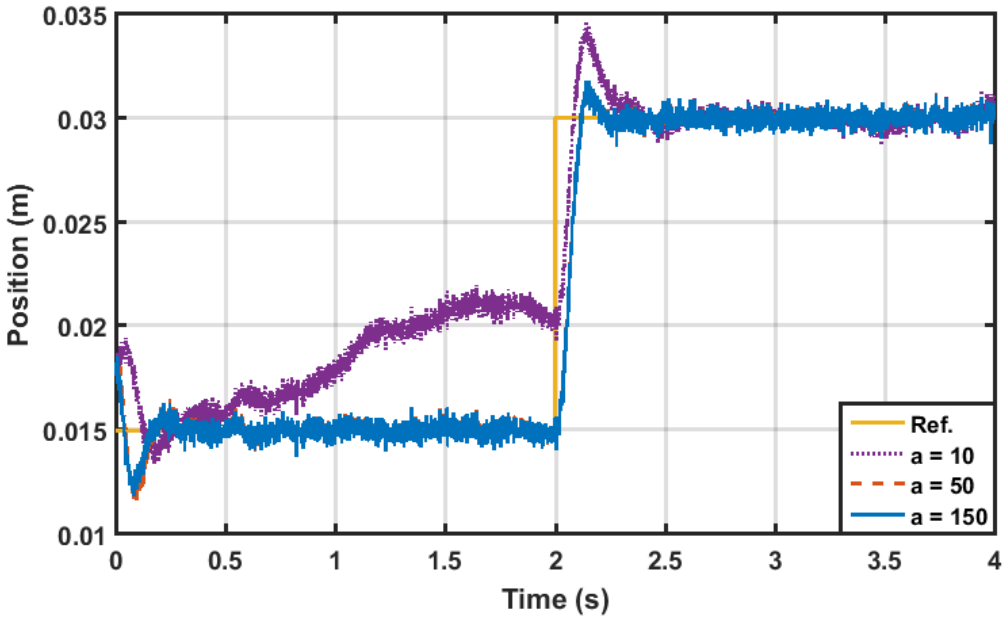

Figure 3.10: Step response with different observer tuning parameters

For maximum noise limits to be taken into account, the maximum linear gains of the

non-linear observer are chosen , for the system to be less susceptible to noise and have an adequate margin of stability a needs to be set to 50 and $\epsilon = 0.5$ with this noise level.

3.4 Sliding mode observer for magnetic levitation system

In the case of designing an observer for linear/ linearised system, a high value of the linear Luenberger observer gain "L" will make the estimated states converge very quickly to the system states. Nevertheless the initial estimator error can be prohibitively large leading to the so-called peaking phenomenon.

The aforementioned problem justifies utilizing sliding mode observer. The sliding mode observer drives the estimated states to hypersurface (sliding surface) around zero estimated error utilizing instead non-linear high gain. This non-linear gain can be implemented with any scaled function such as *signum*, saturation, or *tanh* function. This kind of non-linear gain will maintain the observer trajectories slide along a surface once the estimated states hit this sliding surface where the observed outputs exactly match the the measured outputs. Hence, this attractive feature would reduce the sensitivity of the estimated states to many types of noise (Drakunov, 1983; Utkin et al., 2009).

3.4.1 Sliding mode observer design

According to Drakunov (1992), sliding mode observer can be adequate for non-linear systems. The observer dynamics for non-linear Maglev system, with a special case where system has no input, can be expressed as

$$\dot{\hat{x}} = (J(\hat{x}))^{-1} + M(\hat{x}) * sign\,(V(t) - H(\hat{x})) \tag{3.21}$$

where $(J(\hat{x}))^{-1}J$ is the inverse of Jacobian linearisation matrix and The $sign(.)$ is a vector of n dimension that extends the scalar signum function for $z \in \mathbb{R}^n$ as

$$sign(z_i) = \begin{bmatrix} sign(z_1) \\ sign(z_2) \\ sign(z_3) \end{bmatrix} \tag{3.22}$$

and $M(\hat{x})$ is a diagonal matrix suitably positive large gains to guarantee reachability to sliding mode.

$$M(x) \triangleq diag(m_1(\hat{\hat{x}}), m_2(\hat{x}), m_3(\hat{x})) \tag{3.23}$$

whereas $H(x(t))$ is a vector of system output $h(x)$ that equals to $y(t)$ assuming inverse of Jacobian linearisation matrix exits to have well defined observer and repeated Lie derivative of $h(x)$. In practice

$$H(x) \triangleq \begin{bmatrix} h_1(x) \\ h_2(x) \\ h_3(x) \end{bmatrix} \triangleq \begin{bmatrix} h(x) \\ L_f h(x) \\ L_f^2 h(x) \end{bmatrix} \tag{3.24}$$

The rate of change of the observation error over time / observation error dynamics in terms of the transformed state can be written as

$$\dot{e} = \frac{d}{dt}\left[H(x) - H(\hat{x})\right] \tag{3.25}$$

thus

$$\begin{bmatrix} \dot{e_1} \\ \dot{e_2} \\ \dot{e_3} \end{bmatrix} = \begin{bmatrix} h_2(x) - m_1(\hat{x}).sign(v_1(t) - h_1(\hat{x}(t))) \\ h_3(x) - m_2(\hat{x}).sign(v_2(t) - h_2(\hat{x}(t))) \\ h_4(x) - m_3(\hat{x}).sign(v_3(t) - h_3(\hat{x}(t))) \end{bmatrix} \tag{3.26}$$

To conclude, the necessary condition for the observability of non-linear MIMO system form (Slotine et al., 1986a):

> "*In order for the system to be observable one must be able to perform successive differential operations on $H(x)$ until an implicit inversion can be performed to obtain x*".

In the other words, the system is said to be observable as long as the calculated Jacobian linearisation matrix is square matrix and invertible (Drakunov, 1992).

However, the sufficient condition for the error dynamics $\dot{e_1}$ to reach $e_1 = 0$ sliding surface in finite time is when $m_i(\hat{x}) \geq |h_{i+i}(x(t))|$ beside that when it comes to the sliding mode observer with an input, additional conditions are necessary for the observation error being independent of that input. The observer then

$$\dot{\hat{x}} = (J(\hat{x}))^{-1} + \beta(\hat{x})\ sign\,(V(t) - H(\hat{x})) + \ B(\hat{x})\,u \tag{3.27}$$

Slotine in (Slotine et al., 1986a) simplified the observer structure to reduced-order observer in companion form for non-linear system with modified sufficient condition in terms of single measured state (output) as

$$\dot{\hat{x}}_n = -\alpha_n\,\tilde{x}_1 + f(x) - \beta_n\,sign(\tilde{x}_1) + B(\hat{x})u \tag{3.28}$$

with a condition of $K_{n+1}/K_n \geq a$ and the value of a should be positive i.e. $a \geq 0$ to place all the poles in left-side of s-plane.

In the same way, the reduced-order sliding mode observer for magnetic levitation ball system can be express as

$$\begin{aligned} \dot{\hat{x}}_1 &= f_1 - \alpha_1\,\tilde{x}_1 - \beta_1\,sign\,(\tilde{x}_1) \\ \dot{\hat{x}}_2 &= f_2 - \alpha_2\,\tilde{x}_1 - \beta_2\,sign\,(\tilde{x}_1) \\ \dot{\hat{x}}_3 &= f_3 - \alpha_3\,\tilde{x}_1 - \beta_3\,sign\,(\tilde{x}_1) + \tfrac{1}{L}\,u \end{aligned} \tag{3.29}$$

where

$$\begin{aligned} f_1 &= \hat{x}_2 \\ f_2 &= g - \tfrac{c}{m}\left(\tfrac{\hat{x}_3}{\hat{x}_2}\right)^2 \\ f_3 &= \tfrac{R}{L}\,\hat{x}_3 + \tfrac{2\,c}{L}\left(\tfrac{\hat{x}_2\hat{x}_3}{\hat{x}_1^2}\right) \end{aligned} \tag{3.30}$$

and $\tilde{x}_1$ is the estimation error for the estimated state x_1, that is the measured position of the object which can be written as

$$\tilde{x}_1 = \hat{x}_1 - x_1 \tag{3.31}$$

A mathematical representation of signum function can be written as

$$sign(\tilde{x}_1) = \frac{\tilde{x}_1}{|\tilde{x}_1|} = \begin{cases} -1 & |\tilde{x}_1| < 0 \\ 1 & |\tilde{x}_1| > 0 \end{cases} \tag{3.32}$$

3.4.2 Implementation and results of sliding mode observer

In this section, simulation results of the active magnetic levitation system are presented to demonstrate the feasibility of sliding mode observer. The results are split into two main parts. The first part shows the performance of sliding mode observer in terms of estimation of system sates and noise rejection. Then fuzzy sliding mode observer is introduced to improve the trajectory tracking in the presence of the some uncertainties.

Simulations were carried out with same system parameters that shown in subsection 3.3.2.1. For different set-points the initial conditions of the object were set at 18 mm and 14 mm for the system model and the observer respectively. Simulations were obtained using full-order sliding mode observer-based controller for Maglev system via LQR-feedback linearisation to avoid any extra chattering caused by the controller (see Figure 3.11).

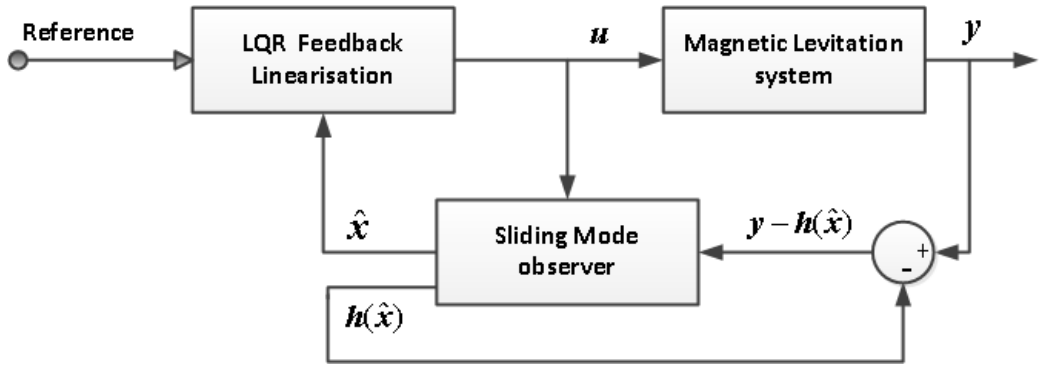

Figure 3.11: Full-order sliding mode observer-based controller for Maglev system via LQR-feedback linearisation

To verify the robustness of the observer, measurement noise was introduced using Gaussian noise generator in Matlab Simulink with zero mean value and covariance of c(.) and sampling time Ts(.) in second.

Consider a third order Maglev system with single measurement, that is the position of the object, which is corrupted by noise $\xi = \xi(t)$. In these results, the conventional sign

function in equation (3.29), $sign\,(\tilde{x}_1)$, can be replaced by the saturation boundary layer function to achieve decrease in switching and discontinuous action in the control loop (Utkin et al., 2009). The saturation function can be expressed as

$$sat(\tilde{x}_1) = \frac{\tilde{x}_1}{|\tilde{x}_1| + \phi} = \begin{cases} \frac{\tilde{x}_1}{\phi} & \left|\frac{\tilde{x}_1}{\phi}\right| \leq 1 \\ sign\left(\frac{\tilde{x}_1}{\phi}\right) & \left|\frac{\tilde{x}_1}{\phi}\right| > 1 \end{cases} \tag{3.33}$$

i.e. for large value of ϕ, $sat(\tilde{x}_1) = sign(\tilde{x}_1)$. However, around the origin with small ϕ-vicinity, the boundary layer is continuous i.e. $sat(\tilde{x}_1) \neq sign(\tilde{x}_1)$. Equation (3.29) can be rewritten as

$$\begin{aligned} \dot{\hat{x}}_1 &= f_1 - \alpha_1\,(\tilde{x}_1 + \xi) - \beta_1\, sat\,(\tilde{x}_1 + \xi) \\ \dot{\hat{x}}_2 &= f_2 - \alpha_2\,(\tilde{x}_1 + \xi) - \beta_2\, sat\,(\tilde{x}_1 + \xi) \\ \dot{\hat{x}}_3 &= f_3 - \alpha_3\,(\tilde{x}_1 + \xi) - \beta_3\, sat\,(\tilde{x}_1 + \xi) + \tfrac{1}{L}\,u \end{aligned} \tag{3.34}$$

The presence of the term $\tilde{x}_1 + \xi$ would involve fairly stochastic analysis. However, useful insight can be obtained by using appropriate approximation, that is assuming ξ is deterministic signal with bounded spectrum (Slotine et al., 1986b)

$$0 \leq w < w_{-} \quad or \quad F_{\xi}(w) = 0$$

where $F_v(w)$ is the Fourier transform of the noise v

Figures 3.12 to 3.14 show the estimated states $\hat{x_1}$, $\hat{x_2}$ and $\hat{x_3}$versus the position, velocity and current states from simulated non-linear Maglev model, when the system input was step of 0.018 for 2 second then step down to the value of 0.015 for another 2 seconds in presence of mass uncertainty of 10%. Initial conditions of the model were [0.018, 0, 0.9039] whereas the initial conditions for the observer were [0.014, 0, 0.7030].

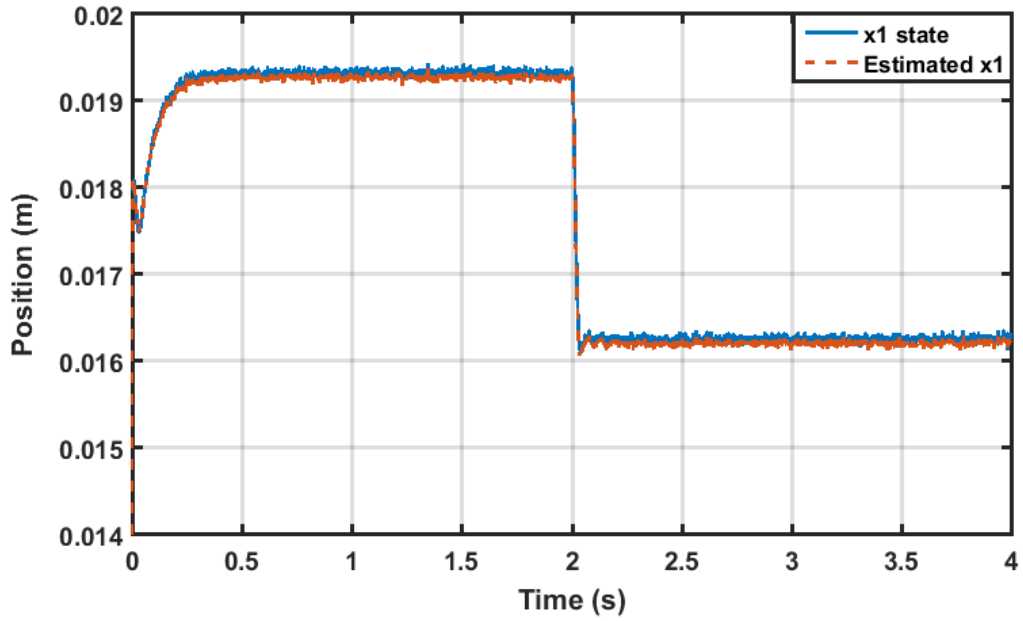

Figure 3.12: Estimated position using full-order sliding mode observer-based controller via LQR-linearisation in presence of mass uncertainty 10%

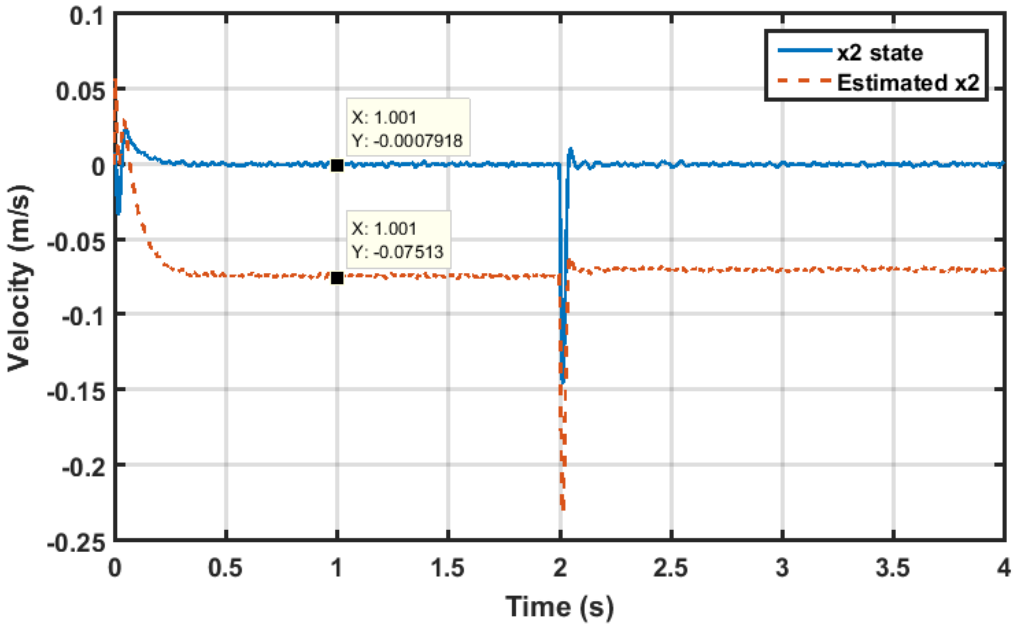

Figure 3.13: Estimated velocity using full-order sliding mode observer-based controller via LQR-linearisation in presence of mass uncertainty 10%

It is noted that relatively good tracking performance for the combined observer has been achieved. The velocity estimation had an estimation error of 0.0739 m/s in steady-state of 10% of mass mismatch whereas in presence of mass uncertainty with the value of 50%, the steady-state estimation error for the velocity increased to be 0.3827 (see Figure

3.15).

Observer gains α_1, α_2 and α_3 were initially tuned using optimization algorithm (Improved spiral Dynamic Algorithm (ISDA)) (Nasir and Tokhi, 2015) to the values of 745.5461, 300 and 597.2114 respectively, and for β_1, β_2 and β_3 gains to 736.2675, 3000 and 299.9370

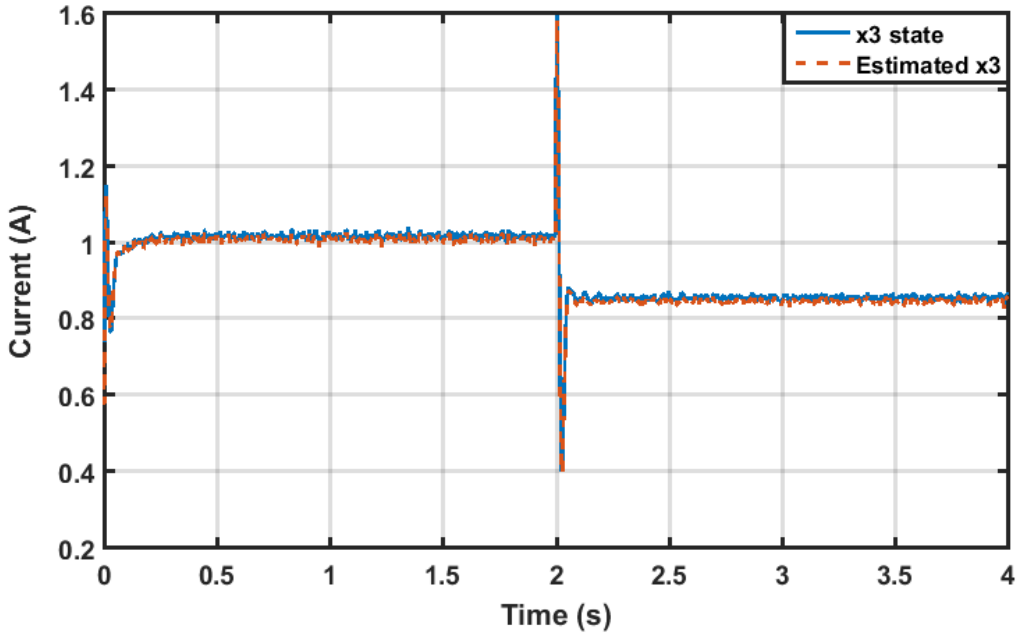

Figure 3.14: Estimated current using full-order sliding mode observer-based controller via LQR-linearisation in presence of mass uncertainty 10%

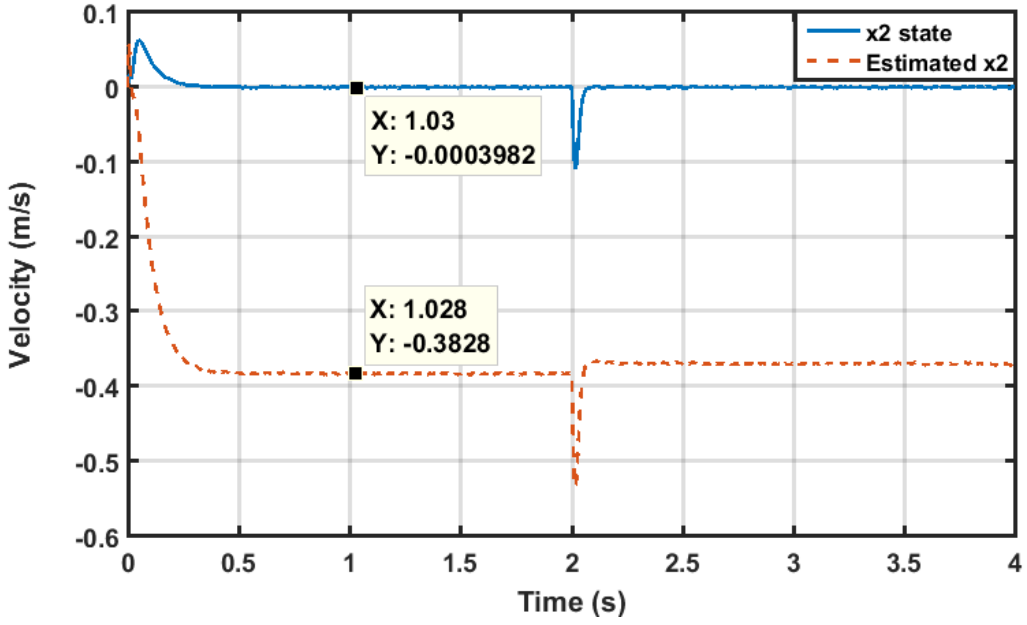

Figure 3.15: Estimated velocity using full-order sliding mode observer-based controller via LQR-linearisation in presence of mass uncertainty 50%

in the mentioned order, the maximum mass uncertainty with this tuning was only 50%. However, the maximum uncertainty increased to 125% just by increasing α_2 to 8500 and β_2 to value of 9000.

If disturbance rejection with zero steady-state error is needed, at the same time to eliminate the estimation error, then integral action must be included in the control law (Alvarez-Ramirez et al., 1998; Werner, 1999). The proposed observer was compared with the observer that was combined with LQi-linearisation as shown in Figure 3.16, in which an integral action was involved in the feedforward path. Figure 3.17 shows a comparison of the tracking of the combined step and ramp reference with different amplitude values for the observer with and without integral action in the presence of 10% mass uncertainty. Sin tracking in the presence of 20% mass uncertainty is shown in Figure 3.18

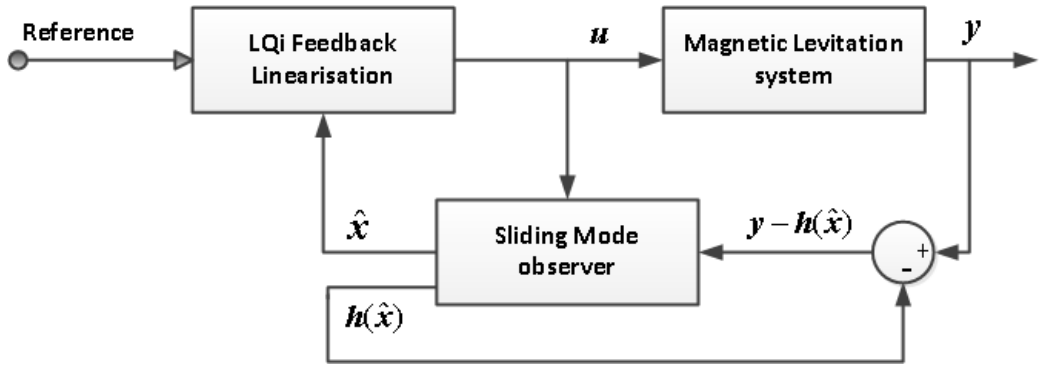

Figure 3.16: Full-order sliding mode observer-based controller for Maglev system via LQi-feedback linearisation

It is noted that integral action eliminated the steady-state error. However, the resultant overshoot for the system with integral action was twice as the system without it, and percentage overshoot of 15% against 7.92%.

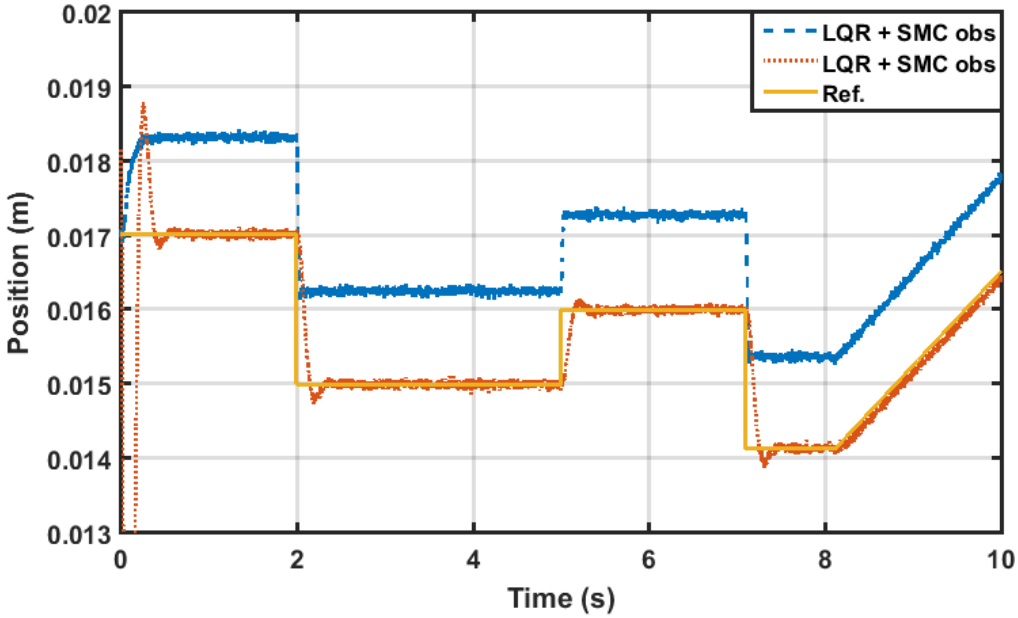

Figure 3.17: System response comparison of the implemented SMC observer with LQR-linearisation versus SMC observer with LQi-linearisation in presence of 10% of mass uncertainty

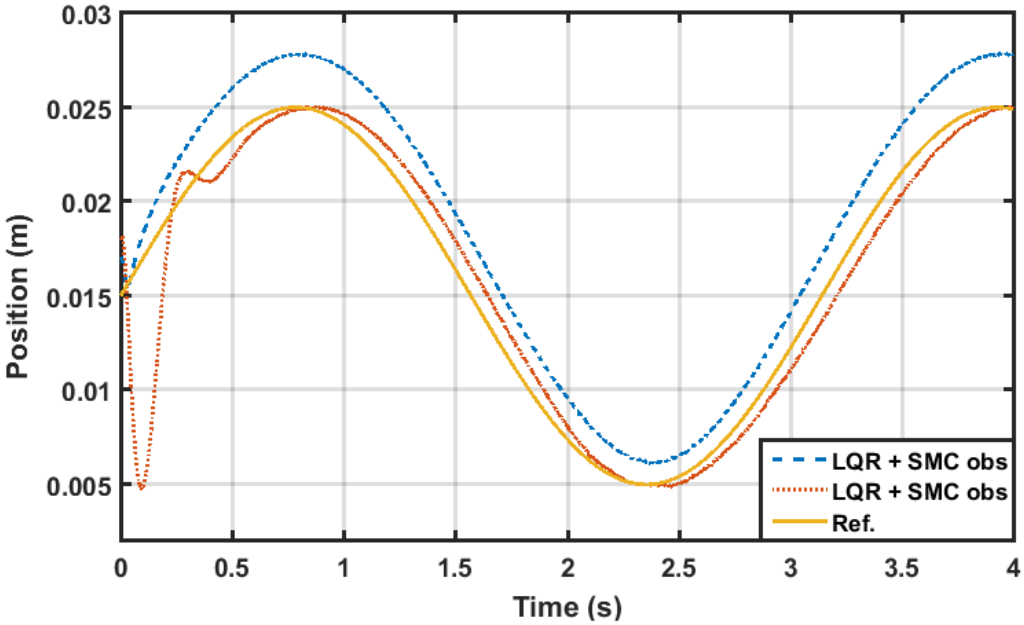

Figure 3.18: Sin response comparison of the implemented SMC observer with LQR-linearisation versus SMC observer with LQi-linearisation in presence of 20% of mass uncertainty

3.5 Fuzzy sliding mode observer

Sliding mode control has become a well-known approach to deal with system parameters mismatch and disturbance because of the concept of equivalent control and sliding mode surface. The use of sliding mode control has been extended to the other control functions apart from stabilization. The approach has been used to construct the state observers. In the literature, the robustness of sliding mode observer with respect to disturbance has been theoretically and experimentally proven. Despite of these advantages of sliding mode control, in general, chattering phenomenon would still be considered a major drawback. Another limitation of using sliding mode observer would be that measurement noise amplification in the state estimation. Fuzzy systems are meant to be employed in a situation of having variation in the system parameters or modelling uncertainties. Hence fuzzy logic should be incorporated with sliding mode control to resolve all restrictions associated with use of sliding mode. In this work, a combination of sliding mode technique and fuzzy singleton-type is proposed.

3.5.1 Fuzzy sliding mode observer design

In this design, the signum function of the proposed sliding mode observer is replaced by fuzzy logic which plays a role in improving the overall performance and the robustness of the resultant observer. To guarantee that the estimated states converge toward the system states, in other words the estimation error tends to zero in finite time and this convergence time should be faster than time constant of system by multiple times, fuzzy rule base is designed in such a way to imitate the needed action from conventional switching function "signum" by reversing fuzzy output to be opposite to the sign of the estimation error to maintain zero estimation error (Firdaus and Tokhi, 2015).

Fuzzy logic structure can be described by four different function blocks, namely Fuzzification, rule- base, inference engine and defuzzification. Figure 3.19 shows the basic structure of fuzzy sliding mode observer. Fizzification is used to map the real data for the estimation error into fuzzy linguistic terms to ensure further fuzzy inferences can be car-

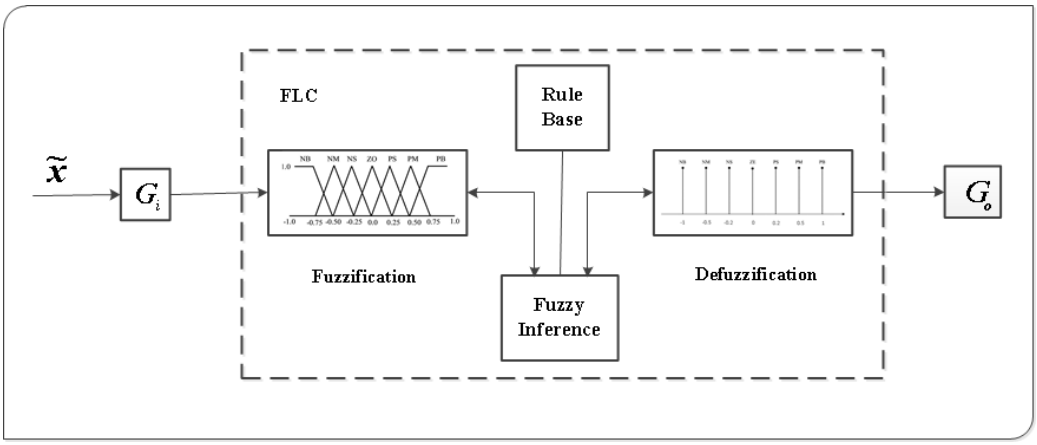

Figure 3.19: Basic structure of fuzzy sliding mode observer

ried out based on the rule-base. The linguistic rules in the rule-base are usually described by fuzzy conditional statements such as

Rule 1: IF $\tilde{x}_1$ is NB, then U_{fo} is PB

Rule 2: IF $\tilde{x}_1$ is NM, then U_{fo} is PM

Rule 3: IF $\tilde{x}_1$ is NS, then U_{fo} is PS

Rule 4: IF $\tilde{x}_1$ is Z, then U_{fo} is Z

Rule 5: IF $\tilde{x}_1$ is PS, then U_{fo} is NS

Rule 6: IF $\tilde{x}_1$ is PM, then U_{fo} is NM

Rule 7: IF $\tilde{x}_1$ is PB, then U_{fo} is NB

The fuzzy linguistic rules are defined here within the range of [-1 , 1] to simplify the notation. Consequently, the actual variations in the input is to be normalized into the interval [-1 , 1] using input scaling factor. Therefore, fuzzy output can be expressed as

$$F_{out} = G_i \, u_{fi} \tag{3.35}$$

where F_{out}, u_{fi} is the fuzzy output and input respectively, G_o (refer to Figure 3.19) is an output amplification factor and G_i is the input scaling factor is to be tuned to ensure that the universe of discourse of the input variable is mapped into unity interval (Chen and Perng, 1994).

A fuzzy set of seven triangular membership functions, namely: Negative Big (NB), Negative Medium (NM), Negative Small (NS), Zero (Z), Positive Small (PS), Positive Medium (PM), and Positive Big (PB) are considered for the input, with the range of [-1, 1] as shown in Figure 3.20.

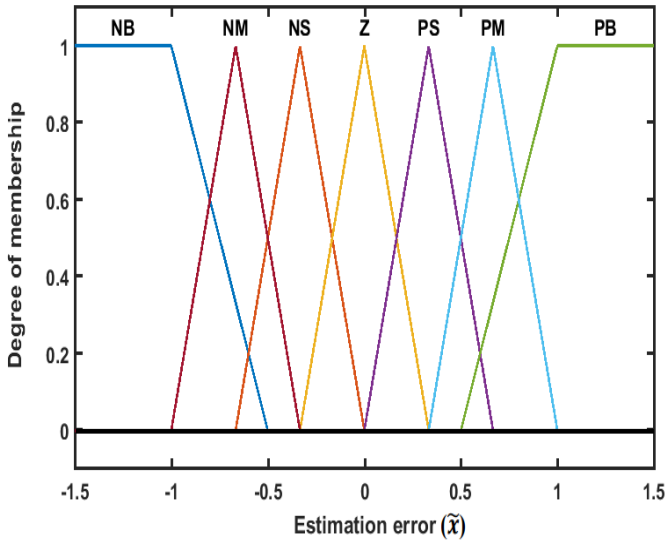

Figure 3.20: Membership functions for fuzzy input 'FU_i'

Triangular Fuzzy Number (TEN) of the membership function used to define a triangular membership can be defined by triple (a_1,a_2 and a_3) with the values of

NB: $a_1 = -\infty$ $a_2 = -1$ $a_3 = -0.5$

NM: $a_1 = -1$ $a_2 = -0.5$ $a_3 = -0.2$

NS: $a_1 = -0.5$ $a_2 = -0.2$ $a_3 = 0$

Z : $a_1 = -0.2$ $a_2 = 0$ $a_3 = 0.2$

PS: $a_1 = 0$ $a_2 = 0.2$ $a_3 = 0.5$

PM: $a_1 = 0.2$ $a_2 = 0.5$ $a_3 = 1$

PB: $a_1 = 0.5$ $a_2 = 1$ $a_3 = \infty$

The output membership is designed using fuzzy singleton method to speed up the estimation process, in which the linguistic variable definition associated with input is the same as the previously defined input. However, the linguistic variable definition for the output was simplified to new form, that is the term set of the output variable is no longer a fuzzy number rather than a crisp value in the base variable space as shown in Figure 3.21.

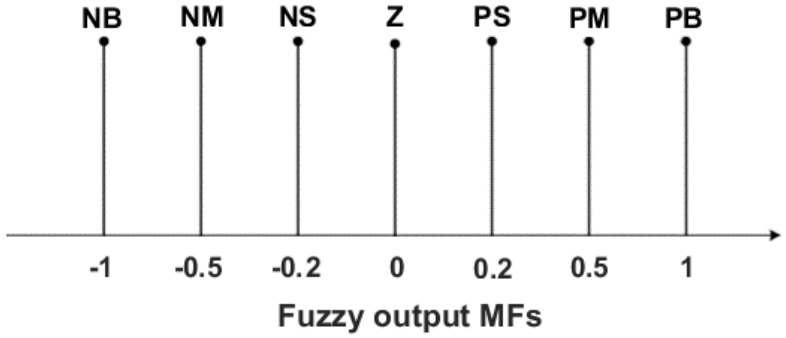

Figure 3.21: Membership functions for fuzzy output 'FU_o' using fuzzy singleton method

The crisp output variable u_{fo} of Fuzzy sliding mode observer (FSMO) using fuzzy singleton method can be calculated by the weighted average defuzzification method as

$$u_{f0} = \frac{\sum_{i=1}^{N} \mu_{Ri}\, u_{fi}}{\sum_{i=1}^{N} \mu_{Ri}} \tag{3.36}$$

where N is the number of the fuzzy set (here N=5), μ_{Ri} is the membership function of i^{th} fuzzy set and u_{f0} is defuzzified value.

3.5.2 Implementation and results of fuzzy sliding mode observer

Computer simulation results are obtained to demonstrate the feasibility of full-order fuzzy sliding mode observer FSMO. This section is divided to two parts where the performance of FSMO is compared with SMO with and without integral action. Firstly, full-order fuzzy sliding mode observer-based controller via LQR-feedback linearisation is compared with Full-order sliding mode observer-based controller via LQR-feedback linearisation, i.e. no integral action is involved in the feedforward path. Figure 3.22 to 3.24 compare the estimation error of step trajectory tracking for full states for both observer assuming no present uncertainty.

It is noted that the performances of both observers were close to each other with little advance to FSMO observer. However, once different mass uncertainty percentages are introduced to the system, the performance of sliding mode observer using boundary layer tended to be better in terms of estimation error compared to FSMO. This because the rate of convergence of SMO using boundary layer is faster than the FSMO. Table 3.3

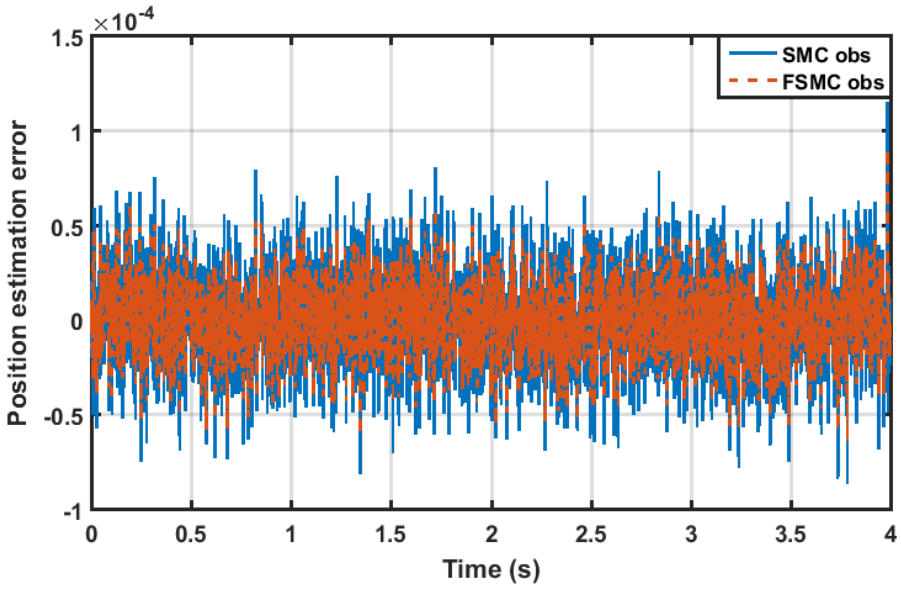

Figure 3.22: Position estimation error of sliding mode observer vs. fuzzy sliding mode observer

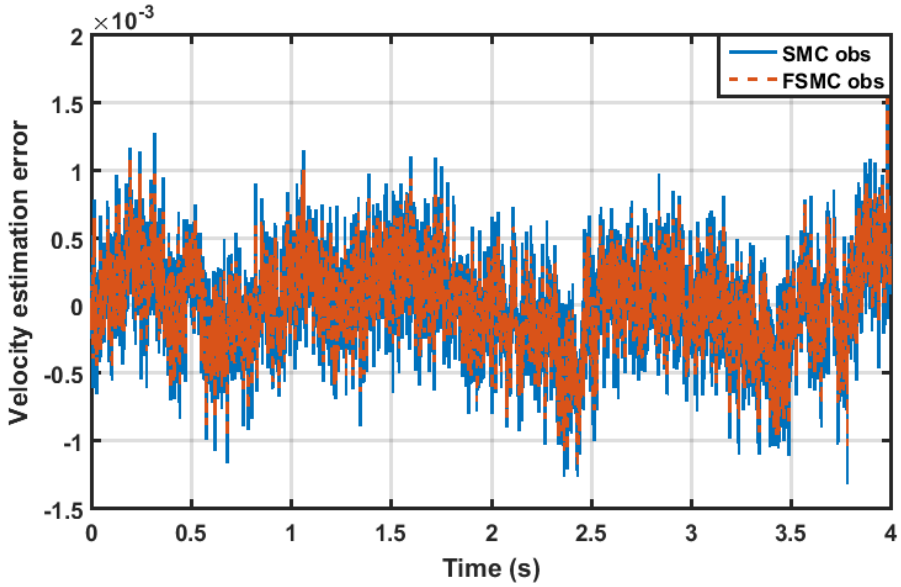

Figure 3.23: Velocity estimation error of sliding mode observer vs. fuzzy sliding mode observer

numerically compares the estimation Integral absolute error (IAE) error of the estimated position of both observers, FSMO and SMO.

The step responses and the control actions with both observers were almost identical, Figures 3.25 and 3.26 compare the corresponding performances and the control actions of FSMO versus SMO , when the input is step of 0.018m for 2s then step down to 0.015m for

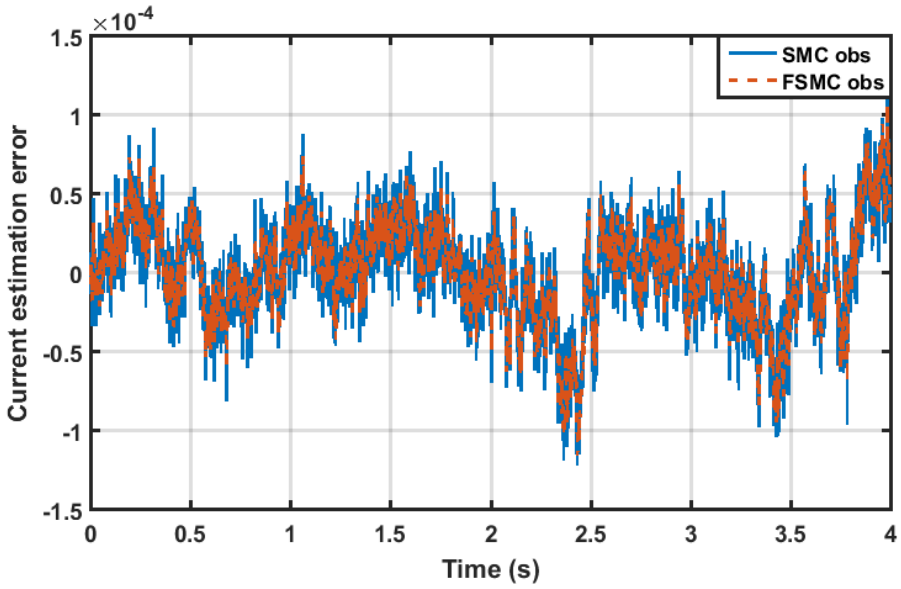

Figure 3.24: Current estimation error of sliding mode observer vs.fuzzy sliding mode observer

the next 2s, in absence of any uncertainty.

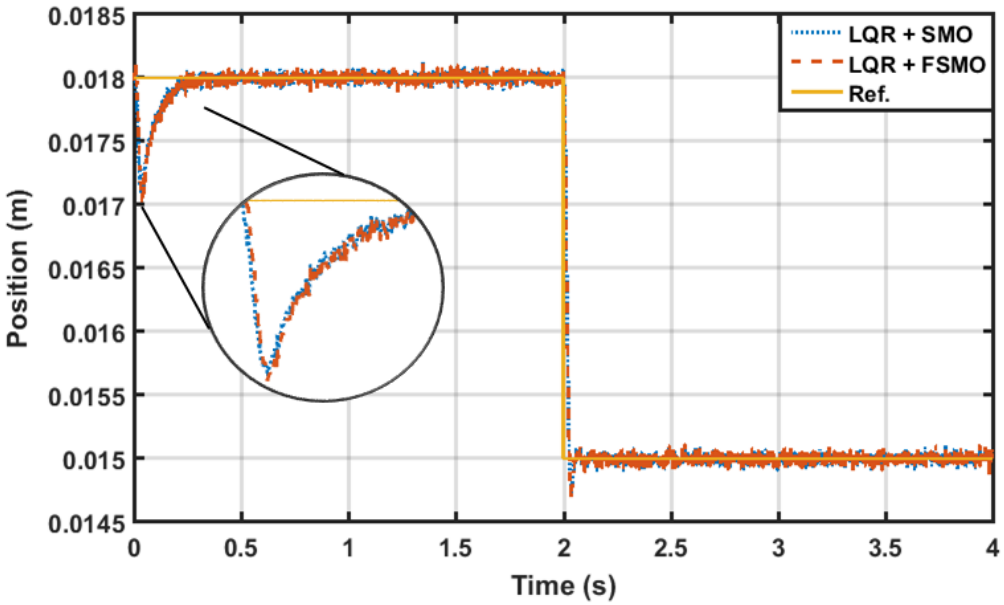

Figure 3.25: Step response comparison between FSMO and SMO without integral action in presence of different percentages of mass uncertainties

Table 3.3: Position estimation IAE comparison between FSMO and SMO without integral action and with different percentages of mass uncertainties

mass uncertainty	IAE error	
(m + %)	FSMO	SMO
10	0.808	0.598
20	1.594	0.792
30	2.408	1.165
40	3.242	1.565
50	4.088	1.971
60	4.945	2.381
70	5.817	2.795
80	6.693	3.217
90	7.580	3.639

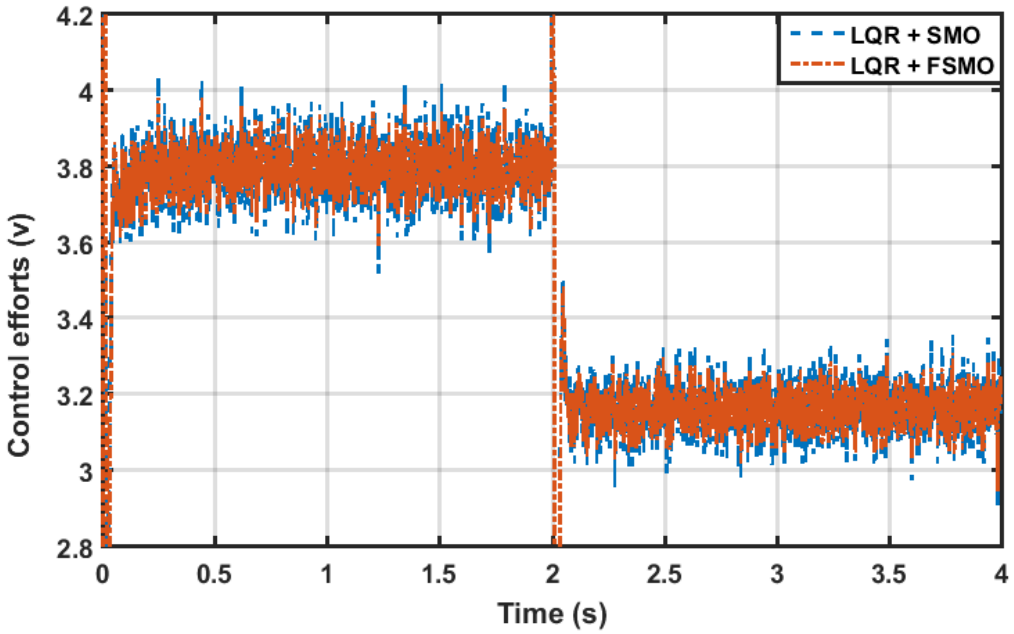

Figure 3.26: Control efforts of FSMO and SMO without integral action and with different percentages of mass uncertainties

On the other hand, once the integral action was implemented to eliminate the steady-state error FSMO provided less estimation error than SMO while combining the observers with LQi-feedback linearisation. Moreover, the maximum mass uncertainty that can be handled by SMO dropped by 30% versus 115% for FSMO. Table 3.4 compares the estimation MSE error of the estimated position, velocity and current of both observers FSMO and SMO with constant input setting at of 0.015m.

Table 3.4: MSE of the estimated position (x_1), velocity (x_2) and current (x_3) for FSMO and SMO with integral action and different percentages of mass uncertainties

mass uncertainty	FSMO			SMO		
(m + %)	x_1	x_2	x_3	x_1	x_2	x_3
0	$2.28 * 10^{-5}$	0.039	0.004	0.014	0.044	0.732
10	$2.31 * 10^{-5}$	0.078	0.008	0.014	0.213	0.753
20	$2.39 * 10^{-5}$	0.127	0.015	0.015	0.415	0.773
30	$2.50 * 10^{-5}$	0.176	0.020	0.015	0.612	0.789
40	$2.70 * 10^{-5}$	0.224	0.03	0.014	0.682	0.775
50	$2.87 * 10^{-5}$	0.271	0.037	-	-	-
60	$2.98 * 10^{-5}$	0.318	0.045	-	-	-
70	$3.02 * 10^{-5}$	0.364	0.054	-	-	-
80	$3.08 * 10^{-5}$	0.409	0.062	-	-	-
90	$3.10 * 10^{-5}$	0.453	0.070	-	-	-
115	$3.54 * 10^{-5}$	0.533	0.094	-	-	-

3.6 Summary

In this chapter, a mathematical non-linear model of highly non-linear unstable Maglev system has been presented in the first part for use in further control design.

In the second and third parts of this chapter, two types of full-order observer, namely non-linear high gain observer and fuzzy sliding mode observer have been designed. Simulation experiments highlight the trade off between the bandwidth and noise- sensitivity, as it should be noticed that increasing value of the linear gain "a" in non-linear observer leads to increasing the high-frequency oscillations due to measurement noise amplification. However, noticeable performance degradation can be noticed when the value of a is smaller than 10.

Furthermore, the simulation results of the siding mode observer and fuzzy sliding mode observer have shown the improvement achieved in the robustness of the observer with fuzzy logic, especially when the integral action is implemented to eliminate the steady-state error. The FSMO can achieve reduced estimation error and can handle larger maximum mass uncertainty compared to SMO.

Chapter 4

LQR-feedback linearisation

4.1 Introduction

Non-linear systems have some features such as multiple isolated equilibrium points, finite escape time and they may exhibit properties such as limit cycle, bifurcation, and chaos. Such properties make non-linear control challenging. As an example finite escape time means that the system output becomes unbounded because one or some of the system states escape to infinity in finite time, which is not the case in a linear system where the system will be unstable when time tends to infinity. Moreover, trajectories of non-linear systems emanate out of an equilibrium point even without perturbation. In contrast, trajectories can reach equilibrium point in finite time (only asymptotically in linear systems).

There are two ways to control a non-linear system. One of these ways is to linearise the system by approximating the non-linear system with a series of linear systems using Taylor series or Jacobian transformation and then apply a linear control technique such as PID, LQR, etc.

The second way to control a non-linear system is to apply a non-linear control method. Again there are two types of methods:

- Techniques that would treat the non-linear system in a limited range of operation as a linear system such as feedback linearisation and gain scheduling.
- Applying direct non-linear control based on Lyapunov stability like sliding mode control, backstepping or non-linear damping.

In this chapter, the indirect non-linear control method is proposed to control highly non-linear Maglev system, where the system is linearised by feeding back the full system state as an input to cancel the non-linearity in the system. Then linear quadratic control is implemented to control the resultant linear system.

4.2 Feedback linearisation scheme

The central idea of the feedback linearisation approach is to cancel the nonlinearity a non-linear system so that the closed-loop dynamics are in (fully or partly) in linear form. Feedback linearisation is achieved by exact feedback and exact state transformations, rather than by linear approximation of the dynamics. Define the transformed states z, for which the equivalent model is in a simpler form, as

$$\begin{bmatrix} z_1 \\ z_2 \\ z_3 \end{bmatrix} = \begin{bmatrix} x_1 \\ x_2 \\ g - \frac{c}{m}\left(\frac{x_3}{x_1}\right)^2 \end{bmatrix} \tag{4.1}$$

To ensure that transformation is invertible, the system states are restricted to $x_1 > 0$ and $x_3 > 0$. In the new coordinates the system equations become

$$\begin{bmatrix} \dot{z}_1 \\ \dot{z}_2 \\ \dot{z}_3 \end{bmatrix} = \begin{bmatrix} z_2 \\ z_3 \\ -\frac{2c}{m}\left(\frac{x_3\dot{x_3}}{x_1^2} - \frac{x_3^2\dot{x_1}}{x_1^3}\right) \end{bmatrix} \tag{4.2}$$

Substituting for $\dot{x}_1$ and $\dot{x}_3$ from equation 3.9 into equation 4.2, yields

$$\begin{bmatrix} \dot{z}_1 \\ \dot{z}_2 \\ \dot{z}_3 \end{bmatrix} = \begin{bmatrix} z_2 \\ z_3 \\ w \end{bmatrix} = \begin{bmatrix} z_2 \\ z_3 \\ \alpha(x) + \beta(x)u \end{bmatrix} \tag{4.3}$$

where

$$\left.\begin{aligned} \alpha(x) &= \frac{2c}{mL}\left(\left(1 - 2\frac{c}{L}\frac{1}{x_1}\right)\frac{x_2 x_3^2}{x_1^3} + \frac{R}{L}\left(\frac{x_3^2}{x_1^2}\right)\right) \\ \beta(x) &= -\frac{2c}{mL}\left(\frac{x_3}{x_1^2}\right) \end{aligned}\right\} \tag{4.4}$$

The nonlinearities can be cancelled by the control law of the from

$$u = \frac{1}{\beta(x)}\left[w - \alpha(x)\right] \tag{4.5}$$

where w is an equivalent input (synthetic control), leading to a linear input-state relation of the form

$$\begin{bmatrix} \dot{z}_1 \\ \dot{z}_2 \\ \dot{z}_3 \end{bmatrix} = \begin{bmatrix} 0 & 1 & 0 \\ 0 & 0 & 1 \\ 0 & 0 & 0 \end{bmatrix} \begin{bmatrix} z_1 \\ z_2 \\ z_3 \end{bmatrix} + \begin{bmatrix} 0 \\ 0 \\ 1 \end{bmatrix} w \tag{4.6}$$

The transformed system using feedback linearisation can be expressed in state variable form as

$$\dot{z}(t) = A\, z(t) + B\, w(t) \tag{4.7}$$

Before proceeding to design the controller, the new transformed system needs to be verified that it is controllable. Satisfaction of this property means that the states of the system can be driven anywhere in finite time as desired. Rank of the controllability matrix

$\begin{bmatrix} A & AB & A^2B \end{bmatrix}_{(3\times3)}$ = (number of states).

The controller makes use of the states of the transformed system z and the reference input r to produce the command for the process through its new command input w which can be written as

$$w(t) = -K\, z(t) + K_r\, r \tag{4.8}$$

here K is the gain vector to be designed using LQR, K_r is the feed-forward gain and r is the reference input.

4.3 Full state feedback control

The stability of the new dynamics can be achieved using a linear state feedback control law that achieves the given requirements.

$$w(t) = -K\, z(t) \tag{4.9}$$

In this research, linear quadratic regulation method is used to determine full state-feedback control gain matrix K, by seeking to minimize a cost function J

$$J(z) := \min_{w(.)} = \int_0^\infty z^T Q_z\, z(t) + w^T Q_w\, w(t)\, dt \tag{4.10}$$

subject to the constrains

$$\dot{z}(t) = A\, z(t) + B\, w(t) \qquad \forall z(0) = z_0 \tag{4.11}$$

where $Q_z(3 \times 3)$ and $Q_w(1 \times 1)$ are typically positive semi-definite and positive definite matrices respectively. Tuning these parameters will balance the relative importance between the control accuracy versus effort. The solution to the LQR problem is a linear

control law of the form:

$$w(t) = -Q_w^{-1}\, B^T P\, z(t) \tag{4.12}$$

where P is a positive definite matrix which satisfies the algebraic Riccati equation

$$PA + A^T P - P\, B\, Q_w^{-1} B^T P + Q_z = 0 \tag{4.13}$$

Thus, the LQR method is used for determining the optimal state-feedback control matrix '$K = Q_w^{-1}\, B^T P$' to allocate the eigenvalues of the closed-loop system $\lambda(A - BK)$ on the left half plane. Since the design of the state feedback matrix K is based on solving the regulator problem (no reference inputs), the stable closed-loop system will reach a steady state to a constant input reference signal but steady state errors may be present.

4.4 Tracking control design

One of most significant advantages of having a controller with two degrees of freedom, where feed-forward and feedback control are combined, is that the control design problem can be split into two parts. The function of feedback control might be meant to provide effective disturbance attenuation and improve overall robustness, whereas the function of the feed-forward may be independently designed to obtain the desired response to the reference and also to reduce the effects of measured disturbance (see Figure 4.1).

Feed-forward is a powerful technique that simply complements the feedback control in presence of a reference input. This tracking control design can be used to reduce the impact of the measured disturbance as well as improving the response to reference signal.

4.4.1 Static feed-forward gain

Combination of feedback and feed-forward is considered as one of the major advantage of modern control with two degrees of freedom, with which the control actions can be split into feedback $F_b(t)$ that can reduce the effect of disturbance and maintain system

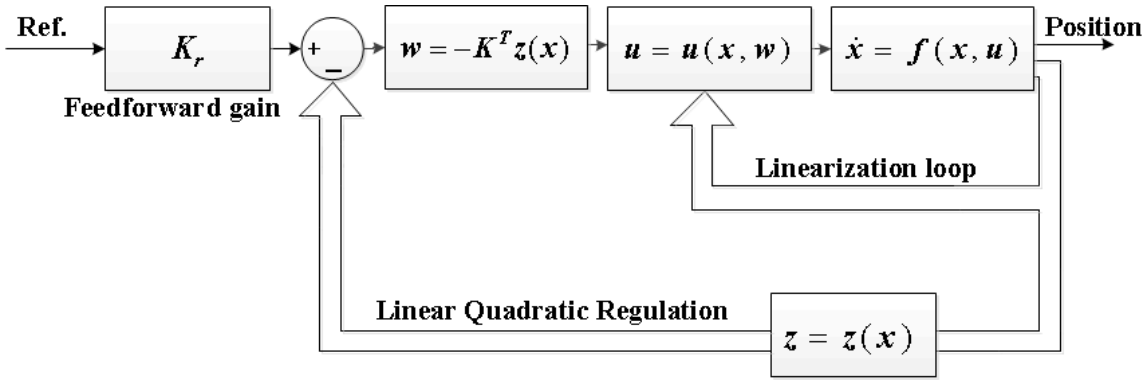

Figure 4.1: Simulation scheme for control of the non-linear model of the Magnetic levitation using exact input-state feedback linearisation

robustness, and feed-forward $F_f(t)$ which can be independently designed to overcome the measured disturbances and improve tracking control.

Feedforward gain does not affect the stability of the system, which is completely determined by the eigenvalues of $\lambda\,(A - B\,K)$ but it has only an effect on the steady state solution. Hence a scalar feedforward gain K_r is introduced to track the reference signal and to remove the steady state error. The transformed closed-loop system equations can be written as

$$\dot{z}(t) = (A - BK)\,z(t) + B\,K_r\,r(t) \tag{4.14}$$

Particularly, the equilibrium point (i.e no change in the system dynamics that is when $\dot{z}(t)$) and steady-state output for the asymptotically stable closed loop system are given as

$$z_e = -(A - B\,K)^{-1} B\,K_r\,r \tag{4.15a}$$

and

$$y_{r,e} = C\,z_e \tag{4.15b}$$

Thus for zero steady state tacking error K_r should be chosen such that $y_{r,e} = r$ (the desired

output value). Solving equations (4.15a) and (4.15b) for scalar gain K_r yields

$$K_r = -1/(C(A - B\,K)^{-1}B) \tag{4.16}$$

4.4.2 Feed-forward control with integral action "LQi"

In this section, the modification of feed-forward control using static gain is described. The new algorithm combining both integral action and feed-forward gain are described in the next stage. LQR is considered as a proportional state feedback control technique in which the controller does not have an integral action. This implies that the steady state error is not zero when the system is subjected to a disturbance. Hence, in case of having disturbance or if nonzero reference are expected the control law of proportional feedback is a consequence of LQ problem formulation. Recall the equations of disturbance free plant where the system is linearised using feedback linearisation described by equation 4.11:

$$\dot{z}(t) = A\,z(t) + B\,w(t)$$

This structure is modified in a way so that the resultant controller can deal with the unwanted disturbance. The basic idea is to augment the state vector with a new state 'i' to describe the integral of the difference between the set-point and the measured output as

$$\frac{d}{dt}\begin{bmatrix} z \\ i \end{bmatrix} = \begin{bmatrix} A\,z + B\,w \\ r - y_{r,e} \end{bmatrix} = \begin{bmatrix} A\,z + B\,w \\ r - C\,z_e \end{bmatrix} \tag{4.17}$$

Thus the new representation of the overall plant can be rewritten with the augmented state-space as

$$\frac{d}{dt}\begin{bmatrix} z \\ i \end{bmatrix} = \begin{bmatrix} A & 0 \\ -C & 0 \end{bmatrix}\begin{bmatrix} z \\ i \end{bmatrix} + \begin{bmatrix} B \\ 0 \end{bmatrix} w + \begin{bmatrix} 0 \\ I \end{bmatrix} r \tag{4.18}$$

where the augmented state matrix and input vector are respectively represented by

$$A_{aug} = \begin{bmatrix} A & 0 \\ -C & 0 \end{bmatrix} \quad \text{and} \quad B_{aug} = \begin{bmatrix} B \\ 0 \end{bmatrix} \tag{4.19}$$

with the control law:

$$w = -\begin{bmatrix} K & -K_i \end{bmatrix} \begin{bmatrix} z \\ i \end{bmatrix} + K_r\, r \tag{4.20}$$

or it can be expressed in such form as

$$w = -K_{aug}\, z_{aug} + K_r\, r \tag{4.21}$$

thus the overall closed-loop system can be written as follows:

$$\frac{d}{dt}\begin{bmatrix} z \\ i \end{bmatrix} = (A_{aug} - B_{aug}) * \begin{bmatrix} K & -K_i \end{bmatrix} \begin{bmatrix} z \\ i \end{bmatrix} + \begin{bmatrix} B\, K_r \\ I \end{bmatrix} * r \tag{4.22}$$

The controller needs to be designed so that the poles of the closed-loop are chosen for the system to be stable, i.e the real part of the eigenvalues of the augmented state matrix 'A_{aug}' must be negative. The block diagram of closed-loop system with integral control is shown in Figure 4.2.

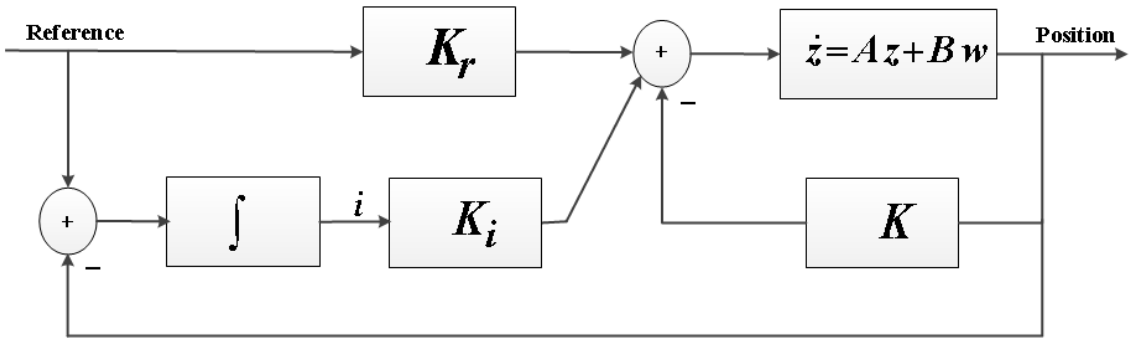

Figure 4.2: Block diagram of the closed-loop system with integral control

4.5 Implementation and results

This section presents simulation results assessing the performance of the proposed controllers. Two types of tests are presented in this section. Firstly, the optimal control based LQR-feedback linearisation for magnetic levitation using static feed-forward gain in section 4.4.1. Then feedback linearisation with integral action in the feed-forward scheme in section 4.4.2.

4.5.1 LQR-feedback linearisation

The simulation results are obtained from the algorithm coded in MATLAB 2015b in Simulink. Using personal computer (PC) with the specifications of processor CPU Intel (R) core (TM) i5-2400 and RAM of 8.00 GB and Windows 7 professional operation system.

Firstly, The non-linear model of magnetic levitation and controller design are simulated in Simulink and the without observer, i.e feedback the states from the model assuming all the states are measurable as shown in Figure 4.3 .

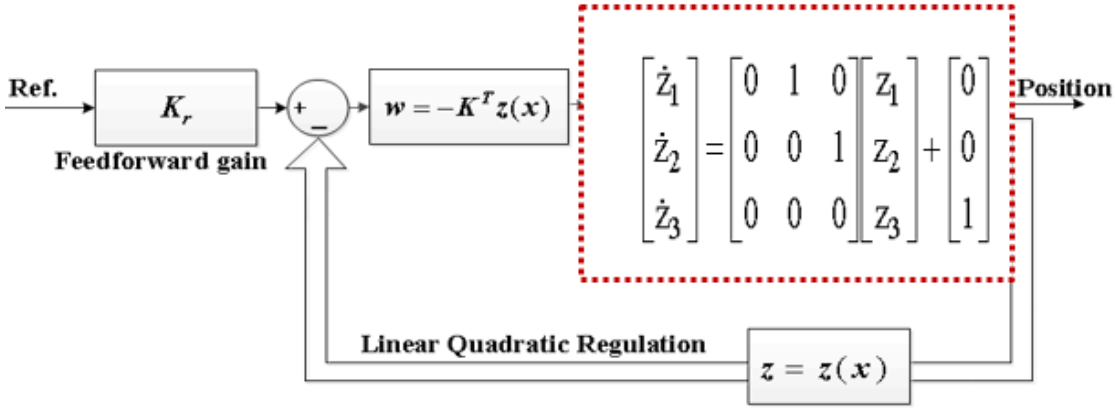

Figure 4.3: LQR-feedback linearisation plus feed-forward gain

LQR minimizes a performance index (i.e. quadratic cost function) which mainly has two penalty matrices: state weighting matrix Q_z and control weighting matrix Q_w.Both of these parameters greatly influence the performance of the LQR controller. However, it is not a trivial task to tune those two matrices.

Initially the weights of the LQR are assumed as Q_w=1 and $Q_z = C^T * C$ and since it

is position control based, the output vector can be written as $C = \begin{bmatrix} 1 & 0 & 0 \end{bmatrix}$

$$Q_z = C^T * C = \begin{bmatrix} 1 \\ 0 \\ 0 \end{bmatrix} \begin{bmatrix} 1 & 0 & 0 \end{bmatrix} = \begin{bmatrix} 1 & 0 & 0 \\ 0 & 0 & 0 \\ 0 & 0 & 0 \end{bmatrix} \tag{4.23}$$

Hence, the corresponding cost function will pose equal importance on the control effort and to fast convergence of the state variables. This implies to start with $Q_w = 1$ and $Q_z = diag(\ 1 \quad 0 \quad 0\ )$. State feedback gain can be calculated using Matlab command:

$$K = lqr(Sys, Q_z, Q_w)$$

and

$$Sys = ss(A, B, C, 0);$$

where $K(1 \times 3)$ is vector of constant gain for position, velocity and current states respectively. Adjusting these parameters intuitively by trial and error to maintain the smallest possible error between the reference input and the system output for an acceptable control effort, form the initial results of system response and the control effort highlights the range of interest for optimization. As seen in Figure 4.4 the system response with $Q_z = diag(\ 1000 \quad 0 \quad 0\ )$ i.e $Q_{z11} = 1000$ is relatively slow, whereas with Q_{z11} set to the value $1e^5$ would show reasonably fast response. The control effort reached about 25 v and only around 8 v when the control weighting Q_{z11} was set to $1e^{-4}$ and 0.1 respectively as shown in Figure 4.5.

The classic approaches are labour-intensive, time consuming and do not guarantee the expected performance. Furthermore, these techniques only aim to minimize the quadratic performance index and do not consider other control objectives such as minimizing the overshoot, rise time, settling time, and steady state error. Based on aforementioned results, the searching range for both parameters are specified. The state weighting matrix and

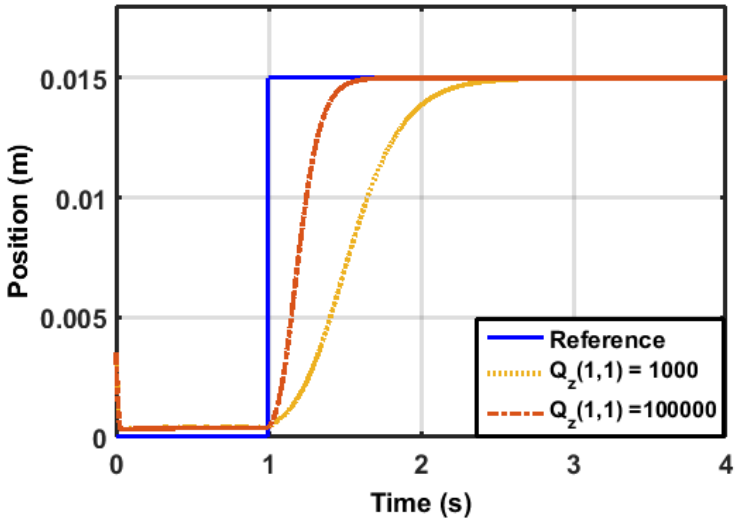

Figure 4.4: System response for different manual setting of state weighting matrix

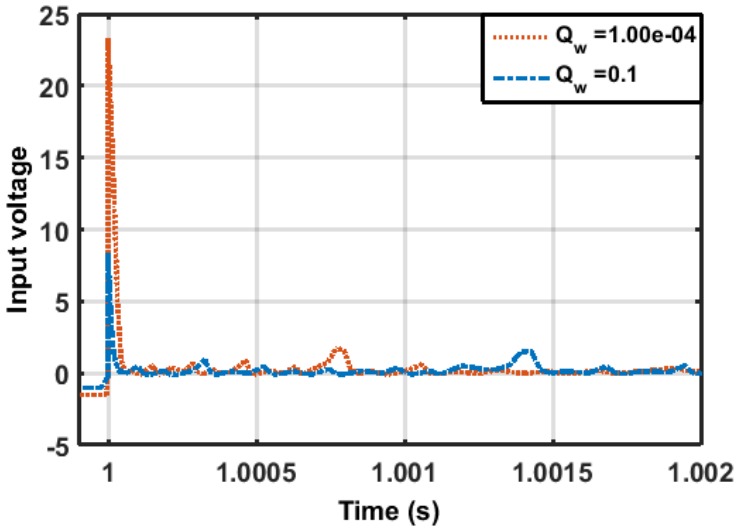

Figure 4.5: Control effort for different settings of control weighting matrix

control weighting matrix are refined as $Q_z = diag(\ 9.31 \times 10^4 \quad 0.7287 \quad 0.7378\ )$ and $Q_w = 6.34 \times 10^{-4}$ using the improved spiral dynamic algorithm (ISDA) (Nasir and Tokhi, 2015) to obtain a satisfactory performance (see Figures 4.6 and 4.7).

Further results were obtained using the proposed non-linear observer (HGO) with LQR-feedback linearisation with static gain (shown in Figure 4.8), as previous results were based on the assumption that all the states were available for the optimal controller. However, this is not the case since the only measurement available is the position of the object.

The linear gain "G" of the proposed observer was calculated according to the formula

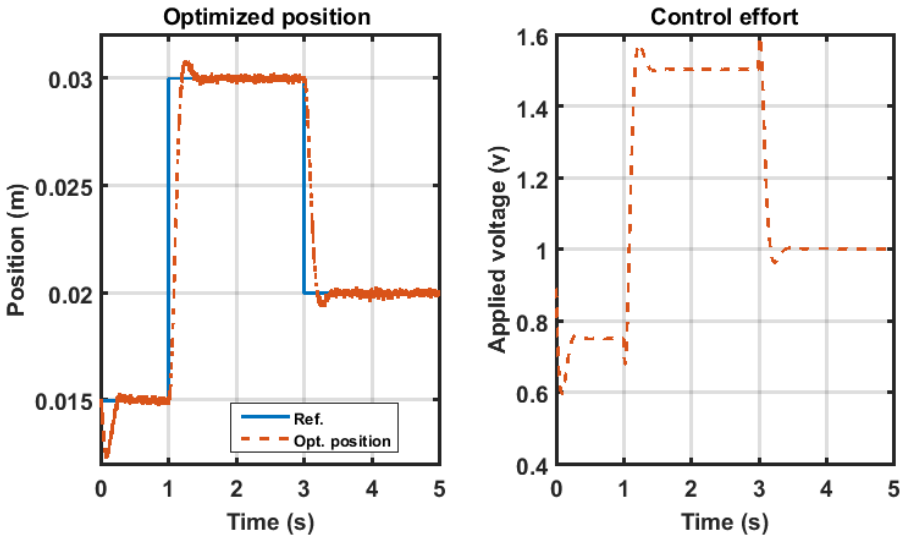

Figure 4.6: Optimized controlled position and the control effort using ISDA with step input

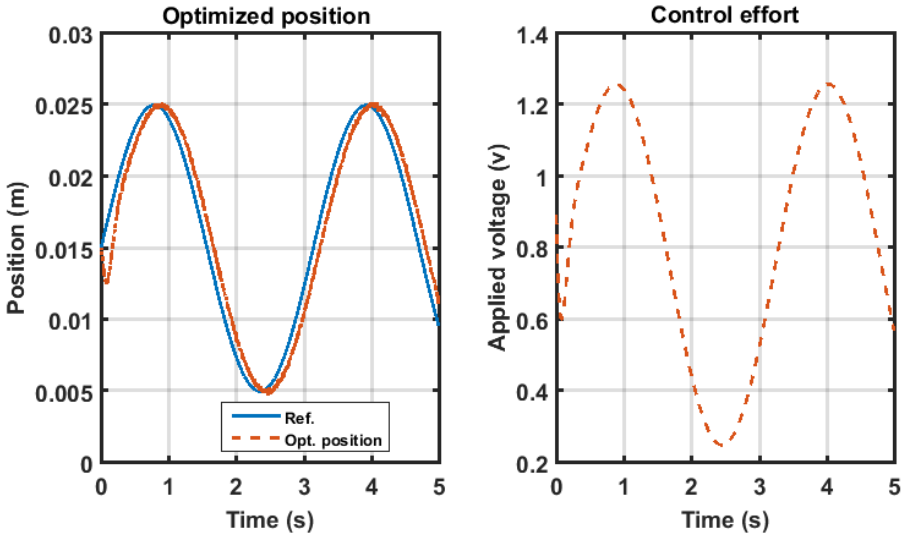

Figure 4.7: Optimized controlled position and the control effort using ISDA with sine input

that was used in (Baranowski and Piatek, 2008; Khalil, 2008; Khalil and Praly, 2014) in the form of

$$G = \begin{bmatrix} G_1 \\ G_2 \\ G_3 \end{bmatrix} = \begin{bmatrix} \frac{3\,a}{\epsilon} \\ \frac{3\,a^2}{\epsilon} \\ \frac{a^3}{\epsilon} \end{bmatrix} \tag{4.24}$$

where $G_1 = 3a$, $G_2 = 3a^2$, $G_3 = a^3$ and $\epsilon \in (0, 1]$, a is a tuning parameter to be tuned to meet the requirements. In this work ϵ has been set within the specified range to the value

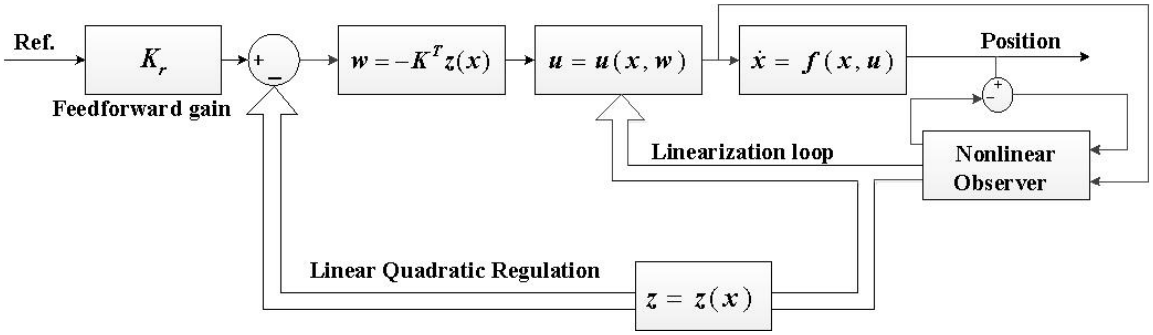

Figure 4.8: State feedback with full-order estimator for Maglev

of 0.5 and a should be at least 10. This results in

$$G = \begin{bmatrix} 6a \\ 12a^2 \\ 8a^3 \end{bmatrix}$$

These gains need to be tuned so that the dynamics of the observer should be faster than the system dynamics "pushing the observer poles further on the left side of S-plane".

At the beginning, the parameters of state weighting matrix Q_z and control weighting matrix Q_w are tuned manually to maintain the smallest possible error taking into account the control effort to be acceptable, and further to have an idea about the optimization range for the tuning parameters for the controller. Figure 4.9 shows the response and control effort of the controlled system with the controller settings of $Qw = 0.0001$ and $Qz = diag(1e5\ 0\ 0)$ (which correspond to the closed-loop poles –31.6228, –15.8114 + 27.3861 i, –15.8114–27.3861 i), the observer parameters a and ϵ set to values of 150 and 0.5 respectively, and the initial conditions set to $x_1(0) = 0.018,\ x_2(0) = 0$ and $x_3(0) = \sqrt{m \times g \times 18 \times 10^{-3}}$ = 0.894.

Further, controller parameters were tuned using (ISDA) algorithm (Nasir and Tokhi, 2015) to obtain a satisfactory performance. Number of search points and maximum iteration number were set to 20 and 50 respectively. Gains for both state weighting matrix of $Qz = diag(V_1\ V_2\ V_3)$ and control weighting matrix of $Qw = V_4$ were distributed within the range after many adjustments and trials as shown in Table 4.1

The best optimum cost function value achieved among many trials was 4.9709×10^{-06}

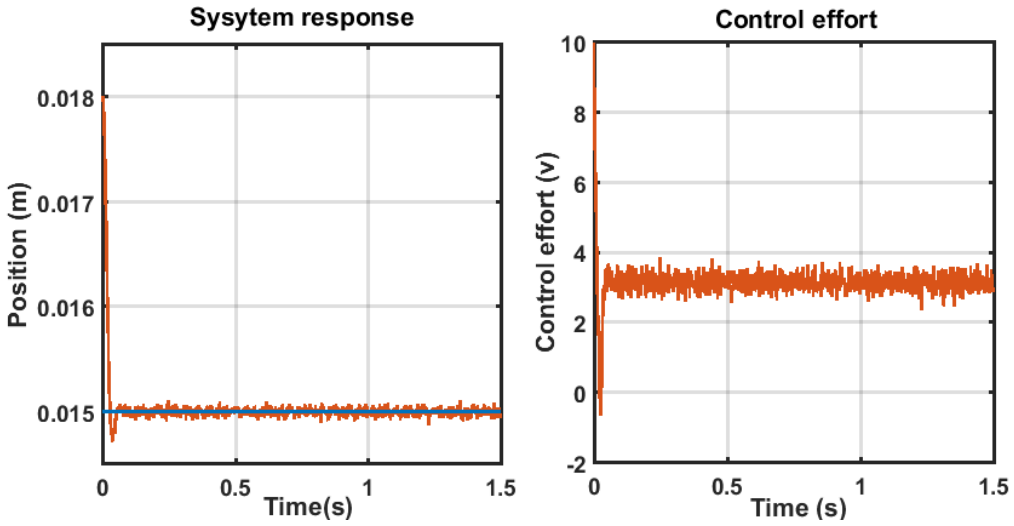

Figure 4.9: System response and control efforts with manual tuned controller

Table 4.1: Optimization range for state and control weighting matrix

Parameter No.	Minimum	Maximum
V1	10^{7}	10^{8}
V2	500	10^{3}
V3	0	10
V4	10^{-4}	10^{-2}

and the optimal gain values were $V_1 = 6.691210^{07}$, $V_2 = 548.7702$, $V_3 = 548.7702$ and $V_4 = 55 \times 10^{-04}$. This results in LQR-feedback gains for the three feedback states as $K_1 = 2.7714 \times 10^{05}$, $K_2 = 8.5622 \times 10^{03}$ and $K_3 = 131.3964$ with the feed-forward gain value equal to $k_r = 2.7714 \times 10^{05}$. The corresponding poles for closed-loop system with these settings are $-65.2696, -33.0634 + 56.1511\,i$, –33.0634–56.1511 i)

There were improvements in terms of system performance as well as the control actions for the controller using the optimised gains compared to the response and control efforts achieved with the manually tuned controller. Table 4.2 highlights some of the performance indices for both controllers. As noted, the position overshoot was reduced further with optimized controller than the manually tuned one. In contrast, the system response was slowed to 3.6 ms instead of 2.8 ms. Figure 4.10 and Figure 4.11 compare the step and sine response for the system with the manually tuned and optimized controllers.

The performance of the system might seem to be not significantly improved. However, the generated control signals from the optimized system were remarkably much smoother

Table 4.2: Performance indices for manual tuned and optimized controller

Performance index	Manual tuning	Optimization
Percentage overshoot (%)	10.5	7.35
Rise time (ms)	**2.8**	**3.6**

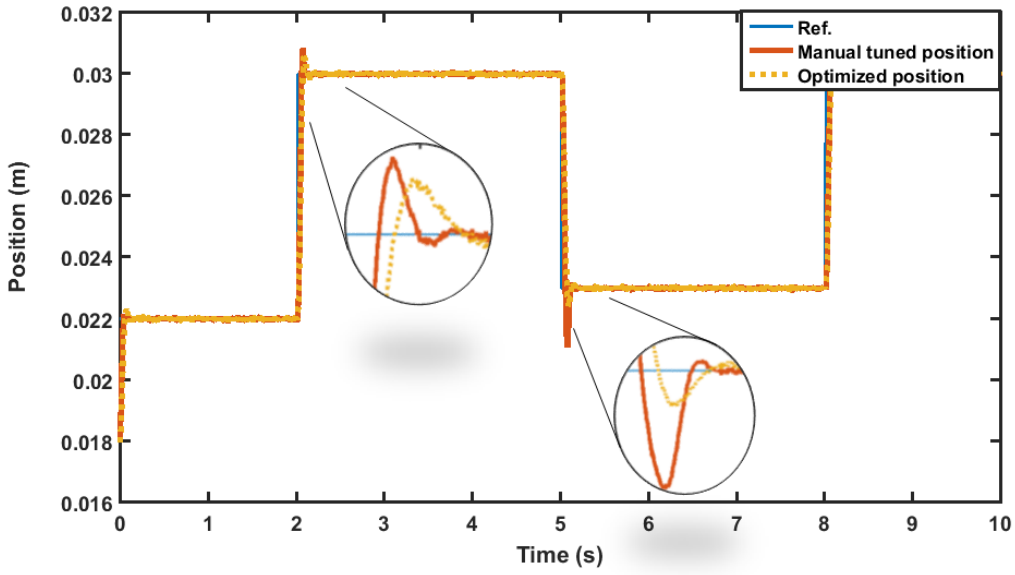

Figure 4.10: Step response comparison between manually tuned and optimised LQR-feedback controllers

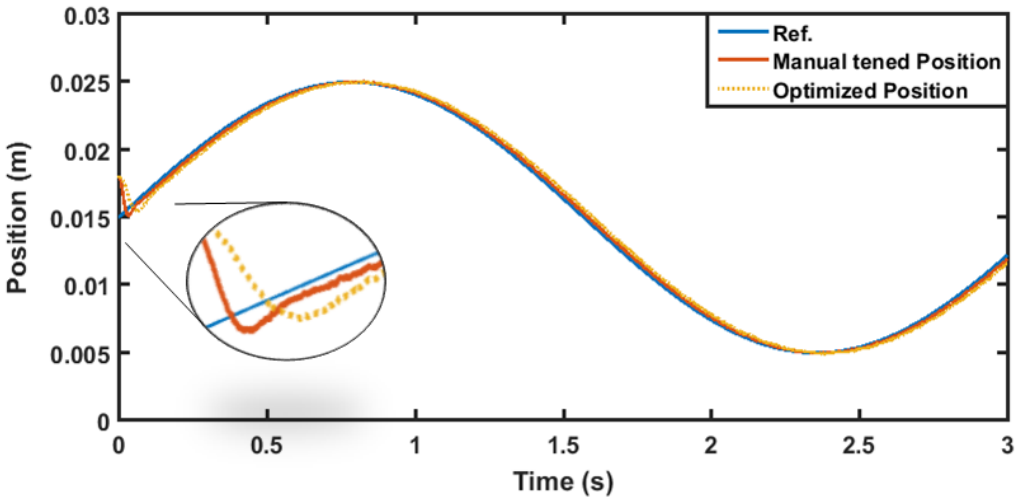

Figure 4.11: Sine response comparison between manually tuned and optimised LQR-feedback controllers

than those with the manually tuned controller as depicted in Figures 4.12 and 4.13

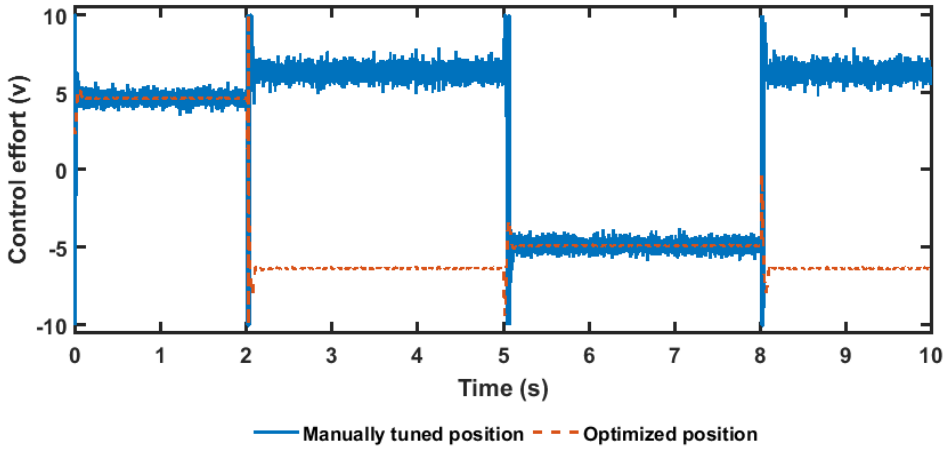

Figure 4.12: Step control actions comparison between manually tuned and optimised LQR-feedback controllers

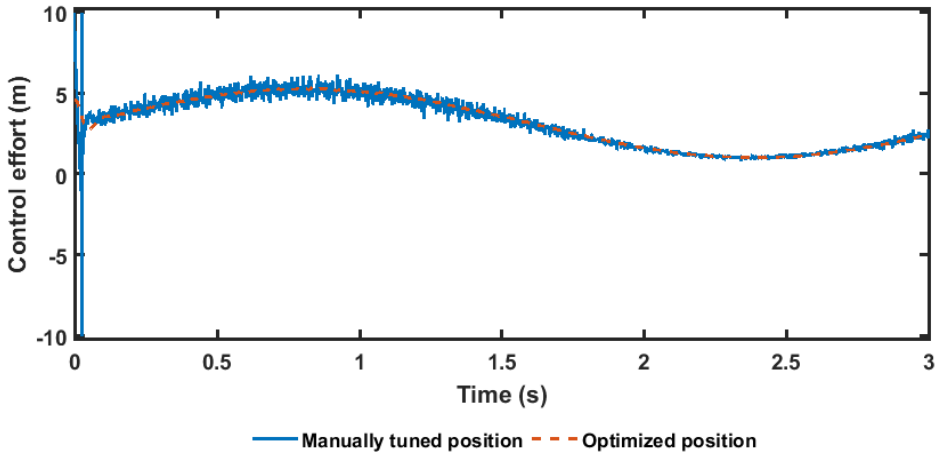

Figure 4.13: Sine control actions comparison between manually tuned and optimised LQR-feedback controllers

Finally, both controllers were tested for robustness in the presence of mass uncertainty in percentage values of 5,10, 20, 50 and 80 % so that the mass value in the mathematical model of the system was higher than the one used in controller and observer designs.

For a comparative assessment, integral of absolute error over time was used, where the error is the difference between the set-point and the measured output (feedback signal). IAE can be calculated using the equation:

$$\text{IAE} = \int^{t} |e(t)|\, dt \tag{4.25}$$

Table 4.3 presents an IAE error comparison between the given controllers with constant input of 0.015. As noted, IAE values with 10% mass mismatch were relatively low. Closer inspection of the table shows that the response improved moderately especially when mass uncertainty was increased to 80% as IAE error was just about 9.5 for the optimized controller whereas it was around 61 for manually tuned controller.

Sample of simulation results with 50 and 80% mismatch are shown in Figures 4.14 and 4.15 comparing the robustness of manual tuned controller with optimized controller using (ISDA) (Nasir and Tokhi, 2015). The single most striking observation to emerge from the performance comparison was the response from both controllers has steady-state error and this error increased with percent uncertainty.

Table 4.3: Mass uncertainty versus IAE error of LQR-feedback linearisation with different tuned gains

mass uncertainty	IAE error	
(m + %)	initial gains	optimized gains
10	**5.9331**	**7.5241**
20	10.0165	7.7168
30	8.3709	7.9838
50	10.6649	8.5557
80	60.8029	9.5957

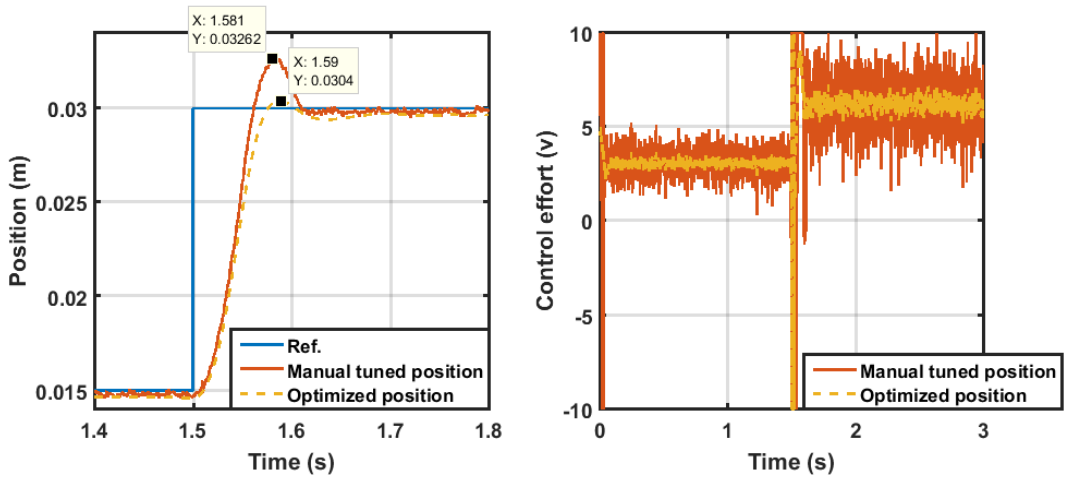

Figure 4.14: System response and control efforts with mass uncertainty of 50 % for both manual and optimized tuned controller

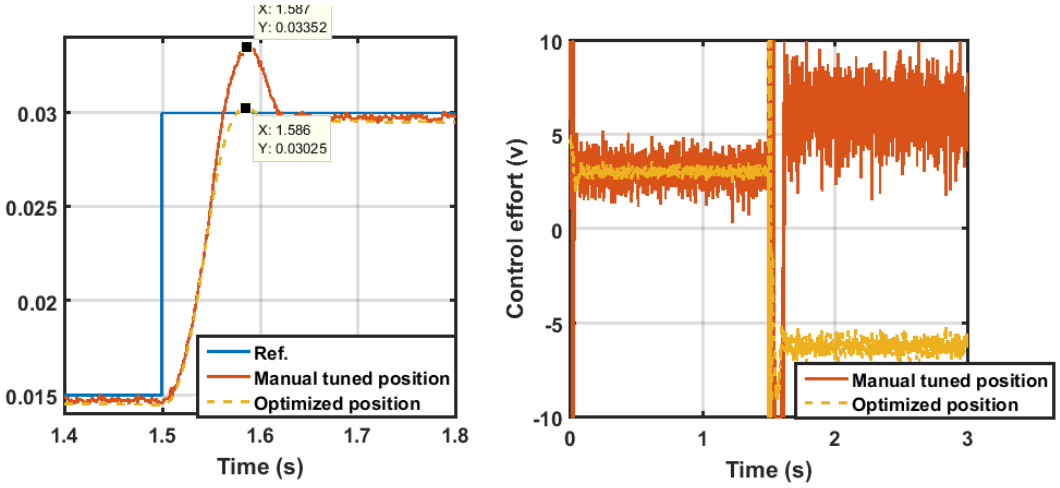

Figure 4.15: System response and control efforts with mass uncertainty of 80 % for both manual and optimized tuned controller

4.5.2 LQi-feedback linearisation

In addition to non-linearity feature of the Maglev system, any change in the operating condition would introduce additional modelling errors. That is why from a design point of view it is important to be able to measure the robust properties of the closed-loop system. In this section an integral control action is included to remove the steady-state error in case of parameters mismatch, subsequently improving the robustness of the proposed controller.

Consider the augmented system with an integral control action in terms of augmented states matrix 'A_{aug}' and input vector 'B_{aug}' as expressed in equation 4.22. Experimentally it can be constructed using a script command in Matlab as

$$Sys_1 = ss(A_{aug}, B_{aug}, C_{aug}, 0)$$

Then the augmented gains vector 'K_{aug}' can be calculated by running the Matlab command

$$K_{aug} = lqi(Sys_1, Q_{zaug}, Q_w)$$

where $Q_{zaug} = diag([V1, V2, V3, V4])$ and V is gains vector that was used to regulate the deviation in the trajectories of the state variable (z(t)), whereas Q_w is to penalize the input signal. k_i can be obtained from $K_{aug}(1 \times 4) = [K \; -k_i]$ as the fourth element in the

vector;

$$k_i = -K_{aug}(1, 4)$$

For a step signal with initial value of 0.033 m, then step down to 0.02, finally to the value of 0.015 m and step time of 10 s, initial conditions for both controller and non-linear observer were fixed to the values of 0.018 m for position with the corresponding current of 0.9039 A, and the initial velocity was set to zero. Three of the best optimized controller "Opt 1, Opt 2 and Opt 3" were tested in terms of tracking the prescribed trajectory and control actions. The optimized gains for both state weighting matrix of $Qz = diag(V_1\ V_2\ V_3 V_4)$ and control weighting matrix $Qw = V_5$ are as shown in Table 4.4

Table 4.4: Optimization gains for state and control weighting matrix

Parameter No.	**Opt 1**	**Opt 2**	**Opt 3**
V1	6.72×10^6	2.71×10^6	2.71×10^5
V2	2.32×10^4	10^5	6900
V3	9.67×10^3	0	0
V4	1.61×10^9	4.43×10^9	3.77×10^8
V5	0.0061	9×10^{-4}	9×10^{-6}

Figure 4.16 shows that the performance of Opt 2 and Opt 3 were close to each other. However, the control effort provided by Opt 2 was much smoother than those with Opt 1 and Opt 3, see Figure 4.17).

The results are summarized in Table 4.5, in which a comparison between the performance indices for optimization results 2 and 3, whereas Opt 1 results are excluded because of slow response and a very noisy control action.

Table 4.5: Performance indices for Opt 2 and Opt 3

Performance index	Opt 2	Opt 3
Percentage overshoot (%)	**3.266**	**3.266**
Peak time (s)	1.187	1.302
Rise time (s)	0.086	0.146
Settling time (s)	0.143	0.214

Sample of simulation results for step response with 30 mismatch and 50% mismatch

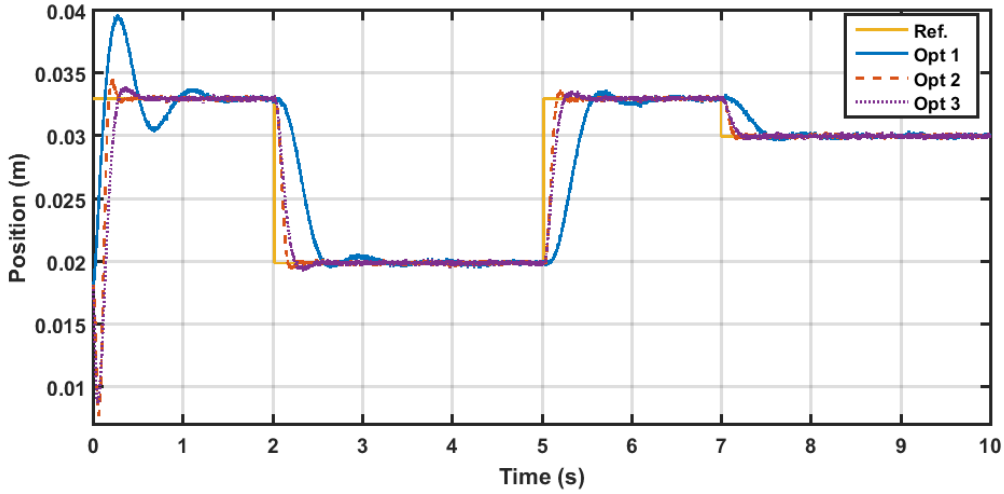

Figure 4.16: System response of the proposed controller LQi for Opt 1, Opt 2 and Opt 3

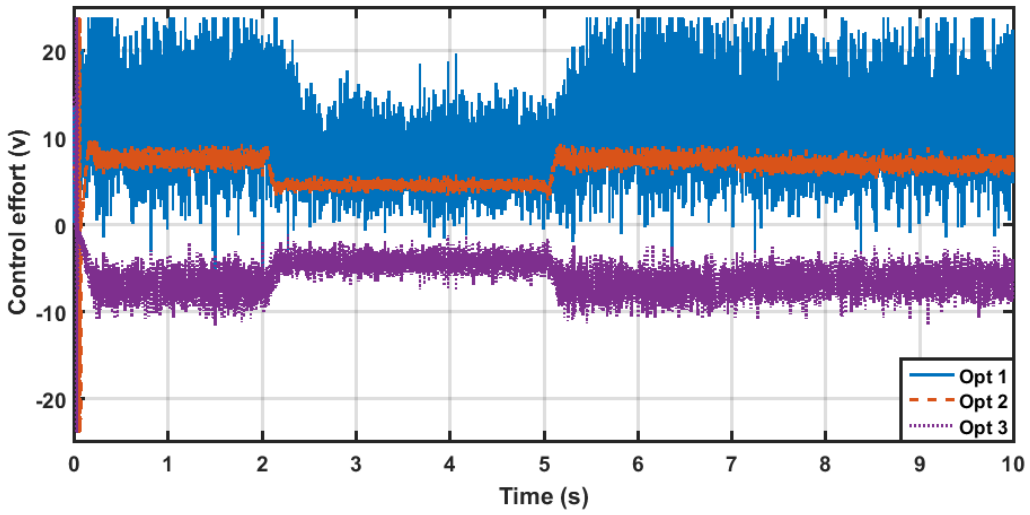

Figure 4.17: Control action of the proposed controller LQi for Opt 1, Opt 2 and Opt 3

with sine reference amplitude of 0.1 and frequency 2 rad/sec are shown in Figures 4.18 and 4.19. The figures also show comparison and control efforts of Opt 2 and Opt 3 in the presence of mass uncertainty. It can be seen that response speeds of both controllers were much closer to each other in the presence of mass uncertainty. However, the control action provided by Opt 2 was smoother than that with Opt 3 control action and Opt 2 still achieved less overshoot 3.67 % compared to Opt 3 (4.87 %).

Based on the results achieved Opt 2 was considered as final fine-tuning for the parameters of the proposed LQi controller. The feedback gains were thus obtained as $K_1 = 1.87 \times 10^5$, $K_1 = 7.17 \times 10^3$ and $K_3 = 119.71$ the integral gain $k_i = 2.21 \times 10^6$ and proportional gain k_r was set to zero.

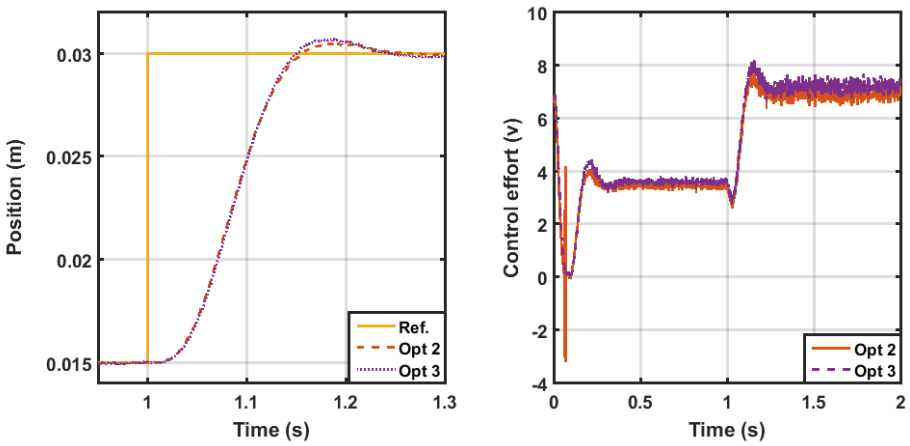

Figure 4.18: Step response and control efforts for Opt 2 and Opt 3

4.6 Comparison and discussion

In this section, the obtained results using LQR-feedback linearisation with static feed-forward gain is compared with those of LQi results. Mainly this section will focus on the performance of both controllers in the presence of mass uncertainty. Figure 4.20 compares between step responses of the system with LQR and with LQi with mass uncertainty of 80%, although the responses with integral action were slowed down, rise time of the system with the LQR was about 0.045 second whereas for the system with LQi was up to 0.078 second. However, integral action helped to eliminate steady-state error, as well as it produced smoother control actions than the LQR action especially around the high edge of step input (see Figure 4.21).

Numerically Table 4.6 compares Integral squared error (ISE) of LQR and LQi in the

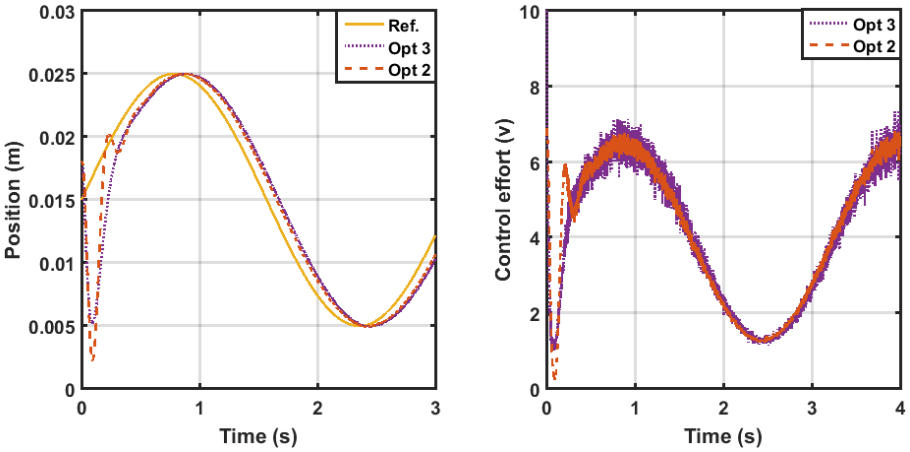

Figure 4.19: Sine response and control efforts for Opt 2 and Opt 3

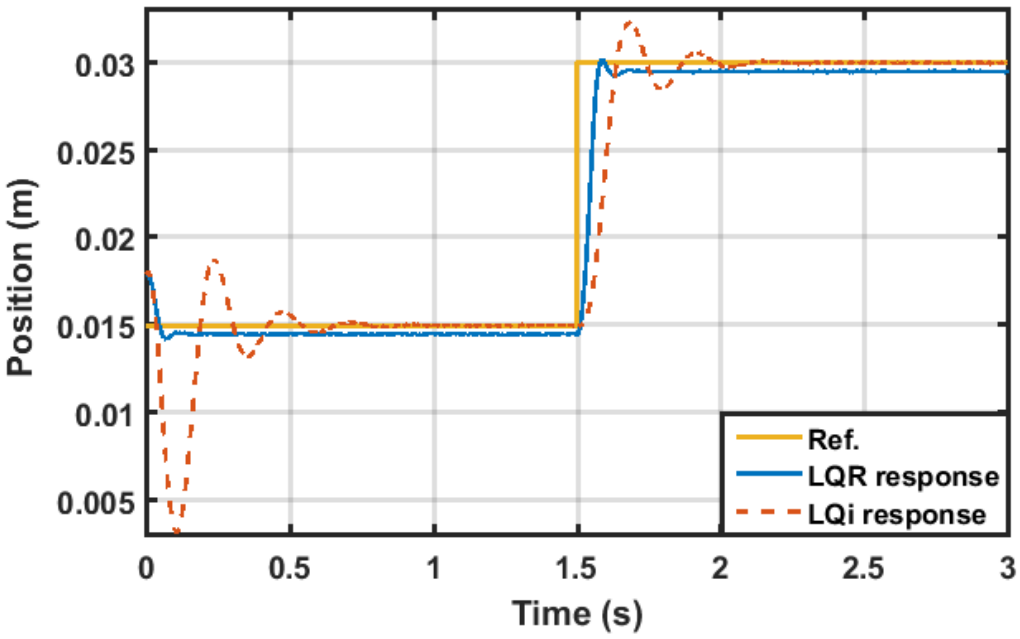

Figure 4.20: Comparison between step response of LQR and LQi in presence of 80% mass uncertainty

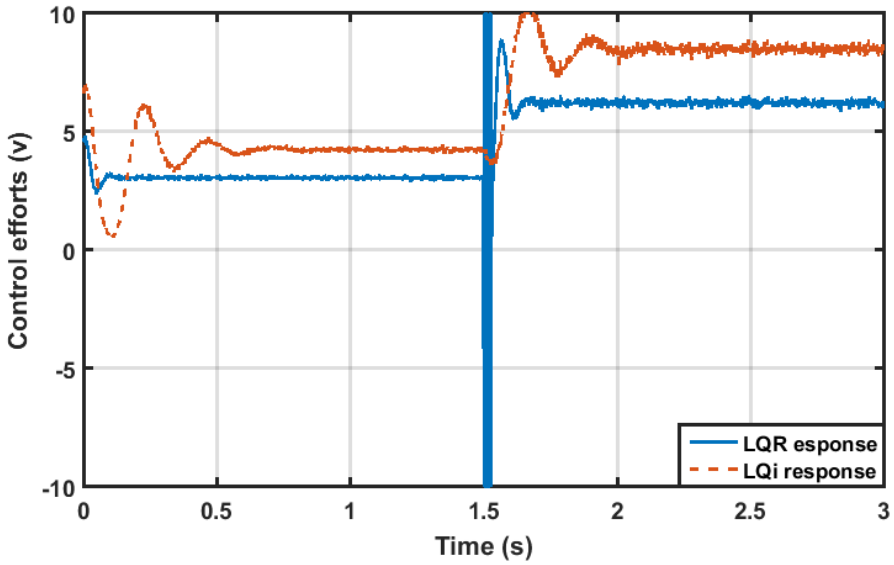

Figure 4.21: comparison between control efforts of LQR and LQi in presence of 80% mass uncertainty

presence of different mass uncertainty with step input of 0.015 for 1.5 s then step up to 0.03 and simulation run time of 3 second.

Table 4.6: ISE error for LQR and LQi in the presence of mass uncertainty

mass uncertainty	ISE	
(m + %)	LQR	LQi
5	58.42	3.54
10	86.14	3.59
20	105.45	3.62
30	157.04	3.73
50	193.4	3.91
80	196.53	4.75

4.7 Summary

In this chapter, an indirect non-linear control strategy has been discussed, where feedback linearisation was used to linearise a non-linear Maglev system into the new z coordinate system, therefore, the system can be treated as a linear system in a limited range of operation. Unmeasured states were estimated using non-linear high gain observer. Optimal control LQR based on full- states feedback was designed to stabilize the transformed linear system in the absence of reference. Reference tracking and disturbance rejection is assigned firstly to static feed-forward gain. This kind of strategy introduced steady-state error in presence of mass uncertainty when the obtained results were evaluated. Then integral action was implemented to improve the robustness to parameters mismatch. Optimization algorithm (ISDA) was used to optimize the controller parameters. The results show the new closed-loop system with integral action has the ability to maintain stable suspension well and to suppress the disturbance caused by noise or parameters mismatch.

Chapter 5

Sliding Mode Control

5.1 Introduction

Sliding mode control is considered as a direct ways to control a non-linear control method based on Lyaponov stability theory. Sliding mode control is a form of Variable Structure Control (VSC) which was investigated first in early 1960s by Emelyanov and several co-researches in the Soviet Union, the ideas did not appear outside of Russia until the mid 1970s when a book by Itkis (1976) and a survey paper by Utkin (1977) were published in English (Edwards and Spurgeon, 1998). It is a practical switching feedback control (discontinuous non-linear control) in which the gains in every feedback path switch between two values in accordance to some rules. The idea is based on bang-bang control theory that was used in early days in high speed switching circuitry and computer products.

The law of this variable structure control is designed in effective way to provide the robustness of controlling non-linear plants against any disturbances and the measurement noise. The control law can be divided into two main parts, namely continuous and discontinuous control law. The continuous control law needs to be designed in a way to drive the state trajectories of non-linear plants in the state space to well-chosen surface. Whereas discontinuous control law essentially utilizes a high speed switching control to maintain the state trajectories on a surface all the time. This surface can be called switching surface because in case the plant trajectory is above the surface the control input needs to switch from one gain to another to bring the trajectory back to the surface and visa versa, if the state trajectory dropped down the surface a control path needs to switch in opposite di-

rection to drive the trajectory back toward the surface (DeCarlo et al., 1988). The surface can at the same time be called sliding surface on which the plant's trajectory slide alone to guarantee the stability of the system which means output feedback trajectories of the closed loop system converge to Lyapunov stable equilibrium points (zero dynamic system).

5.2 Sliding mode control approach

The state variables for the magnetic ball levitation system are described as $\underline{x} = \begin{bmatrix} x_1 & x_2 & x_3 \end{bmatrix}^T$, with the position of the object, velocity and coil current. Define the vector of the desired values as $\underline{x}_d = \begin{bmatrix} r_1 & r_2 & r_3 \end{bmatrix}^T$, where r_1 represents the desired position and r_2 and r_3 equal to zero. Then the vector of tracking error is defined as

$$E = \begin{bmatrix} e & \dot{e} & \ddot{e} \end{bmatrix} = \begin{bmatrix} e_1 & e_2 & e_3 \end{bmatrix} \tag{5.1}$$

A sliding mode controller can be effectively applied to a non-linear system in spite of parameter uncertainties and external disturbances. The dynamics of a nonlinear system can be described in the state space form as follows

$$\dot{x}(t) = f(x;t) + g(x;t)\, u(t) \tag{5.2}$$

For a control system, generally the sliding surface is a function of the system states $\sigma(x;t)$ which can be selected as

$$\sigma(x;t) = S\, x(t) \tag{5.3}$$

where S is a matrix of positive constant elements with a dimension of $[m \times n]$. For a 3rd order system, the time varying surface $\sigma(t)$ can be defined in terms of tracking error instead of a function of system states as

$$\sigma(t) = \left(\frac{d}{dt} + s\right)^{3-1} E \tag{5.4}$$

where s is strictly positive constant and indicates the slope of sliding surface. Thus from equation (5.4), the sliding surface can be written as

$$\sigma(t) = \begin{bmatrix} s^2 & 2s & 1 \end{bmatrix} \begin{bmatrix} e_1 \\ e_2 \\ e_3 \end{bmatrix} \tag{5.5}$$

or it can be simplified as follows

$$\sigma(t) = \begin{bmatrix} s_1 & s_2 & 1 \end{bmatrix} \begin{bmatrix} e_1 \\ e_2 \\ e_3 \end{bmatrix} \tag{5.6}$$

where $s_2 = 2\sqrt{s_1}$.

The next step is to design a control input which can bring the system trajectories towards sliding surface (see Figure 5.1). Considering the dynamical system in equation (5.2), the developed control law is required to drive the system's trajectories towards the sliding surface in finite time $t \leq t_r$ and maintain motion on the surface " $\sigma = 0$" thereafter in the presence of disturbance.

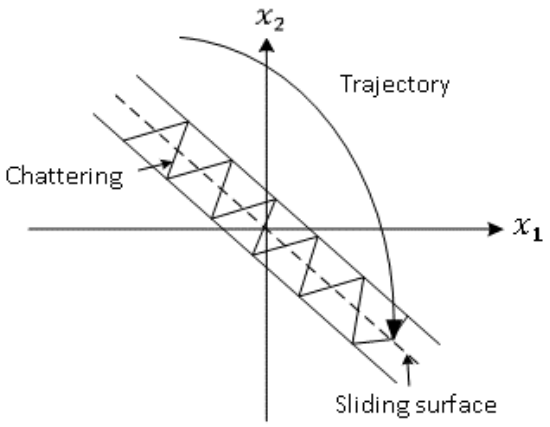

Figure 5.1: Sliding surface

A stability control law is designed using Lyapunov stability condition $\sigma^T \dot{\sigma} < 0$. The

general form of the control law for the sliding mode controller can be written as

$$u = u_{eq} + u_n = -Kx \tag{5.7}$$

where u_{eq} and u_n are the equivalent control and natural control receptively. u_{eq} can be interpreted as a continuous control law to maintain the dynamics of the system on both sides of the sliding surface " i.e $\dot{\sigma} = 0$"(Slotine et al., 1991), while the natural control u_n is discontinuous control law to be designed to account for nonzero uncertainties (DeCarlo et al., 1988).

Substituting for $u(t)$ from equation (5.7) into equation (5.2), yields the closed-loop dynamics of the system as

$$\dot{x}(t) = f(x;t) + g(x)\,(u_{eq} + u_n) \tag{5.8}$$

5.2.1 Equivalent control

The controllability condition of the system to ensure the existence of control signal that can bring the system trajectory closer to the sliding mode is

$$\left|\frac{\partial \sigma}{\partial x} g(x,t)\right| = 0 \tag{5.9}$$

i.e the matrix product $\frac{\partial \sigma}{\partial x} g(x,t)$ is non-singular for all t and x.

Once the sliding mode is achieved where $\sigma(x) = 0$ the sliding trajectories in this mode $\sigma(x)$ should be constant. The sliding motion along the sliding mode, that is described by the differential equation of the sliding mode trajectories, should equal to zero to guarantee the system would slide toward the equilibrium along the sliding mode surface, i.e.

$$\dot{\sigma}(x) = 0 \tag{5.10}$$

Hence, the necessary condition for the output trajectory to reach the sliding surface σ is that $\dot{\sigma} = 0$ which is expressed using the chain rule as $\frac{\partial \sigma}{\partial x}\dot{x} = 0$. Substituting for $\dot{x}$ from

equation 5.2 yields

$$\left[\frac{\partial\sigma}{\partial x}\right]\dot{x} = \left[\frac{\partial\sigma}{\partial x}\right]\left[f(x,t) + g(x,t)\,u\right] = 0 \tag{5.11}$$

and in terms of sliding constant S it can be written as

$$\dot{\sigma} = S\dot{x}(t) = 0 \tag{5.12}$$

Thus the equivalent control is augmented by auxiliary control effort termed as hitting the sliding surface (i.e u_n=0) and determined to solve equation 5.11, expressed as

$$u_{eq} = \left(\left[\frac{\partial\sigma}{\partial x}\right] g(x,t)\right)^{-1}\left[\frac{\partial\sigma}{\partial x}\right] f(x,t) \tag{5.13}$$

Since the sliding motion is equal to S which can be calculated from equation (5.2), i.e $\frac{\partial\sigma}{\partial x} = S$. The so-called equivalent control with respect to sliding constant S can be written as

$$u_{eq} = -(S\,\hat{g}(x))^{-1} S\,\hat{f}(x,t) \tag{5.14}$$

where $\hat{g}(x)$ and $\hat{f}(x)$ are based on best estimated model as can be illustrated in Figure 5.2

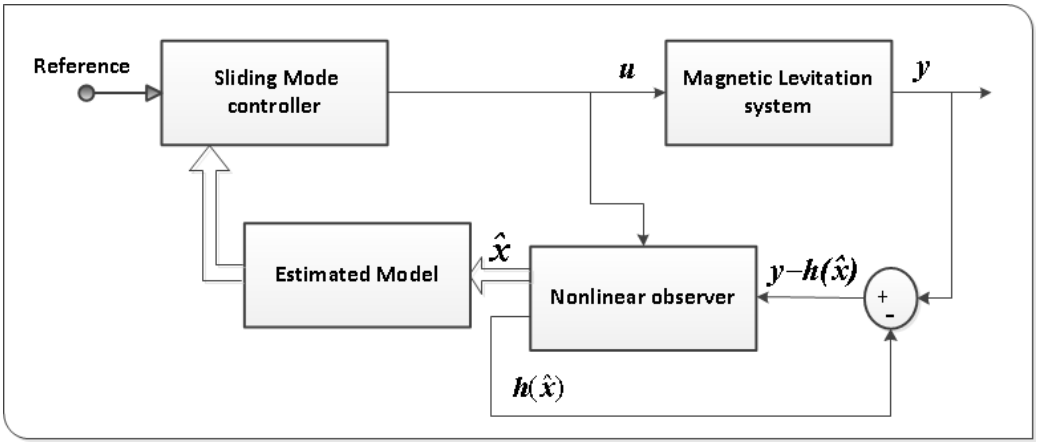

Figure 5.2: Sliding mode control block diagram

5.2.2 Natural control

The natural control is used to maintain the status trajectory on sliding surface using signum function which requires infinite switching on the part of actuator and the control signal.

To ensure sliding mode exists a sliding mode control of the following form is applied

$$u = u_{eq} + u_n$$

The sliding mode control to control the non-linear Maglev system with Non-linear high-gain observer (NHGO) is illustrated in Figure 5.3

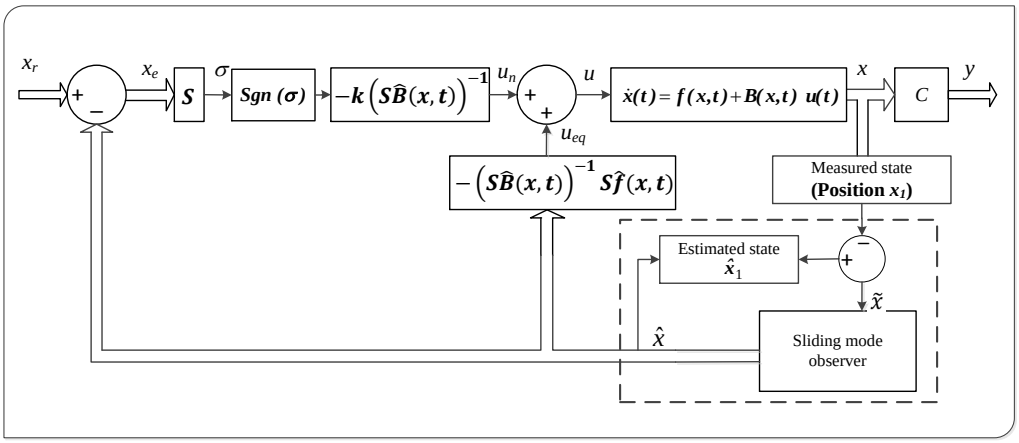

Figure 5.3: The sliding mode control details including natural and equivalent control

For system in equation (5.2), consider the Lyapunov function candidate

$$V(\sigma(x)) = \frac{1}{2}\sigma^T(x)\,\sigma(x) = \frac{1}{2}\left\|\sigma(x)\right\|_2 \tag{5.15}$$

where $\|\sigma(x)\|_2$ is the distance away from the sliding surface $\sigma(x) = 0$. Sliding mode will exist if

$$\sigma^T(x)\,\dot{\sigma}(x) = \frac{\partial V}{\partial \sigma}\frac{\partial \sigma}{\partial t} = \frac{\partial V}{\partial t} < 0 \tag{5.16}$$

in neighbourhood of sliding surface.

For this equality $\sigma^T(x)\,\dot{\sigma}(x)$ is to remain all the time less than zero, which means that convergence of the system trajectories towards the sliding surface is guaranteed by selecting feedback law so that σ and $\dot{\sigma}$ have opposite signs such as

- u(x) can make $\dot{\sigma}$ to be negative when σ is positive
- u(x) can make $\dot{\sigma}$ to be positive in case σ is negative

By having this, once the trajectories move away from the surface in positive direction the input signal (system input / controller output) would bring it back to the surface, and this can be achieved by reversing the motion around the sliding surface, i.e by making the rate of change of the sliding surface ($\dot{\sigma}$) to be negative and vice versa.

Thus the control law of discrete/ natural $u_n(x)$ can be chosen so that

$$u_n(x) = \begin{cases} u^-(x) & if\ \sigma(x) > 0 \\ u^+(x) & if\ \sigma(x) < 0 \end{cases} \tag{5.17}$$

or it can be expressed mathematically in general form as

$$u_n = -M\ sign(\sigma) \tag{5.18}$$

the resultant form can be scaled as expressed in (Firdaus and Tokhi, 2016) as

$$u_n = -M(S\,\hat{g}(x))^{-1} sign(\sigma) \tag{5.19}$$

5.3 Fuzzy sliding mode control

The essential purpose of using this technique is to improve the switching function of natural control (u_n) with fuzzy logic. The proposed method endeavours to eliminate the chattering phenomenon during sliding mode condition on the sliding surface. The general structure of Fuzzy sliding mode controller (FSMC) is shown in Figure 5.4. The membership functions of fuzzy input (U_n) and output (FU_n) are created through the the values of

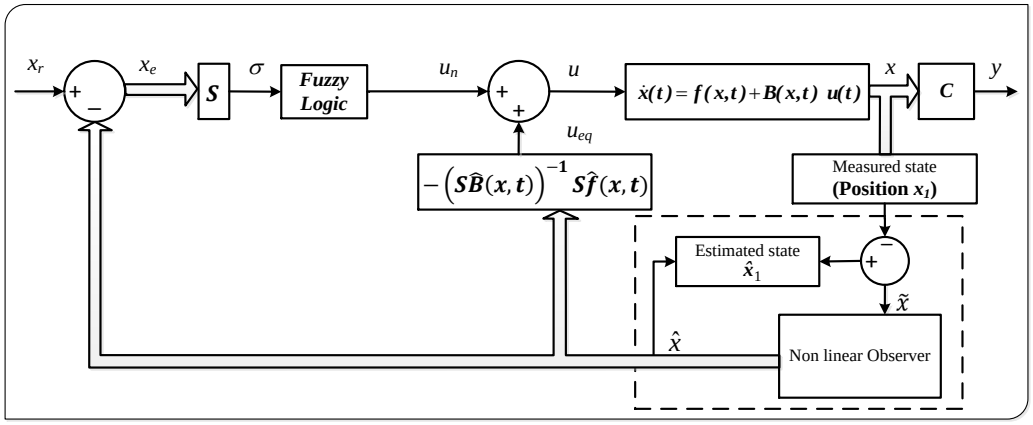

Figure 5.4: General structure of FSMC

sliding surface (σ) as shown in Figure 5.5. Here only input membership function is shown here, since in this work two types of membership function for the output were used, and output membership functions will be shown later. Fuzzy sets of seven membership functions, namely: Negative Big (NB), Negative Medium (NM), Negative Small (NS), Zero (Z), Positive Small (PS), Positive Medium (PM), and Positive Big (PB) are used, with the range [-1, 1] for both input and output.

Considering the fuzzy input and output, the rules-base to produce the desired natural control (u_n) can be set up as in Table 5.1

Table 5.1: The Fuzzy rule base for FSMC

σ / u_{fn}	NB	NM	NS	Z	PS	PM	PB
	PB	PM	PS	Z	NS	NM	NB

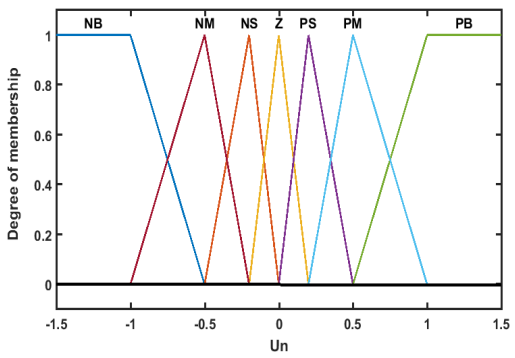

Figure 5.5: Membership functions for fuzzy input 'U_n'

The natural control obtained after defuzzification process can be expressed as

$$u_n = G_u \, u_{fn} \tag{5.20}$$

where G_n is a gain to factorise the output signal, while u_{fn} represents the crisp values obtained from the FLC. Thus the overall control signal of FSMC can be written as (see Figure5.6)

$$u = -(S \, \hat{g}(x))^{-1} S \, \hat{f}(x,t) + G_u \, u_{fn} \tag{5.21}$$

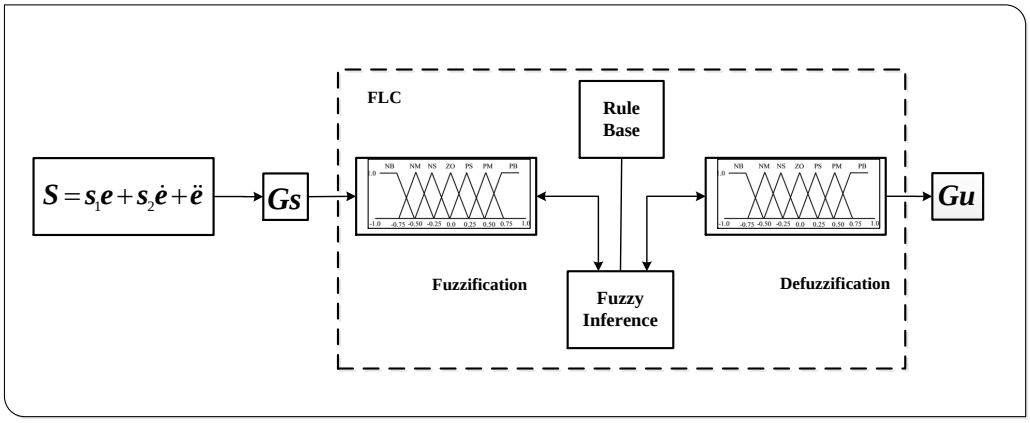

Figure 5.6: FSMC block diagram in detail

5.4 Implementation and results

This section presents simulation results assessing the performance of the SMC. The results are split to two main sub-sections, where in the first part results of SMC with SMO observer are presented, and in the second part results obtained by FSMC and FSMO are presented and discussed. A comparative assessment of the performances of both controllers is also presented.

5.4.1 Sliding mode controller

The simulation results were obtained from the algorithm which was coded in MATLAB 2015b Simulink using a personal computer with the same specifications stated in section 4.5.1. The system parameters were as shown previously in Table **??**.

Sliding mode control is considered as an optimal control where all the states need to be available, which is not the case here, as the position of the object is the only measured state, whereas the velocity and current are estimated using Sliding mode observer (SMO). The details of the implemented Sliding mode control (SMC) with Sliding mode observer (SMO) are shown in Figure 5.7.

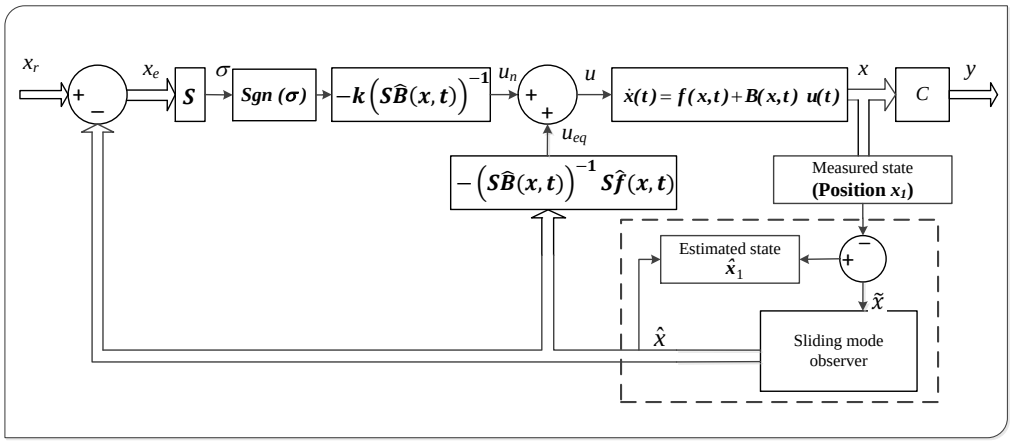

Figure 5.7: SMC with SMO

In the feedback loop continuous control input/ equivalent control input was used to

bring the system states to the sliding surface as described in equation (5.14);

$$u_{eq} = -(S\,\hat{g}(x))^{-1} S\,\hat{f}(x,t)$$

where S is second order sliding mode surface constant defined as vector of $[s_1\ s_2\ 1]$, $\hat{g}(x)$ is the input vector with value of $[0\ 0\ 1/L]$, and $\hat{f}(x,t)$ is the best estimated model of Maglev system that equals to $[\hat{f}_1\ \hat{f}_2\ \hat{f}_3]$ as was expressed in equation (3.31)

$$\begin{aligned}
\hat{f}_1 &= \hat{x}_2 \\
\hat{f}_2 &= g - \frac{c}{m}\left(\frac{\hat{x}_3}{\hat{x}_2}\right)^2 \\
\hat{f}_3 &= \frac{R}{L}\,\hat{x}_3 + \frac{2\,c}{L}\left(\frac{\hat{x}_2\hat{x}_3}{\hat{x}_1^2}\right)
\end{aligned}$$

Discontinuous control input/ natural input in the feed-forward path was used to preserve the sliding trajectories (system trajectories around sliding surface) from moving away from sliding manifold as described in equation 5.19

$$u_n = -M(S\,\hat{g}(x))^{-1} sign(\sigma)$$

where M is the natural gain to be tuned, by which the input is constrained based on the following condition

$$|u_n| \leq M, \quad M > 0 \tag{5.22}$$

and switching function $sign(\sigma)$, well-known function in conventional sliding mode theory, is to reverse the sliding motion by changing the sign of rate of change of the sliding dynamic around sliding surface $\dot{\sigma}(x)$, which can be written as

$$sign(\sigma) = \frac{\sigma}{|\sigma|} = \begin{cases} -1 & |\sigma| < 0 \\ 1 & |\sigma| > 0 \end{cases} \tag{5.23}$$

The simulation results compare the performances obtained using conventional switching

function with those acquired using a boundary layer, where the saturation function was used to solve the chattering problem described as

$$sat(\sigma) = \frac{\sigma}{|\sigma| + \phi} = \begin{cases} \frac{\sigma}{\phi} & \left|\frac{\sigma}{\phi}\right| \leq 1 \\ sign\left(\frac{\sigma}{\phi}\right) & \left|\frac{\sigma}{\phi}\right| > 1 \end{cases} \tag{5.24}$$

A thin boundary layer as shown in Figure 5.8 was introduced in neighborhood of the sliding surface to eliminate the chattering when all trajectories are inside $\phi(t)$ for all time, therefore the input u was interpolated inside $\phi(t)$ as illustrated in Figure 5.9.

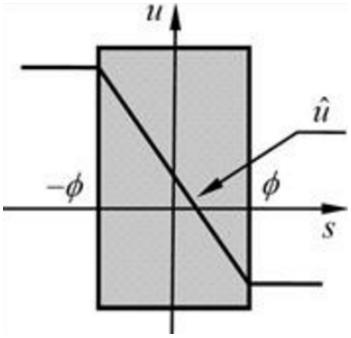

Figure 5.8: Saturation function

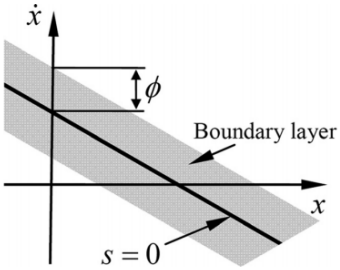

Figure 5.9: Boundary layer

Figure 5.10 shows the sine response of SMC using signum and saturation function to each other in the the presence of 30% mass mismatch. It can be seen that both controllers have achieved similar performances in terms of reference tracking. However, a boundary layer using saturation function helps to improve the smoothness of the control action. Figures 5.11 to 5.13 illustrate the control actions of both controllers in presence of different percentages of mass uncertainty for variety of inputs, constant of 0.015 m, step of 0.018 initially till 1.5 second then step down to 0.015 and finally sine input with frequency of 2

rad/s.

These results were obtained using second order sliding surface with two gains (s_1 and s_2) as presented in equation 5.5 where $s_2 = 2\sqrt{s_1}$ with tuned value of 62.7660 and s_1 = 984.8940, natural gain M was 8786.9907, states were estimated using optimized SMO with six gains shown in Table 5.2 . The maximum percentage mass uncertainty with these tuned parameters was 75%.

Table 5.2: SMO observer parameters used with SMC controller

Parameter	α			β		
	1	2	3	1	2	3
Values	3958.22	10307.34	9509.15	7962.62	6575.31	7223.49

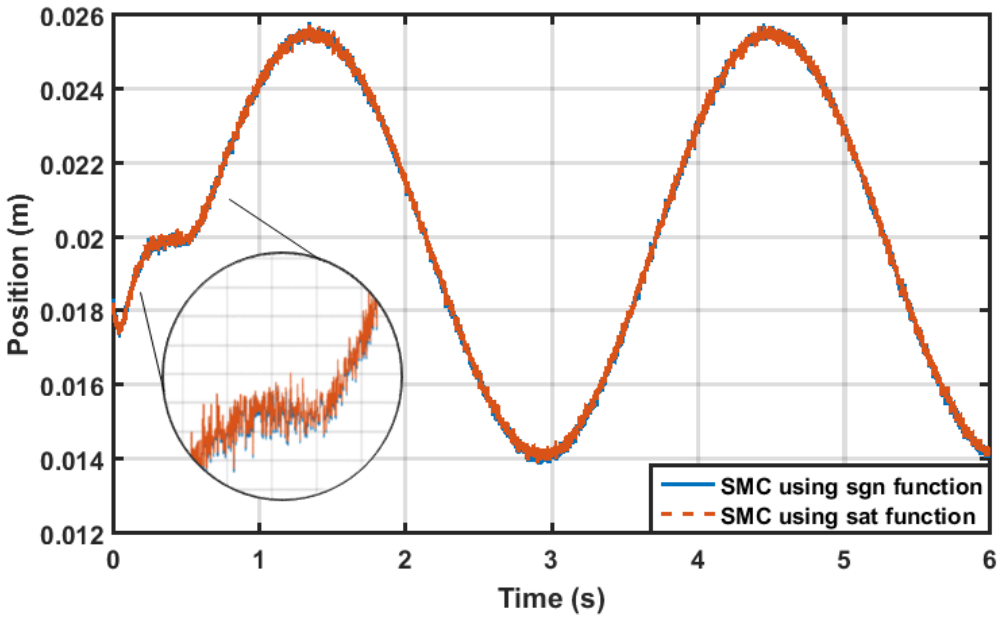

Figure 5.10: Sine response of SMC controller in presence of 30% of mass uncertainty

5.4.2 Fuzzy sliding mode control

In this section simulation results assessing the performance of (FSMC) combined with FSMO are presented. Previous results have highlighted one of the main disadvantages of the SMC method; its dependence on system model, which affects the robustness of the controller. Moreover, there is the chattering phenomenon during sliding mode condition

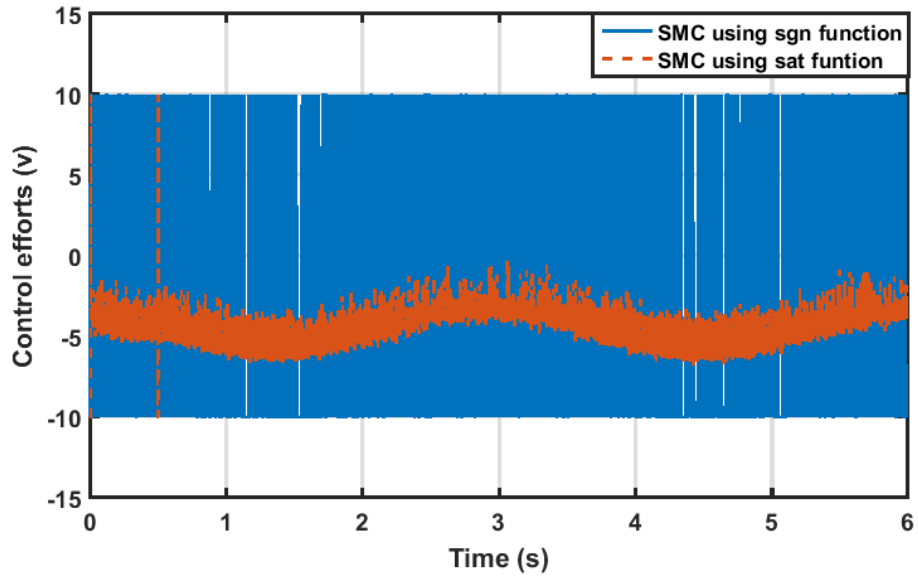

Figure 5.11: Control efforts of SMC controller with sine input in presence of 30% of mass uncertainty

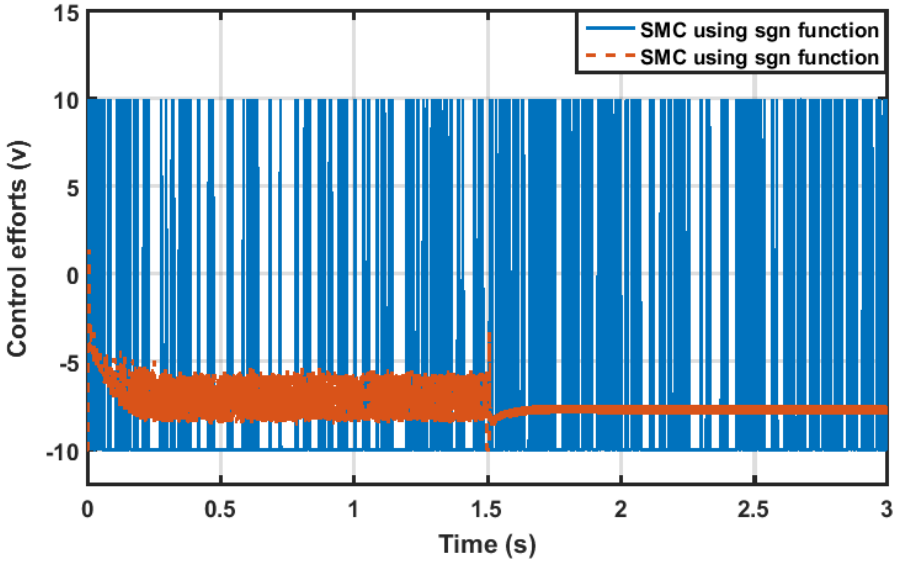

Figure 5.12: Control efforts of SMC controller with step input in presence of 50% of mass uncertainty

in the sliding surface. To overcome these problems FSMC is proposed, since fuzzy logic control is not a model based technique.

In this type of design the same equivalent control as in equation (5.14) was used. FLC was implemented in the natural control input by replacing the switching function to adapt to the sliding surface σ. Triangular membership functions for input U_n and the output FU_n were used in the fuzzification procedure to adjust the thickness of the boundary layer as

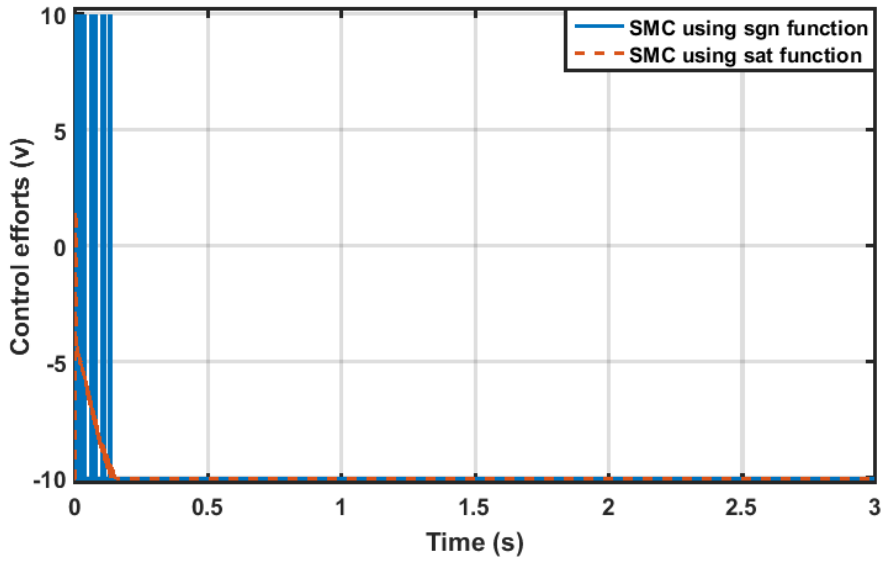

Figure 5.13: Control efforts of SMC controller with constant input in presence of 75% of mass uncertainty

an output. Fuzzy rules were designed for the fuzzy output to always have opposite sign to σ to ensure the sliding trajectories move toward the sliding surface. The rules from Table 5.1 are described as

Rule 1: IF σ is NB, then U_n is PB

Rule 2: IF σ is NM, then U_n is PM

Rule 3: IF σ is NS, then U_n is PS

Rule 4: IF σ is Z, then U_n is Z

Rule 5: IF σ is PS, then U_n is NS

Rule 6: IF σ is PM, then U_n is NM

Rule 7: IF σ is PB, then U_n is NB

Two scaling factors G_s and G_u as shown in Figure 5.6 were used to normalise the input to fuzzy block and to amplify the fuzzy output respectively. These gains are tuned manually.

First simulation results were obtained using fuzzy sets of seven triangular membership functions for output, namely: Negative Big (NB), Negative Medium (NM), Negative Small (NS), Zero (Z), Positive Small (PS), Positive Medium (PM), and Positive Big (PB), with the range of [-1, 1] as shown in Figure 5.14. The crisp output variable of FSMC was calculated by centroid defuzzification method. Triangular Fuzzy Number (TEN) of the

membership function used to define a triangular membership by triple (a_1,a_2 and a_3) with the values

NB: $a_1 = -\infty$ $a_2 = -1$ $a_3 = -0.5$

NM: $a_1 = -1$ $a_2 = -0.5$ $a_3 = -0.2$

NS: $a_1 = -0.5$ $a_2 = -0.2$ $a_3 = 0$

Z : $a_1 = -0.2$ $a_2 = 0$ $a_3 = 0.2$

PS: $a_1 = 0$ $a_2 = 0.2$ $a_3 = 0.5$

PM: $a_1 = 0.2$ $a_2 = 0.5$ $a_3 = 1$

PB: $a_1 = 0.5$ $a_2 = 1$ $a_3 = \infty$

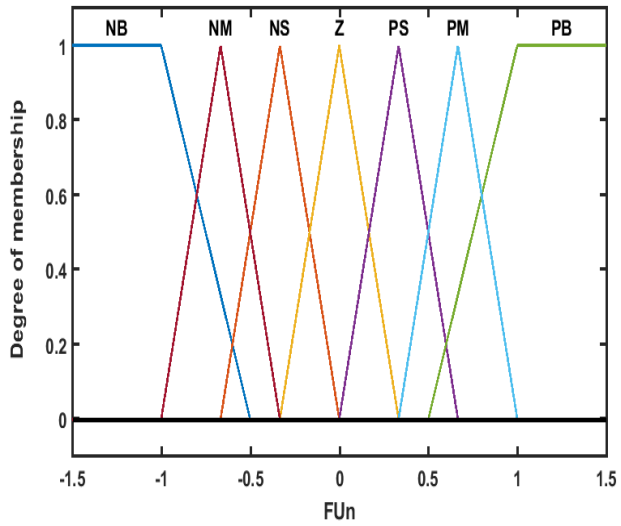

Figure 5.14: Membership functions for fuzzy output "FU_n"

The same equivalent control was used with second order sliding surface with two tuned gains $s1 = 34026$ and $s2 = 368.9228$, whereas the scaling factors in natural control were set to the values of 10^{-5} and 7000 for G_s and G_u respectively. Fuzzy sliding mode observer (FSMO) was used to estimate the states using Fuzzy inference system (Mamdani) (fis) file which was designed using fuzzy toolbox in Matlab. The same fuzzy sets of seven membership function for input and output were implemented in FSMO observer. The scaling factors for the observer were given the same values used in the controller and α_1 to α_3 were given values of 736.2675, 9000 and 299.9370 respectively. Figures 5.15 and 5.16 show step and sine responses and control actions for FSMC with FSMO.

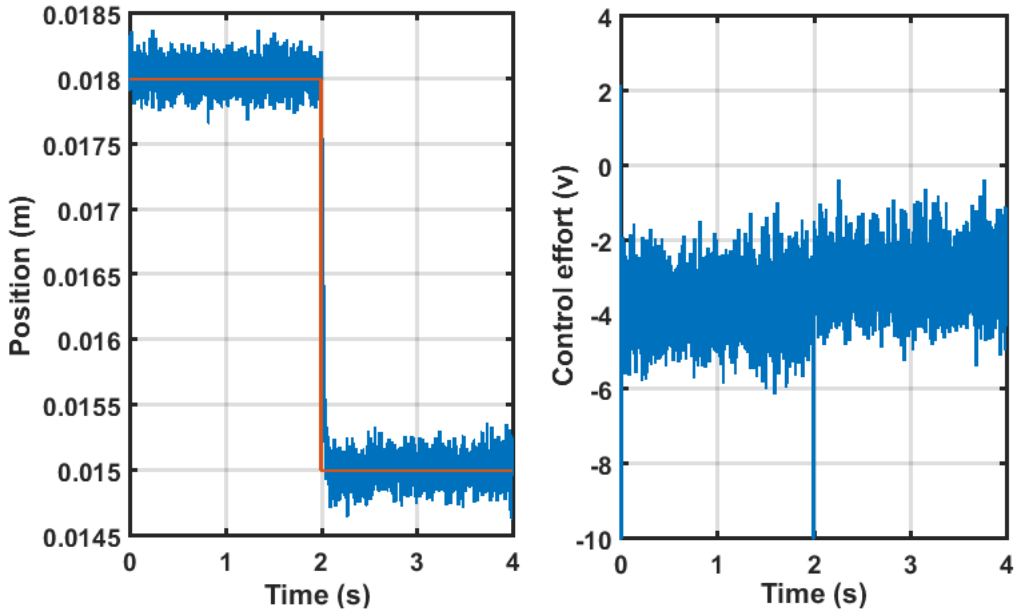

Figure 5.15: Step response and control actions for FSMC controller with FSMO observer using fis file

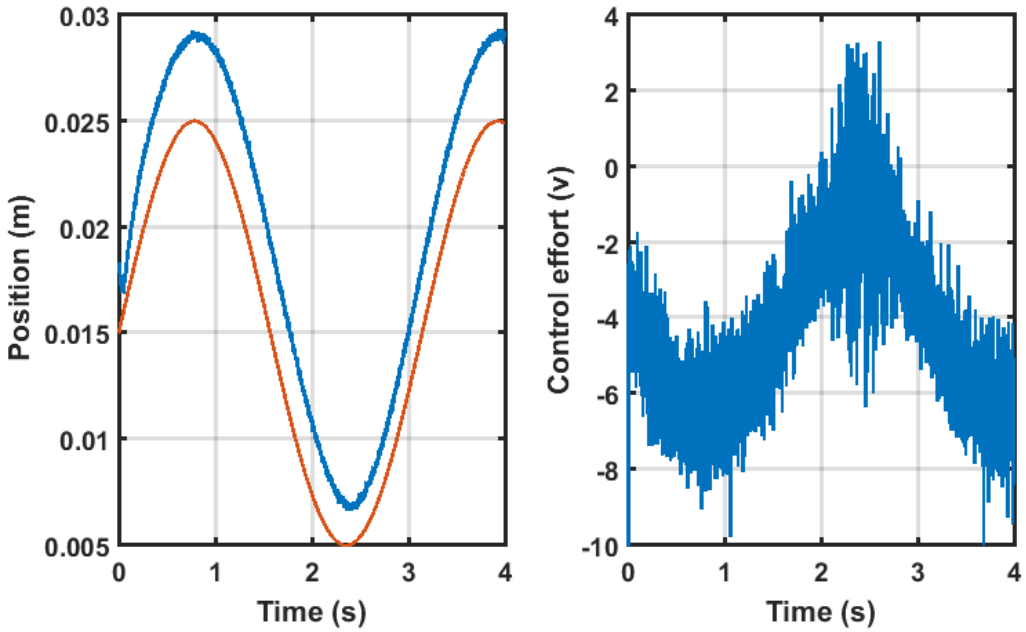

Figure 5.16: Sine response and control actions for FSMC controller with FSMO observer using fis file in presence of 20% of mass uncertainty

Further results were obtained using the fuzzy singleton method, in which the linguistic variable definition associated with input was the same as the previously defined input. However, the linguistic variable definition for the output was simplified to a new form; the set of output variable was no longer a fuzzy number but was a crisp value in the base

variable space as shown in Figure 5.17. The crisp output variable u_{fs} of FSMC using fuzzy singleton method can be calculated by the weighted average defuzzification method as

$$u_{fs} = \frac{\sum_{i=1}^{5} \mu_{Ri}\, u_{fsi}}{\sum_{i=1}^{5} \mu_{Ri}} \tag{5.25}$$

All control parameters for the controller (both equivalent and natural control) and the

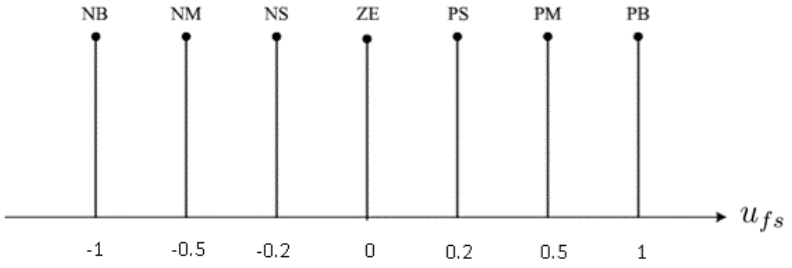

Figure 5.17: Membership functions for fuzzy output 'FU_n' using fuzzy singleton method

observer were the same as the ones used previously in FSMC using fis file. The only change was that the membership function for fuzzy output of singleton- type replaced the classic triangular membership functions for the output.

Figures 5.18 to 5.22 compare the performance of FSMC controller with observer using the classic approach (fis file) with FSMC using fuzzy singleton method for both controller and observer in the presence of different percent mass uncertainties and different inputs. Figures 5.21 and 5.23 show the corresponding control actions.

Although the control actions for both techniques seem to be close to each other, better response can be obtained using fuzzy singleton method.

Table 5.3 shows a numerical comparison between both techniques for constant input of 0.015 for 4s. It is noted that the maximum uncertainty percentage for FSMC using classic approach was 90% against 113% for FSMC using fuzzy singleton output membership function. Moreover, simulation results show a significant reduction in computation time which was just 4.08 second for FSMC using singleton by contrast to FSMC using fis. file that was 57.96 s.

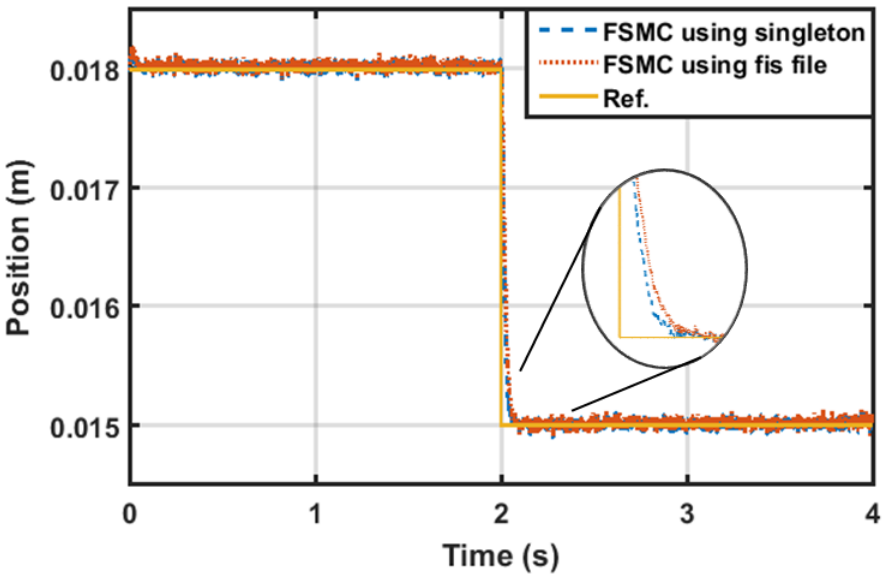

Figure 5.18: A comparison between step response for FSMC using singleton method and using fis.

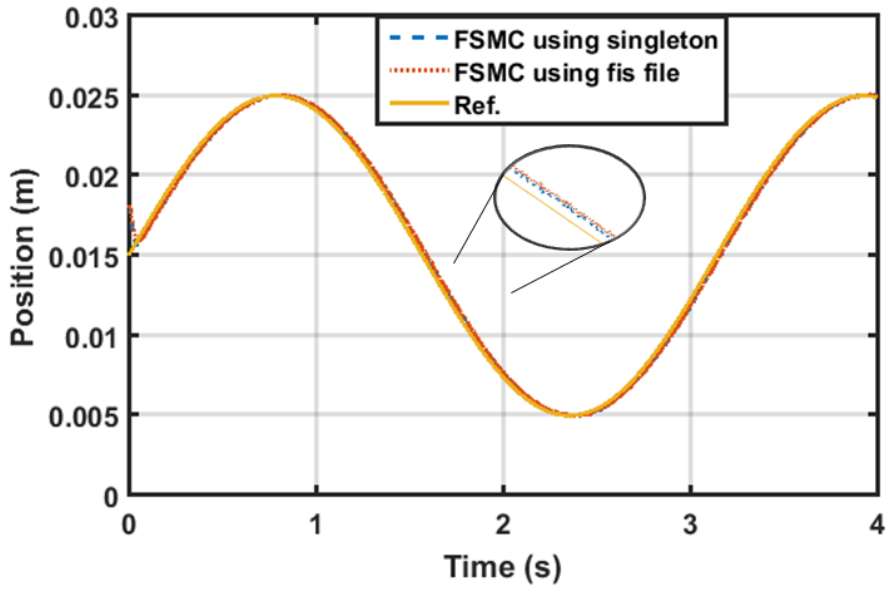

Figure 5.19: A comparison between sine response for FSMC using singleton method and using fis.

5.5 Comparison and discussion

In this section, a comparison between SMC and FSMC is presented. For a fair comparison the states were estimated using the same Non-linear high-gain observer (NHGO) with the tuned parameters $a = 50$ and $\epsilon = 0.5$. A block diagram representation of active magnetic levitation with the implemented controllers (SMC/FSMC) with Non-linear high-

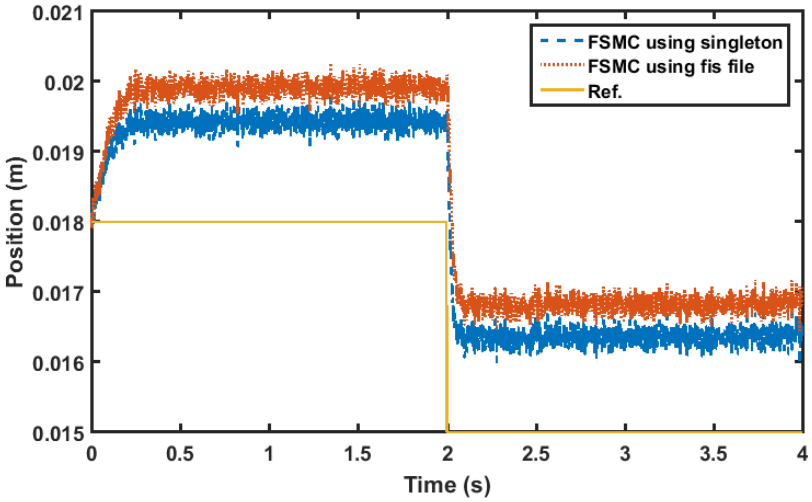

Figure 5.20: A comparison between step response for FSMC using singleton method and using fis. file in presence of 10% mass uncertainty

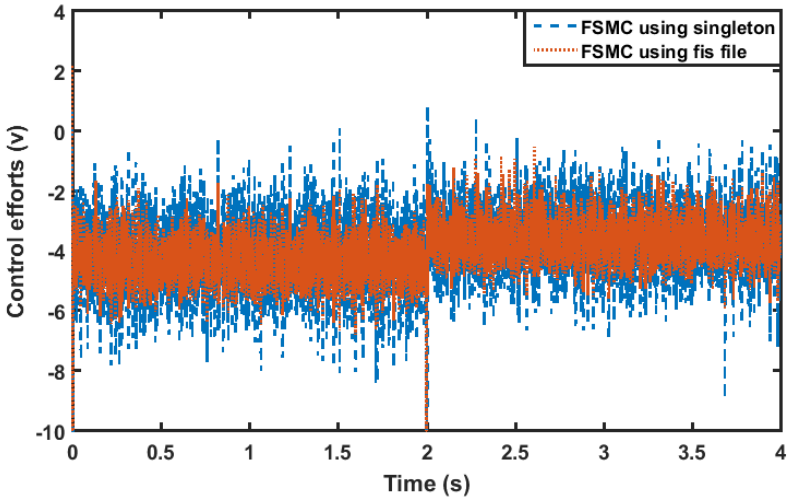

Figure 5.21: A comparison between control efforts for FSMC using singleton method and using fis. file in presence of 10% mass uncertainty with step input

gain observer (NHGO) is shown in Figure 5.24.

Initially, the set point for the system was located at 15 mm with initial position of $x_{1e} = 18 \times 10^{-3}$ m, $x_{2e} = 0$ m/s and the obtained initial current as $x_{3e} = \sqrt{m \times g \times 18 \times 10^{-3}}$ = 0.9039 A. Figure 5.25 shows the performances of SMC and FSMC. It is noted that both controllers could stabilise the object and track the set point and the response rise time was shorter with FSMC. Moreover, FSMC generated much smoother control signal than SMC as shown in Figure 5.26

Table 5.4 explores the effect of uncertainty in the mass of object in the system with set-

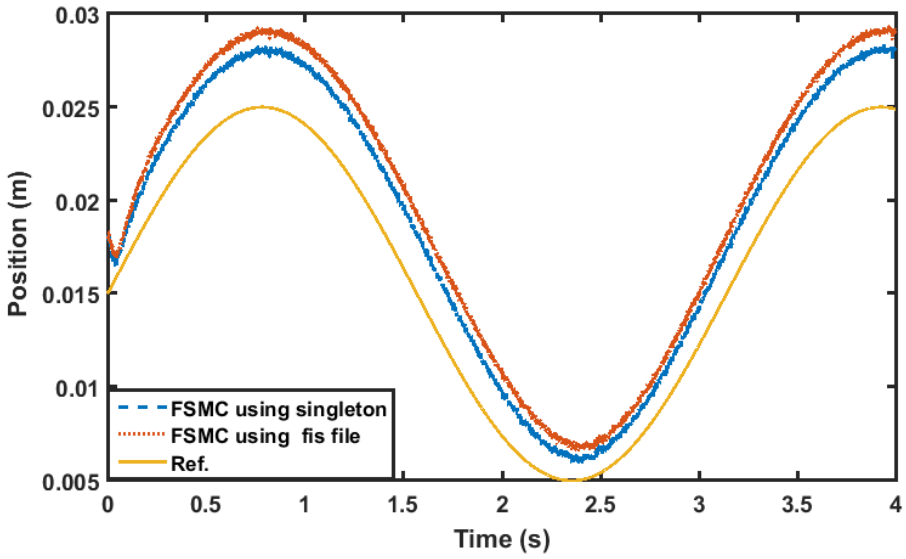

Figure 5.22: A comparison between sine response for FSMC using singleton method and using fis. file in presence of 20% mass uncertainty

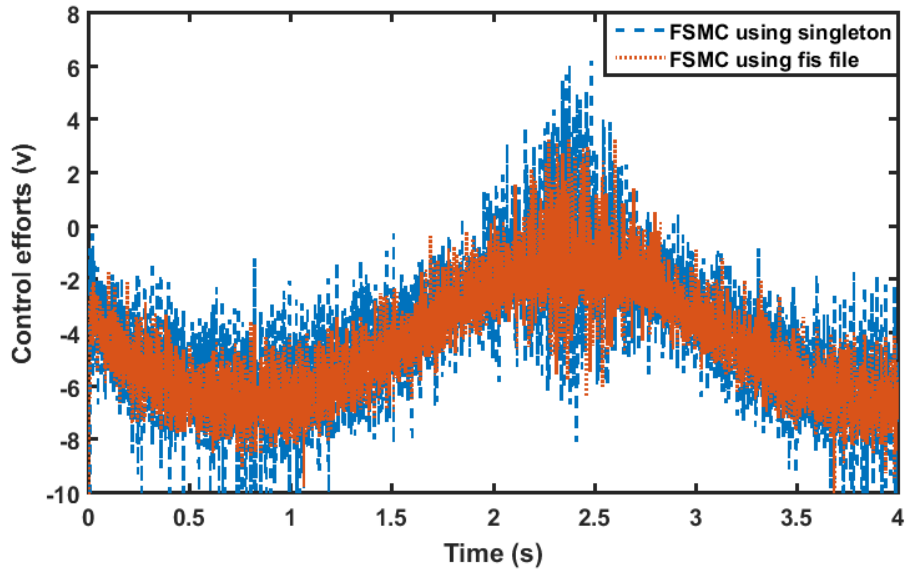

Figure 5.23: A comparison between control efforts for FSMC using singleton method and using fis. file in presence of 20% mass uncertainty with sine input

point of 15 mm, as the mass was decreased to the limit of 70% and increased up to around 255%. It is noted that FSMC achieved the minimum IAE as well as minimum MSE.

Step responses of the magnetic ball system with these two controllers are shown in Figures 5.27-5.30 in the presence of different percentage mass uncertainties.

Table 5.3: ISE error for classic approach versus fuzzy singleton method in presence of mass uncertainty

mass uncertianty	ISE	
(m + %)	Fis. file	singleton
10	63.32	52.63
20	115.79	103.93
30	169.64	153.83
50	281.86	254.21
80	417.03	379.09
90	392.49	**395.45**
100	-	387.37
110	-	298.33
113	-	224.96

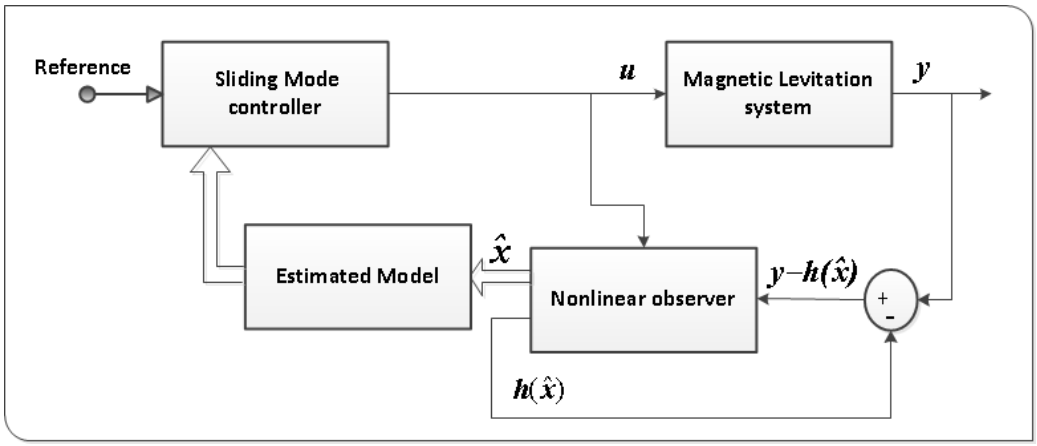

Figure 5.24: Sliding mode control block diagram

Figures 5.31 and 5.32 show the control efforts of SMC and FSMC with mass uncertainties of 80% and 120% respectively. As noted FSMC delivered a smooth control signal and overcame the chattering phenomenon.

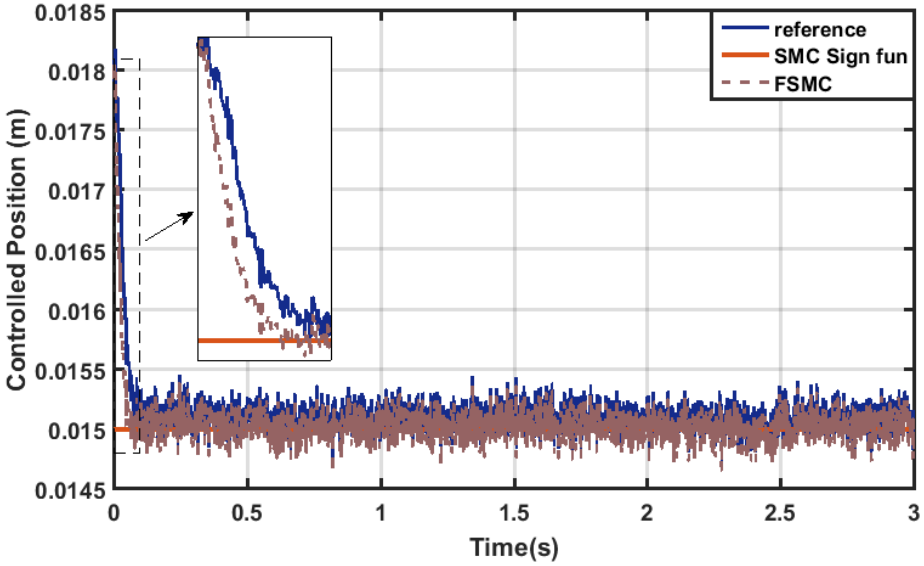

Figure 5.25: System response using SMC and FSMC with set-point of 15 mm

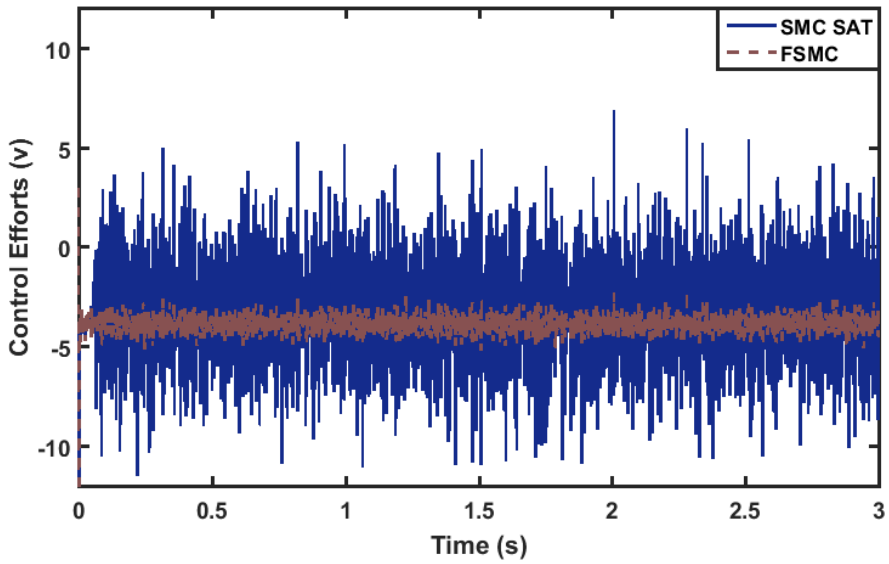

Figure 5.26: The control effort of SMC and FSMC controllers with set-point of 15 mm

Table 5.4: The performance indices for the control schemes with set-point of 15 mm

mass uncertainty	SMC		FSMC	
(m %)	IAE	MSE	IAE	MSE
70	-	-	16.405	8.03×10^{-3}
78*	27.398	4.46×10^{-3}	-	-
80	27.478	4.24×10^{-4}	10.959	5.56×10^{-4}
90	13.933	3.23×10^{-4}	5.631	3.32×10^{-4}
105	5.284	3.94×10^{-4}	2.414	2.85×10^{-4}
110	9.157	5.11×10^{-4}	6.168	3.81×10^{-4}
120	11.095	9.33×10^{-4}	10.966	6.21×10^{-4}
122.3*	28.344	2.70×10^{-3}	-	-
130	-	-	15.848	2.81×10^{-1}
150	-	-	25.848	3.61
180	-	-	41.334	8.03
200	-	-	51.805	9.98
250	-	-	78.624	12.95
255.5*	-	-	81.377	13.17.

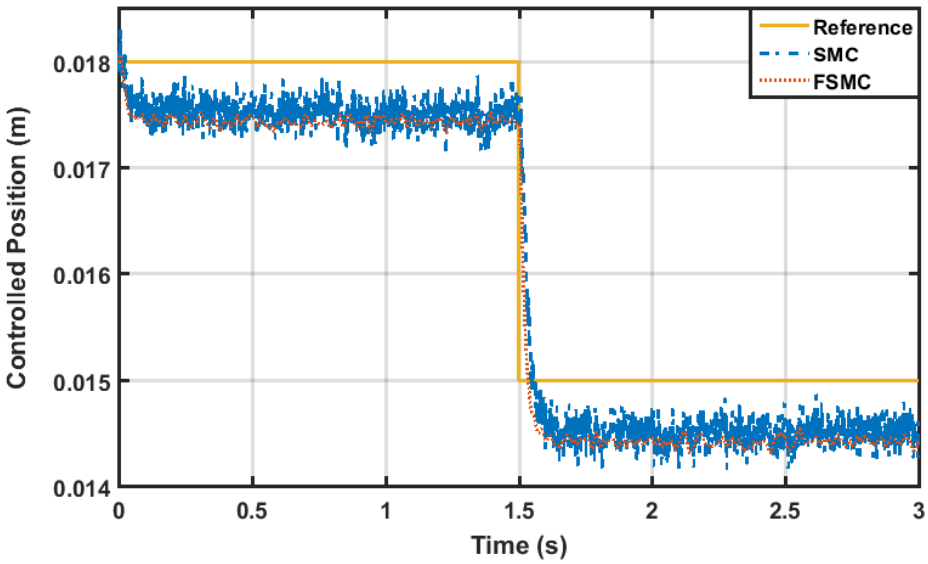

Figure 5.27: System response in the presence of mass uncertainty, m=80%

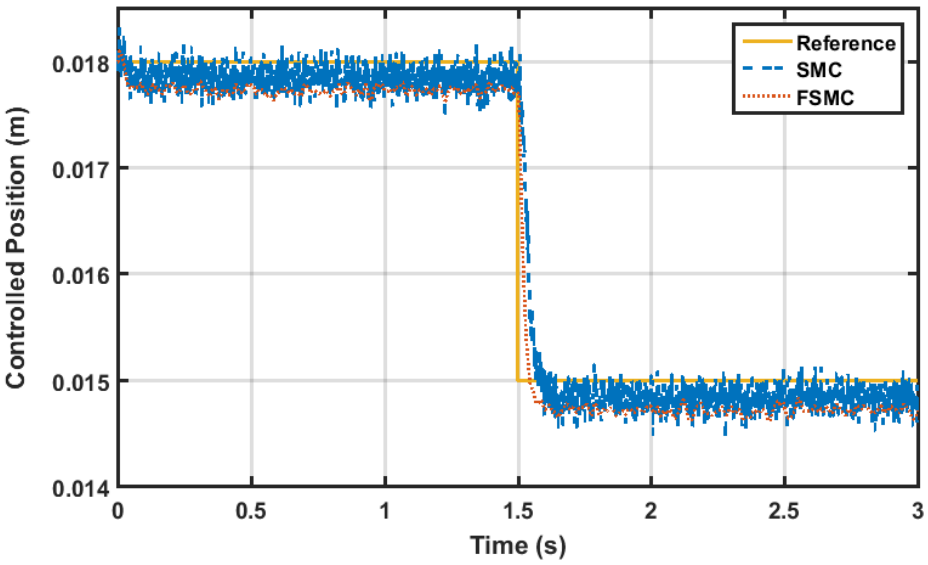

Figure 5.28: System response in the presence of mass uncertainty, m=90%

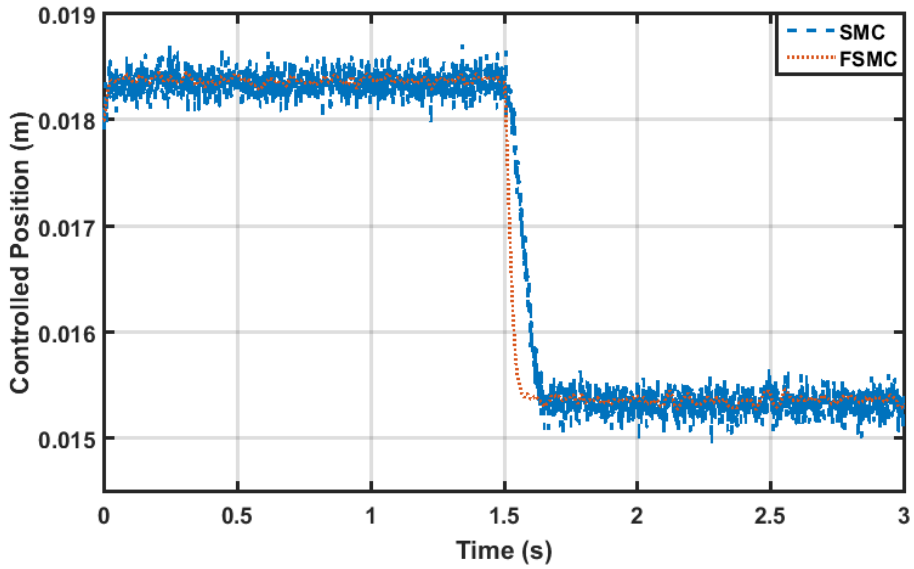

Figure 5.29: System response in the presence of mass uncertainty, m=110%

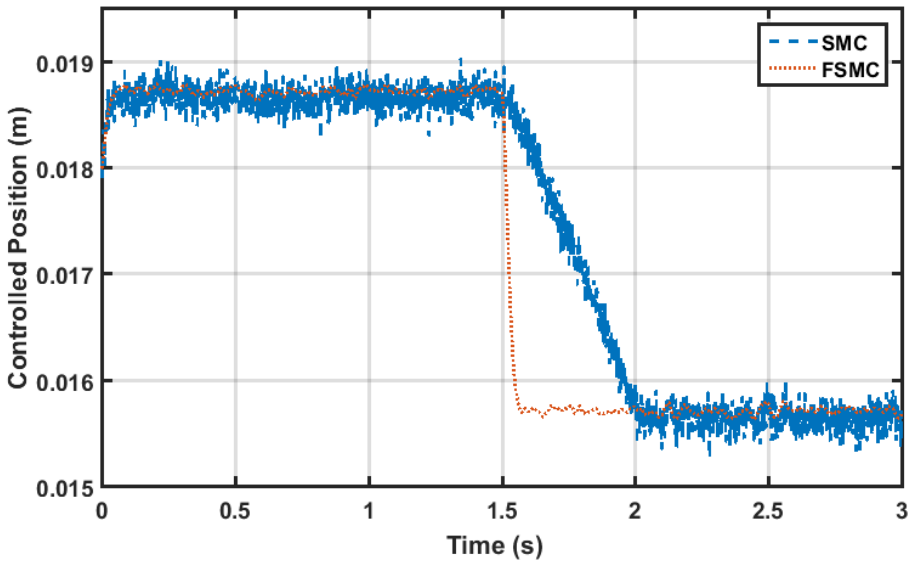

Figure 5.30: System response in the presence of mass uncertainty, m=120%

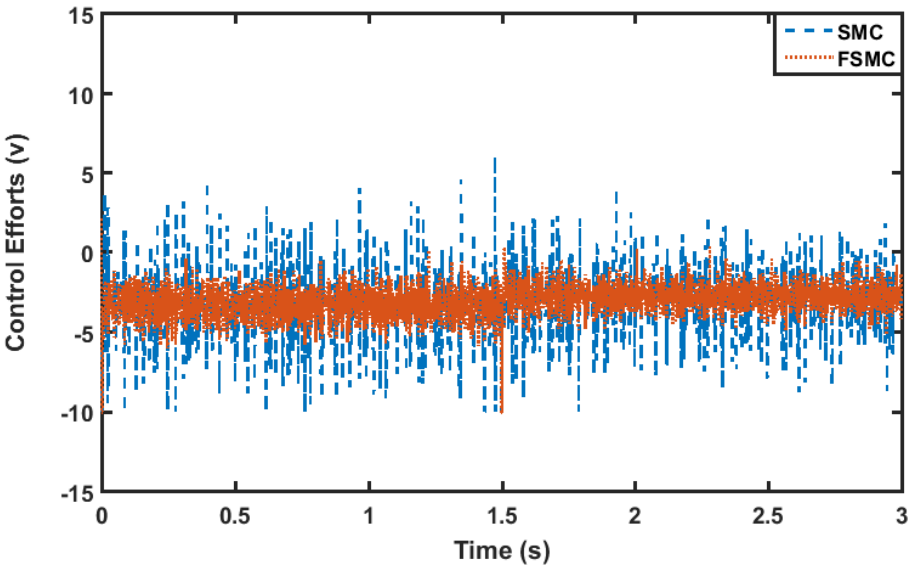

Figure 5.31: The control effort of SMC and FSMC with mass percentage of 80%

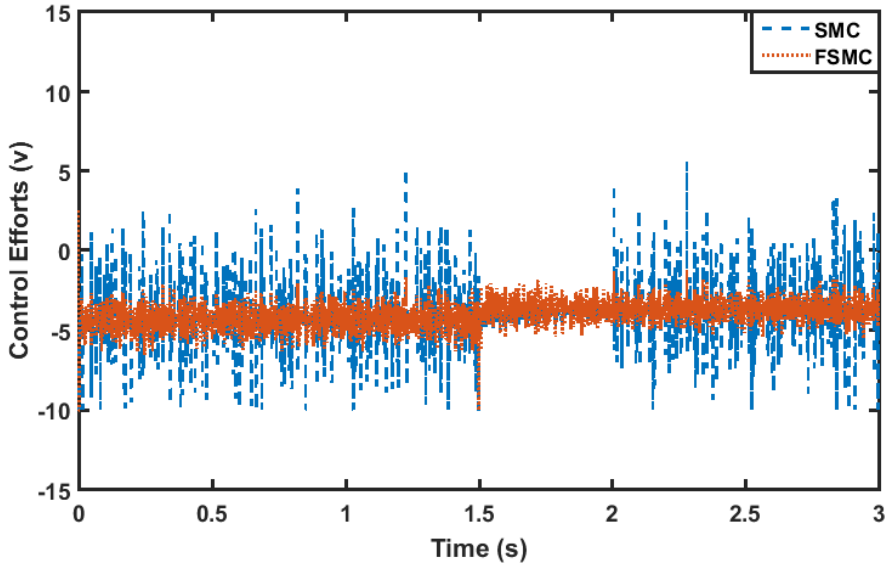

Figure 5.32: The control effort of SMC and FSMC with mass percentage of 120%

5.6 Summary

In this chapter, SMC as a direct nonlinear control method based on Lyapunov stability has been implemented. A classic SMC with a conventional switching function has been compared first with the results acquired using a boundary layer, that is a saturation function. Simulation studies have shown the capability of SMC with a boundary layer to solve the chattering problem, as it provided a smoother bounded control. However, the robustness against mismatch is not improved using such technique.

A fuzzy boundary layer using linguistic fuzzy rules versus the conventional sliding mode control was introduced. The results proved that FSMC is an effective method in reducing the number of switches in the control action without degrading any of the other performance indices. Fuzzy based rules played a role of applying a small or large control efforts to return the trajectories to the selected sliding manifold in case the trajectory leaves the sliding surface.

Finally, the robustness of FSMC against parametric uncertainties was dramatically improved using singleton method where the output variable was characterised by seven fuzzy singletons distributed over the interval [-1, 1].

Chapter 6

Optimization of the controller and observer parameters with Spiral Dynamic Algorithm

6.1 Introduction

Tamura and Yasuda (2011a) proposed an optimization algorithm the so-called Spiral Dynamic Algorithm (SDA) algorithm based on two dimensional metaheuristics logarithmic spiral phenomena. In their study, it is shown that SDA can more effectively produce solutions than Particle swarm optimization (PSO) in the problem of three types of 2-dimensional benchmark. In the same year, the design principle for two dimensional was used to developed n-dimensional optimization SDA algorithm ((Tamura and Yasuda, 2011b)). These algorithms have been inspired by natural motion of the spiral such as hurricanes, spiral galaxies, nautilus shells and whirling currents (some of the motion are shown in Figure 6.1). The strength of this algorithm is referred to its advantages, that is, SDA has a powerful capacity in local search, fast convergence toward a solution. The algorithm has few control variables and it is easy to implement (Benasla et al., 2014).

6.2 Spiral dynamic algorithm

In the search space, SDA utilizes a dynamic step size to provide the motion from one location to another. The search points spread out in the search space in the way they spirally move toward the centre form the outermost layer. Diversification with a large

step size would occur at the beginning of a search point then this step size gets smaller and smaller while the search point converges toward the spiral centre as the number of iterations increases. Figure 6.1 shows some spiral shapes and highlights the continuous reduction in the step size according to different spiral radius values, r, and rotation angle, θ.

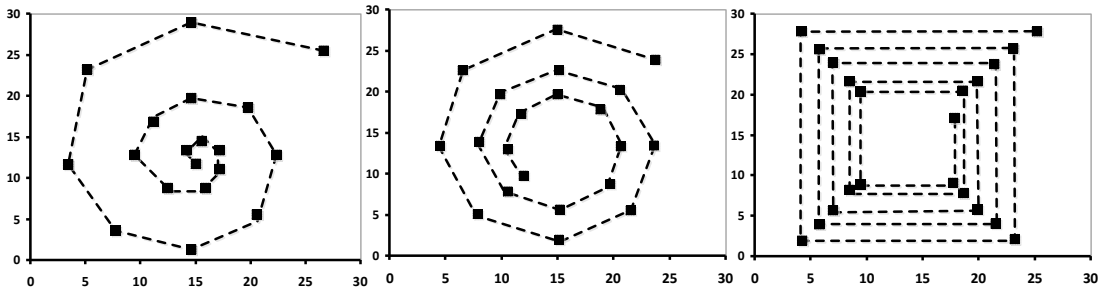

(a) Case 1 (b) Case 2 (c) Case 3

Figure 6.1: Graphical representation of spiral model

The spiral radius r and the rotation angle θ can be considered as crucial parameters as the accuracy and convergence speed of this algorithm mainly depends on the selection of values for these parameters. Figure is adapted from (Tamura and Yasuda, 2011a), where in case 1: $r = 0.9$ and $\theta = \pi/4$, case 2: $r = 0.95$ and $\theta = \pi/4$ and case 3: $r = 0.9$ and $\theta = \pi/2$. The value of rotation angle must lie on the range of 0 to 2π around the origin at each k, while the range of the spiral radius should be within the range of 0 to 1 which represent the convergence rate of the displacement between the search point and the origin at each k.

The spiral radius can be expressed in the dynamic formulation as (Tamura and Yasuda, 2012):

$$x_i(k+1) = S_n(r,\theta)x_i(k) - (S_n(r,\theta) - I_n) \tag{6.1}$$

$$S_n = r\,R^n \tag{6.2}$$

where x represents the coordinate location of the search point, while k represents the iteration number. Table 6.1 describes the rest of notations and parameters of the n-dimensional SDA.

Table 6.1: Spiral dynamic algorithm variables

Symboles	Description
x^*	Spiral centroid point
$x_i(k)$	Position of i_{th} point in k_{th} generation
r	Convergence rate or spiral radius
$\theta_{i,j}$	Rotation angle in the range of $0 \leq \theta \leq 2\pi$
m	Maximum number of search points
R^n	Composition of rotation matrix $n \times n$ in search space base on combination of 2 axes
S^n	Multiplication of a composition of rotational $n \times n$ matrix R^n and radius r
k_{max}	Maximum number of iterations

For n-dimensional SDA, a rotation matrix can be defined as

$$R^n_{i,j}(\theta_{i,j}) = \begin{bmatrix} 1 & & & & & & & & \\ & \ddots & & & & & & & \\ & & 1 & & & & & & \\ & & & cos\theta_{i,j} & \cdots & -sin\theta_{i,j} & & & \\ & & & & 1 & & & & \\ & & & \vdots & \ddots & \vdots & & & \\ & & & & & 1 & & & \\ & & & sin\theta_{i,j} & & cos\theta_{i,j} & & & \\ & & & & & & 1 & & \\ & & & & & & & \ddots & \\ & & & & & & & & 1 \end{bmatrix} \tag{6.3}$$

The objective function, $f(x_i(k))$ is calculated using the corresponding flow chart depicted in Figure 6.2

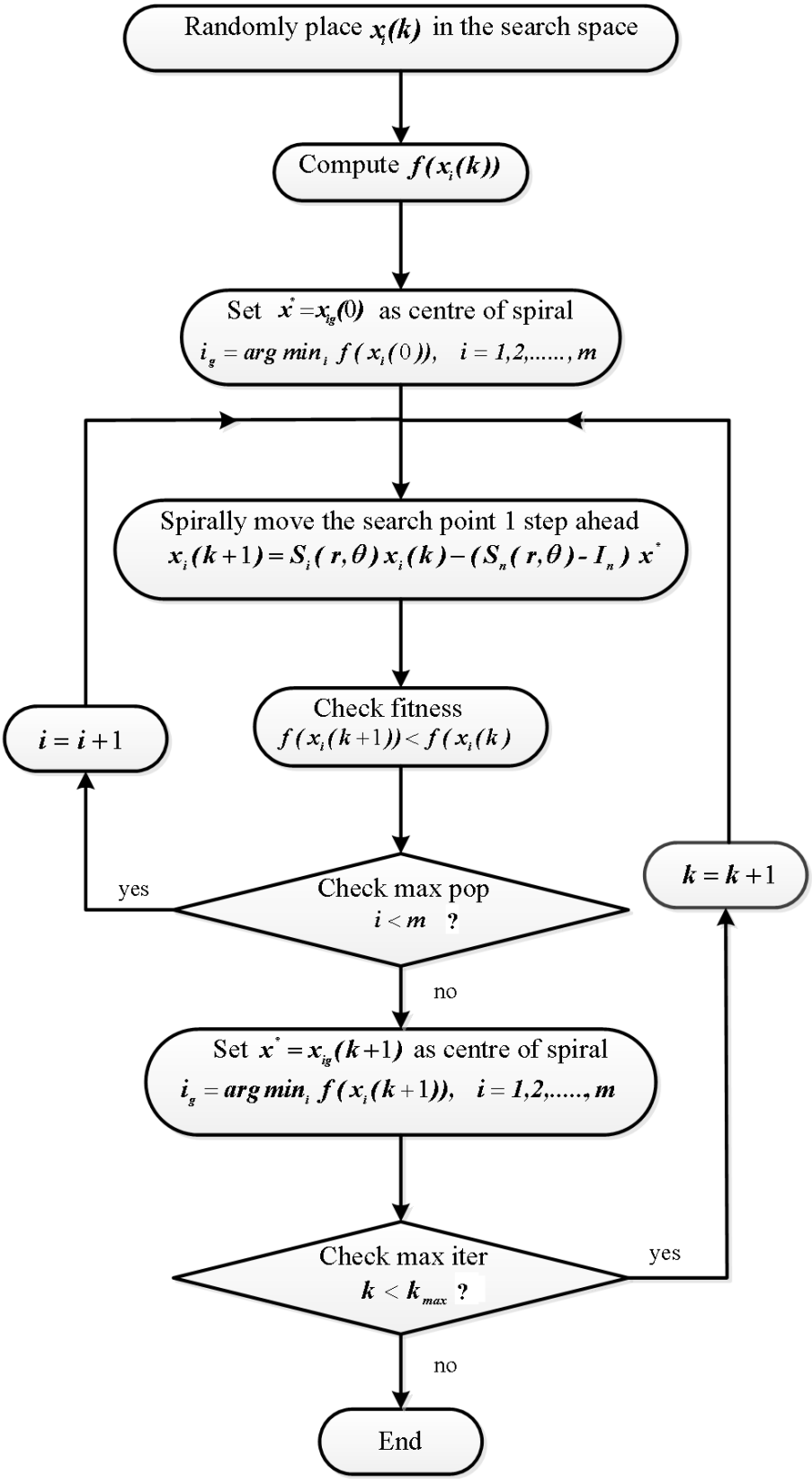

Figure 6.2: SDA flow chart operation

The Pseudo code of the n-dimensional algorithm programmed by Tamura and Yasuda (2011a) can be described by the steps shown below

- Step 0: Preparation

  Set the optimization parameters, number of search points $m \geq 2$, angle $0 \leq \theta \leq 2\pi$, radius $0 < r < 1$ and maximum number of iterations K_{max}.

- Step 1: Initialization

  Initial points to be set randomly to $x_i(k+1) = S_n(r,\theta)x_i(k) - (S_n(r,\theta) - I_n)$

  Set spiral centre point to $x^* = x_{i_g}(0)$, where $i_g = argmin_i f(x_1(0))$ and $i = 1, 2, ..., m$

- Step 2: Updating x_i

  $x_i(k+1) = S_n(r,\theta)\, x_i(k) - (S_n(r,\theta) - I_n)\, x^*$ and $i = 1, 2, ..., m$

- Step 3: Updating x^* $x^* = x_{i_g}(k+1)$,

  $i_g = argmin_i f(x_1(k+1))$

- Step 4: Checking iteration limit Terminate if $k = k_{max}$.

  Otherwise $k = k + 1$ and return to step 2.

In this optimization, the radius r was set to the value of 0.95 and the rotational angle was chosen to be $\pi/4$ to perform the trajectories of the spiral dynamics. The objective or fitness function of SDA is selected in such a way to reduce the error of the object position to as minimum as possible. The performance index of this optimization was the Mean square error (MSE) as follows

$$MSE = \sqrt{\frac{1}{n}\sum_{i=1}^{n}(e)^2} \tag{6.4}$$

In general, optimization can be performed to guarantee reduction of the overall error, which is represented by the summation of weighted multivariate MSE of the processes

optimization as

$$Costfunction = w_1\, MSE_1 + w_2\, MSE_2 + ... + w_q\, MSE_q \tag{6.5}$$

where q represents the total number of the optimized errors and $w_1, w_2, ...$ and w_n are the weighting factors that can take any value within the range of 0 to 1.

6.3 Simulation results

6.3.1 Optimisation of LQi-Feedback linearisation

The control strategy for magnetic levitation system is to stabilize the object (regulation problem since the system is unstable) using three feedback gains (K) and then track the provided reference using feedforward gains (proportional gain K_r and integral gain K_i). Figure 6.3 illustrates the control gains to be optimized using SDA as an optimization algorithm. This implies to optimize four gains of main diagonal of the state weighting matrix, that is $Q_z = diag(V1\,V2\,V3\,V4)$, and the control penalize gain of the control weighting matrix of $Q_w = V5$. The cost function is to minimize the MSE of the position tracking error which can be expressed as

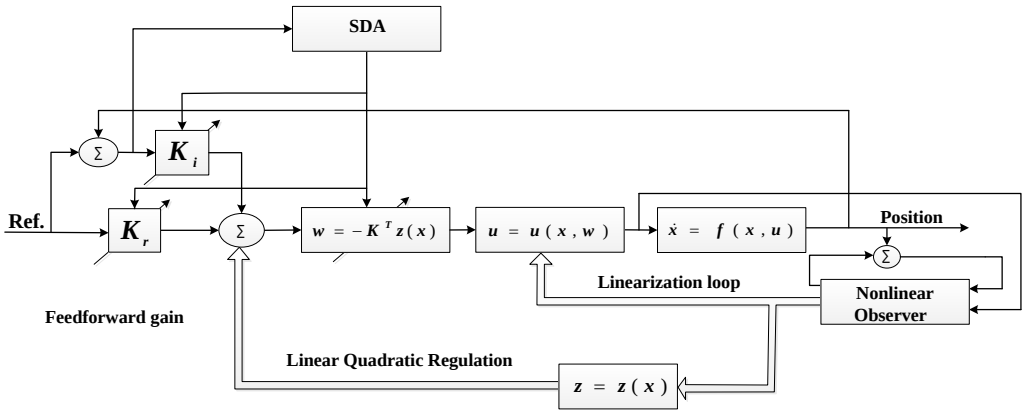

Figure 6.3: Optmization of LQi-feedback linearisation

$$MSE = \sqrt{\frac{1}{n}\sum_{i=1}^{n}(Ref. - x_1)^2} \tag{6.6}$$

where n is dimension of search space, $Ref.$ is the given reference or set-point and x_1 is measured position of the object.

In the SDA implementation process, initially a wide range was assigned for the tuning parameters as shown in Table 6.2 and the number of the search points was only 5 while iteration was 15. One solution selected among several potential solutions, was assessed on this optimization problem of tracking a step input with initial value of 0.015 m for 1.5 s then step up to the value of 0.03 for another 1.5 s. Figure 6.4 shows the SDA fitness cost function for Opt 1

Table 6.2: Optimization range for tuning parameters of LQi-feedback linearisation for Opt 1

	Value	
Gain	minimum	maximum
V_1	10	1×10^6
V_2	1	1×10^4
V_3	1	1×10^4
V_4	1×10^2	1×10^7
V_5	9×10^{-6}	1×10^{-2}

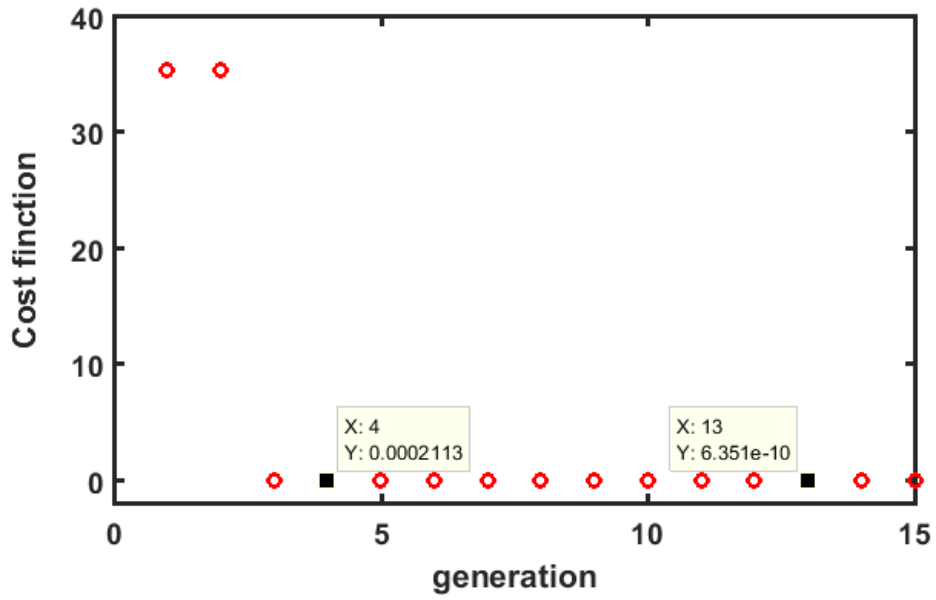

Figure 6.4: SDA fitness cost function for Opt 1 for LQi-feedback linearisation

The best estimated tuned gains were used to modify the range of the search space that was used for optimization trial Opt 2 and Opt 3 as shown in Table 6.3. Number of the search points was 20 and the number of iterations was 50 for Opt 2 while these were 100 and 500 respectively for Opt 3. The resultant optimization gains for state and control

weighting matrix were as mentioned previously in chapter 4 in Table 4.4. A comparison of system response and control efforts for the proposed LQi-feedback linearisation is shown in Figures 4.16 and 4.17 respectively.

Table 6.3: Modified optimization range of tuning parameters of LQi-feedback linearisation for Opt 2 and Opt 3

	Value	
Gain	minimum	maximum
V_1	2.7094×10^5	2.7094×10^7
V_2	6900	10000
V_3	1	10
V_4	4.4324×10^7	9×10^9
V_5	9×10^{-6}	9×10^{-3}

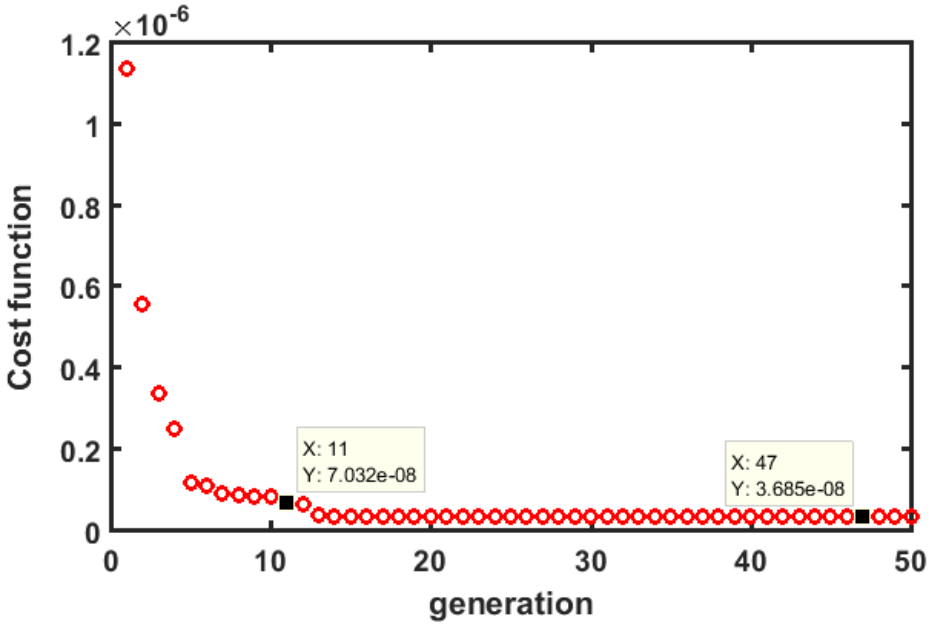

Figure 6.5: SDA fitness cost function for Opt 2 for LQi-feedback linearisation

6.3.2 LQi-feedback linearisation results using SDA versus IWO

To illustrate the efficiency of the SDA optimization algorithm, a comparison was carried out between SDA and Invasive weed optimization (IWO) to find the best solution for this optimization problem. The IWO algorithms is inspired by the growth phenomena of weeds

(Karimkashi and Kishk, 2010). In both optimization algorithm, the same number of search points and generations were used in both optimizations for feasibility and reliability. Table 6.4 shows the optimized gains for the proposed LQi-feedback linearisation obtained using SDA and IWO methods. Although IWO converged faster toward the minimum cost function, the obtained minimum cost function value using SDA (1.56×10^{-18}) was smaller than the one obtained with IWO (2.65×10^{-17}).

Table 6.4: Comparison of optimized LQi-feedback linearisation gains using SDA and IWO

Gain	SDA	IWO
K_1	1.8659×10^5	7.7979×10^5
K_2	7.1656×10^3	2.3506×10^4
K_3	119.7134	273.4662
K_I	-2.2192×10^6	-9.6470×10^6
K_r	0	0

As it can be seen in Figure 6.6, the optimized controller using SDA achieved a faster response than the controller using IWO. The response with SDA based controller settled in 0.197s and that with IWO based controller settled in 0.652 s. Moreover, the percentage overshoot was 5.06% using SDA against 21.26% when IWO was used. The rise time of SDA based system response is less than the one for IWO's response. Table 6.5 compares the performance indices using SDA and IWO.

Table 6.5: Performance indices for LQi-linearisation using SDA Vs. IWO

Performance index	SDA	IWO
Percentage overshoot (%)	5.06	21.26
Peak time (s)	**1.181**	**1.169**
Rise time (s)	**0.084**	**0.070**
Settling time (s)	0.197	0.652

Figure 6.7 shows the control action of LQi-feedback linearisation. It can be seen that the control effort using SDA was smoother than using IWO; the standard deviation of control effort using IWO was twice as much as using SDA, that is 4.3057 against 2.5714.

Furthermore, the power consumed using the SDA optimized controller was two thirds of the power consumption with the IWO optimized controller; the steady state voltage with IWO based system was around 11.2 compared that with SDA based system, which was around 7.21.

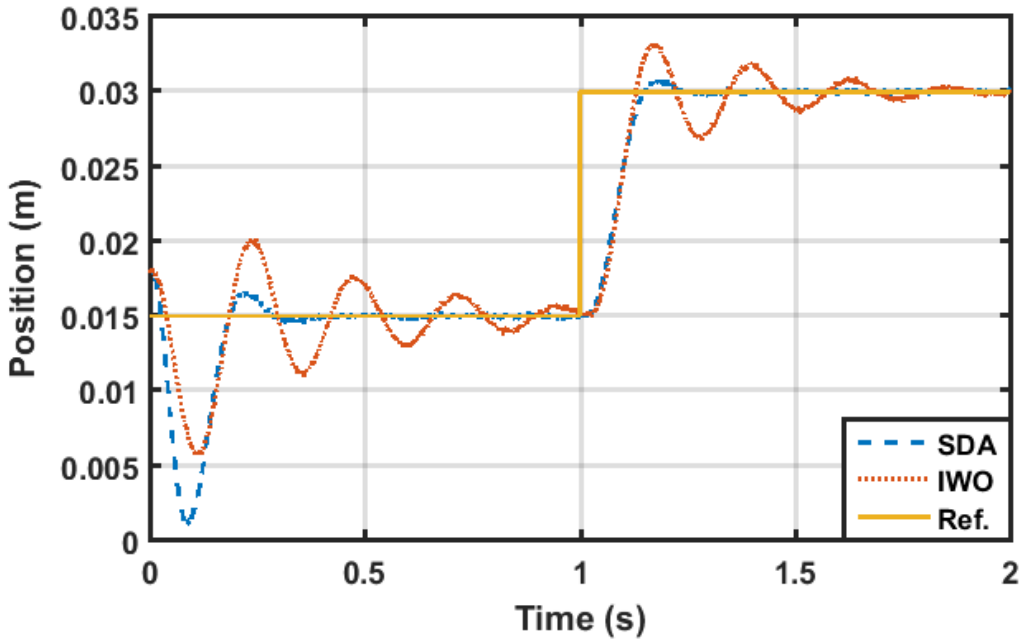

Figure 6.6: LQi-feedback linearisation response using SDA against IWO

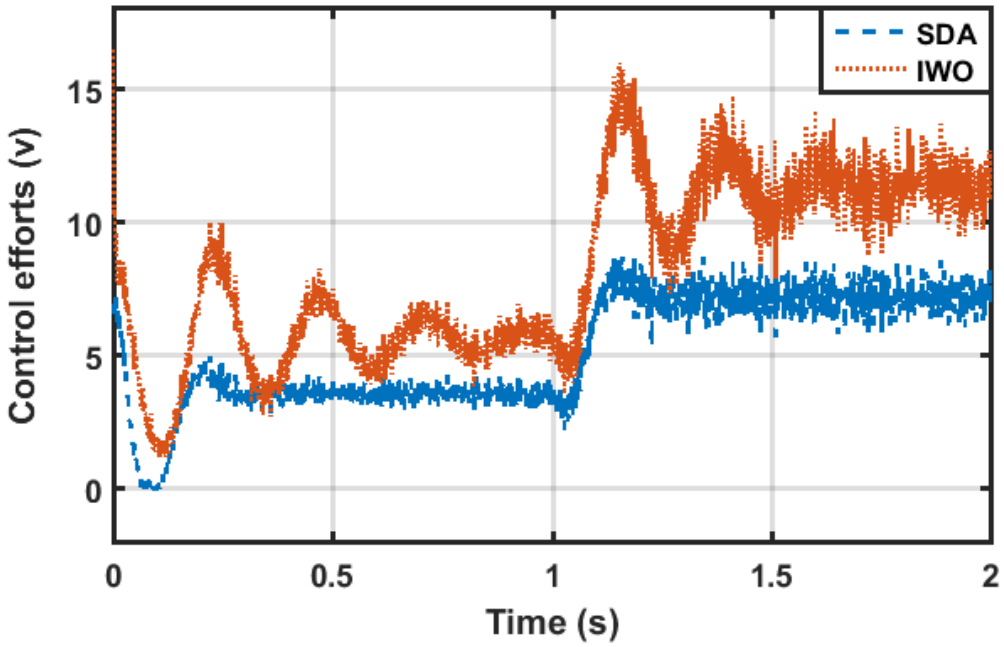

Figure 6.7: LQi-feedback linearisation control efforts using SDA against IWO

6.3.3 Optimization of fuzzy sliding mode control

In this section, SDA is used to optimize fuzzy sliding mode control for Maglev system. Figure 6.8 illustrates the control gains to be optimized. The parameters to be tuned are sliding constants of the sliding surface in equation (5.6), that is s_1 and s_2 where $s_2 = 2\sqrt{s_1}$, and the scaling factors of the fuzzy sliding mode control G_s and G_u. Here, Non-linear high-gain observer (NHGO) is used to estimate the full states with observer gain $a = 30$ and $\epsilon = 0.5$.

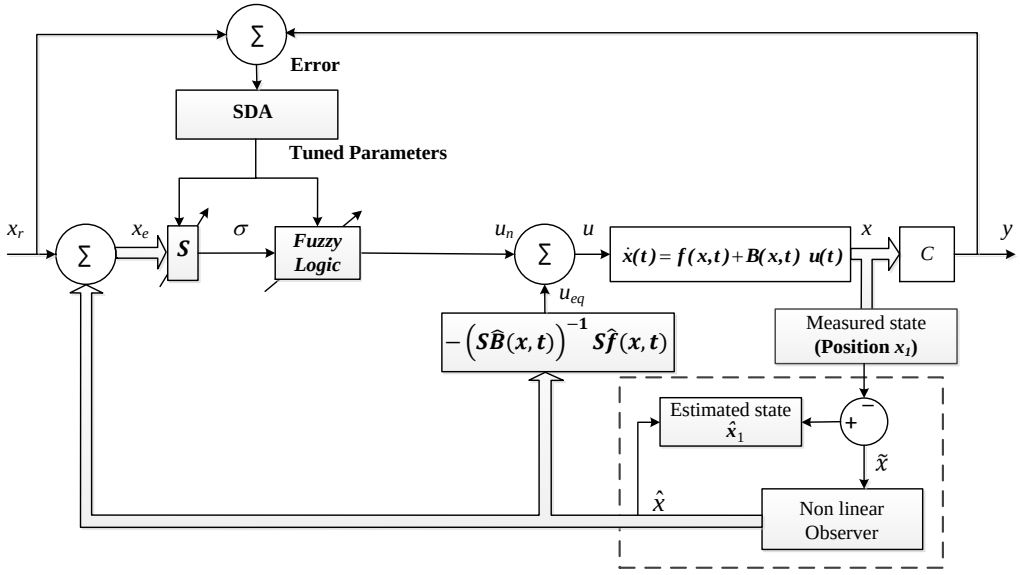

Figure 6.8: Optmization of Fuzzy sliding mode controller (FSMC)

In the SDA process, the range for the tuned parameters was modified after many trials as shown in the Table 6.6. One selected solution among several potential solutions was assessed on the optimization problem of tracking a step input with initial value of 0.018 m for 1.5 s then step down to the value of 0.015 for another 1.5 s. Number of search points was 30 while iteration was 120 for the selected results. The initial conditions were [0.018, 0 , 0.9039] for both the observer and for the mathematical model of Maglev system.

Table 6.6: Optimization range of tuning parameters of FSMC using SDA

	Value	
Gain	minimum	maximum
G_s	2×10^{-3}	5×10^{-3}
G_u	900	1000
s_1	7000	7700

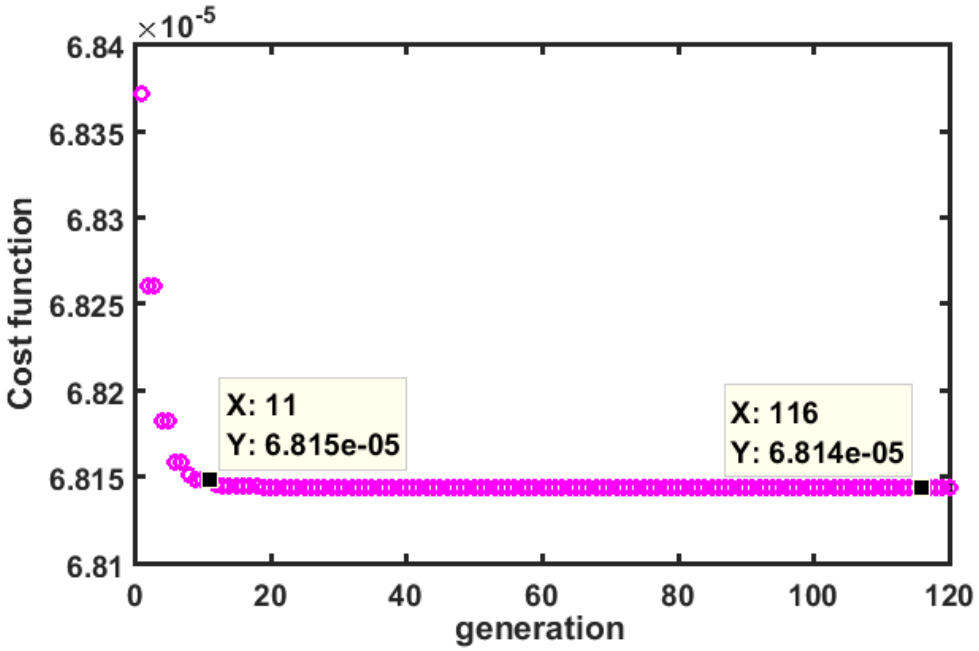

Figure 6.9: SDA fitness cost function for FSMC

6.3.4 FSMC using SDA versus IWO

The same number of search points and generation were used in both SDA and IWO. Although SDA converged faster toward the minimum cost function, where Elapsed time was 2119 s for SDA and 3228s for IWO. However, the obtained minimum cost function value using IWO (1.3624×10^{-5}) was smaller than the one obtained with SDA (6.8145×10^{-5}). Note that the measured position was corrupted by noise. Tuned parameters for the proposed FSMC obtained using SDA and IWO are summarized in Table 6.7.

Table 6.7: Comparison of FSMC gains using SDA and IWO

Gain	SDA	IWO
G_s	2×10^{-3}	6.7761×10^{-5}
G_u	901.5956	2.7092×10^{3}
s_1	7.6993×10^{3}	4.9808×10^{4}

As can be seen in Figure 6.10, the optimized controller using SDA resulted in faster response than the controller using IWO; the response of SDA optimised system settled in 0.175 s and that with IWO optimised system settled in 0.5 s. Moreover, the rise time was 0.056 s using SDA against 0.156 s when IWO was used. However, the steady state error of the tuned FSMC using IWO was less than that using SDA. Table 6.8 compares the performance indices for FSMC using SDA and IWO.

Table 6.8: Performance indices for FSMC response using SDA Vs. IWO

Performance index	SDA	IWO
Percentage overshoot (%)	0	0
Steady state error (m)	1.1×10^{-4}	$\mathbf{2 \times 10^{-5}}$
Rise time (s)	0.056	0.156
Settling time (s)	0.175	0.500

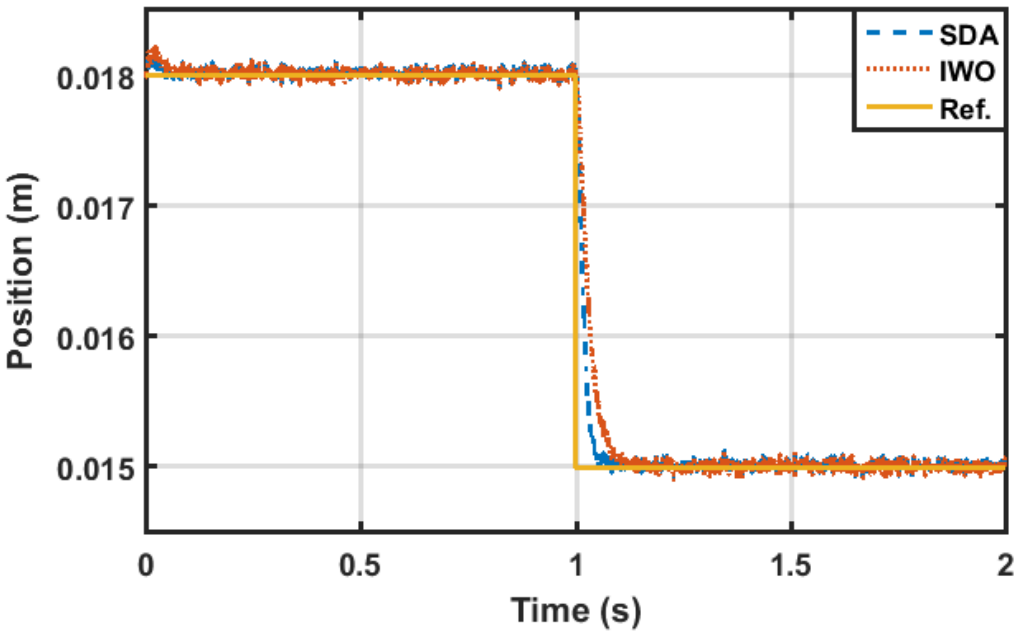

Figure 6.10: FSMC response using SDA against IWO

Figure 6.11 shows the control action of FSMC optimised with SDA and IWO. It can be seen that the control efforts were close to each other with the IWO based effort slightly smoother than using SDA; the standard deviation of control effort of IWO was 0.4906 against 0.5316 for SDA.

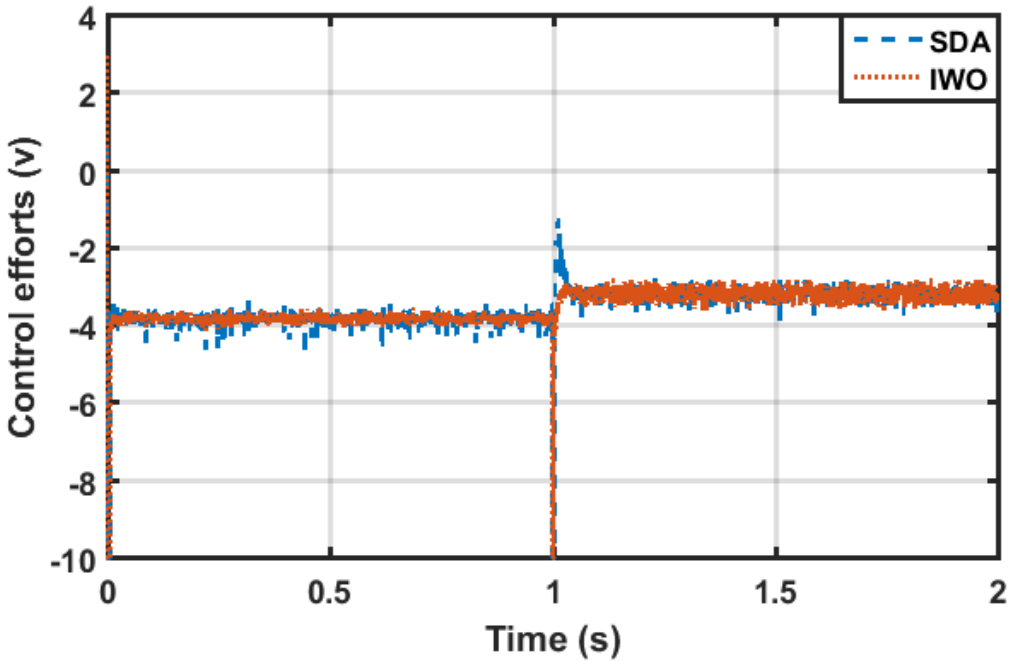

Figure 6.11: FSMC control efforts using SDA against IWO

6.4 Summary

The SDA optimization algorithm mainly used in this research has been presented. The methodology of this algorithm has been discussed first by providing the Pseudo code of the n-dimensional problem reported by Tamura and Yasuda (2011b).

SDA based optimization approach for controlling Maglev system using two types of observer-based non-linear control, namely LQi-linearisation and fuzzy sliding mode control has been presented. A comparative assessment of optimised system responses and control efforts using SDA and IWO has been carried out showing superiority of SDA.

Chapter 7

Conclusion and future works

7.1 Conclusion

A literature review has been conducted in detail to gain knowledge of state of the art in magnetic levitation systems and their applications. Since a Maglev system is a highly non-linear unstable system, it is necessary to focus on understanding the non-linear observer-based controlling methods and any relative work done to resolve the current problem. In this work, a new simplified version of an optimized non-linear observer-based control has been proposed to overcome the non-linearity problem and to improve the robustness and enhance the performance to ensure the system works in a wide operation range.

In continuous-time design, the state variable vector for Maglev system contains the derivative of the position signal. Generally, these signals are noisy, that is why differentiation of the state variable has been avoided as derivative operation would amplify the noise. In this work, two types of non-linear observer have been proposed to tackle this point and to make all state variables available for the optimal control approach. Simulation experiments highlight the trade off between the bandwidth and noise-sensitivity. Linear gain of the non-linear high gain observer has been carefully tuned to balance between inclination of noise rejection and serious degradation in the performance, as the sensitivity of the system to the noise is less with lower value of linear gain to the limit where the system performance becomes worse. Furthermore, the simulation results of the fuzzy sliding mode observer have highlighted the improvements of the observer's robustness compared

to the sliding mode observer without fuzzy logic.

Optimal control LQR based on full-state feedback has been proposed in this work to stabilize the transformed linear system where all state variables have been estimated using non-linear high gain observer. Computer simulation results have shown that using integral action in feedforward path could improve the robustness in the presence of parameter mismatch as compared to using static feed-forward gain, where steady-state error has been introduced in presence of mass uncertainty. Optimization algorithm (ISDA) was used to optimize the controller parameters. It has been shown that the new closed-loop system with integral action has the ability to maintain stable suspension well and to suppress the disturbance caused by noise or parameter mismatch.

SMC based on Lyaponov stability has been implemented. The chattering phnomenon, which refers to oscillations with finite frequency and amplitude in the discontinuous control law, around the sliding surface is considered as a common problem of using conventional switching function in SMC. A fuzzy boundary layer using linguistic fuzzy rules has been introduced as a solution to eliminate the chattering. FSMC is an effective method in reducing the number of switching in the provided control action without degradation in the performance. The robustness of FSMC in the presence of parameter uncertainties has been dramatically improved using singleton method where the output variable has been characterised by seven fuzzy singletons distributed over the interval [-1, 1].

SDA based optimization approach for controlling Maglev system using two types of observer-based non-linear control, namely LQi-linearisation and fuzzy sliding mode control has been presented. A comparative assessment of optimised system responses and control efforts using SDA and IWO has been carried out showing superiority of SDA.

7.2 Recommendation for future works

- In this work, fuzzy boundary layer was introduced as a solution to eliminate the chattering in SMC. Further consideration of fuzzy control parameters such as the parameters of the fuzzy membership function with optimisation may result in enhanced performance of the system and achieve optimal results.

- Some of the system characteristics in time-domain are in conflict with each other. That is, whether to speed up the response and end up with an overshoot or having less overshoot and slow down the performance. Multi objective optimization techniques may be suggested to separately define the conflicted characteristics into standalone objective or different error functions.

- Multi objective optimization would be an appropriate solution to provide a set of solutions to balance between fast response and having smoother control action.

- The implementation of the process on real-world hardware or real-time targets can be carried out to verify the proposed model and controller, that is by applying modelling standards to the real-time hardware verification to make sure of errors that introduced in the development earlier are reduced.

References

Adekanle, O., Guisser, M., Abdelmounim, E., and Aboulfatah, M. (2017). Integral backstepping controller combined with high gain observer for the optimization of grid-connected doubly-fed induction generator. In *2017 International Conference on Wireless Technologies, Embedded and Intelligent Systems (WITS)*, pages 1–7.

Ahsan, M., Masood, N., and Wali, F. (2013). Control of a magnetic levitation system using non-linear robust design tools. In *2013 3rd IEEE International Conference on Computer, Control and Communication (IC4)*, pages 1–6.

Al-Muthairi, N. and Zribi, M. (2004). Sliding mode control of a magnetic levitation system. *Mathematical Problems in Engineering*, 2004(2):93–107.

Allaire, P., Maslen, E., Kim, H., Bearnson, G., and Olsen, D. (1996). Design of a magnetic bearing-supported prototype centrifugal artificial heart pump. *Tribology transactions*, 39(3):663–669.

Alvarez-Ramirez, J., Morales, A., and Cervantes, I. (1998). Robust proportional- integral control. *Industrial & engineering chemistry research*, 37(12):4740–4747.

Aravind, C., Rajparthiban, R., Rajprasad, R., and Wong, Y. (2012). A novel magnetic levitation assisted vertical axis wind turbine—design procedure and analysis. In *Signal Processing and its Applications (CSPA), 2012 IEEE 8th International Colloquium on*, pages 93–98. IEEE.

Atassi, A. N. and Khalil, H. K. (2001). A separation principle for the control of a class of nonlinear systems. *IEEE Transactions on Automatic Control*, 46(5):742–746.

Baranowski, J. and Piatek, P. (2008). Nonlinear dynamical feedback for motion control of magnetic levitation system. In *Power Electronics and Motion Control Conference, 2008. EPE-PEMC 2008. 13th*, pages 1446–1453. IEEE.

Barie, W. and Chiasson, J. (1996). Linear and nonlinear state-space controllers for magnetic levitation. *International Journal of systems science*, 27(11):1153–1163.

Bassani, R. (2011). A passive maglev vehicle with self-regulating aerostatic-aerodynamic pads. *International Journal of Heavy Vehicle Systems*, 18(4):359–389.

Baumann, W. and Rugh, W. (1986). Feedback control of nonlinear systems by extended linearization. *IEEE Transactions on Automatic Control*, 31(1):40–46.

Benallegue, A., Mokhtari, A., and Fridman, L. (2008). High-order sliding-mode observer for a quadrotor uav. *International journal of robust and nonlinear control*, 18(4-5):427–440.

Benasla, L., Belmadani, A., and Rahli, M. (2014). Spiral optimization algorithm for solving combined economic and emission dispatch. *International Journal of Electrical Power & Energy Systems*, 62:163–174.

Bethoux, O., Floquet, T., and Barbot, J. P. (2003). Advanced sliding mode stabilization of a levitation system. In *2003 European Control Conference (ECC)*, pages 501–506.

Bleuler, H., Cole, M., Keogh, P., Larsonneur, R., Maslen, E., Okada, Y., Schweitzer, G., Traxler, A., Schweitzer, G., Maslen, E. H., et al. (2009). *Magnetic bearings: theory, design, and application to rotating machinery*. Springer Science & Business Media.

Chen, C., Paden, B., Antaki, J., Ludlow, J., Paden, D., Crowson, R., and Bearnson, G. (2002). A magnetic suspension theory and its application to the heartquest ventricular assist device. *Artificial Organs*, 26(11):947–951.

Chen, S. L. and Hsiao, Y. H. (2011). Nonlinear high-gain observer for a three-pole active magnetic bearing system. In *2011 8th Asian Control Conference (ASCC)*, pages 155–159.

Chen, Y.-Y. and Perng, C.-F. (1994). Input scaling factors in fuzzy control systems. In *Proceedings of 1994 IEEE 3rd International Fuzzy Systems Conference*, pages 1666–1670 vol.3.

Cho, D., Kato, Y., and Spilman, D. (1993). Sliding mode and classical controllers in magnetic levitation systems. *IEEE control systems*, 13(1):42–48.

Clark, D. J., Jansen, M. J., and Montague, G. T. (2004). An overview of magnetic bearing technology for gas turbine engines.

Cole, M. O., Keogh, P. S., Sahinkaya, M. N., and Burrows, C. R. (2002). Progress towards fault tolerant active control of rotor-magnetic bearing systems. *Department of Mechanical Engineering, University of Bath, UK*.

DeCarlo, R., Zak, S. H., Matthews, G. P., et al. (1988). Variable structure control of nonlinear multivariable systems: a tutorial. *Proceedings of the IEEE*, 76(3):212–232.

Doyle, J. and Stein, G. (1979). Robustness with observers. *IEEE Transactions on Automatic Control*, 24(4):607–611.

Drakunov, S. V. (1983). An adaptive quasioptimal filter with discontinuous parameters. *Avtomatika i Telemekhanika*, (9):76–86.

Drakunov, S. V. (1992). Sliding-mode observers based on equivalent control method. In *Decision and Control, 1992., Proceedings of the 31st IEEE Conference on*, pages 2368–2369. IEEE.

Du, J., Hu, X., Liu, H., and Chen, C. L. P. (2015). Adaptive robust output feedback control for a marine dynamic positioning system based on a high-gain observer. *IEEE Transactions on Neural Networks and Learning Systems*, 26(11):2775–2786.

Edwards, C. and Spurgeon, S. (1998). *Sliding mode control: theory and applications*. Crc Press.

Emelyanov, S. (1967). Variable structure control systems. *Moscow, Nouka*.

Emelyanov, S. (1970). Automatic control systems with variable structure. Technical report, DTIC Document.

Emelyanov, S. and Taran, V. (1963). On design of variable structure control systems for control of linear plants. *Eng. Cybern.*, (2):69–78.

Erbatur, K., Vinter, R. B., and Kaynak, O. (1994). Feedback linearization control for a 3-dof flexible joint elbow manipulator. In *Proceedings of the 1994 IEEE International Conference on Robotics and Automation*, pages 2979–2984 vol.4.

Esfandiari, F. and Khalil, H. (1987). Observer-based design of uncertain systems: recovering state feedback robustness under matching conditions. In *Proc. Allerton Conf*, pages 97–106.

Esfandiari, F. and Khalil, H. K. (1992). Output feedback stabilization of fully linearizable systems. *International Journal of control*, 56(5):1007–1037.

Field, R. and Iannello, V. (1998). A reliable magnetic bearing system for turbomachinery. In *Proceedings of the 6th ISMB*, pages 42–51.

Firdaus, A. R. and Tokhi, M. O. (2015). Robust sliding mode - based interval type-2 fuzzy logic observer for quadcopter uavs. In *2015 19th International Conference on System Theory, Control and Computing (ICSTCC)*, pages 559–564.

Firdaus, A. R. and Tokhi, M. O. (2016). Sliding mode control-based interval type-2 fuzzy logic controller for quadcopter uavs. In *ASSISTIVE ROBOTICS: Proceedings of the 18th International Conference on CLAWAR 2015*, pages 555–563. World Scientific.

Gao, W., Wang, Y., and Homaifa, A. (1995). Discrete-time variable structure control systems. *IEEE transactions on Industrial Electronics*, 42(2):117–122.

Goel, A. and Swarup, A. (2016). A novel high-order sliding mode control of magnetic levitation system. In *2016 IEEE 59th International Midwest Symposium on Circuits and Systems (MWSCAS)*, pages 1–4.

Gosiewski, Z. and Mystkowski, A. (2008). Robust control of active magnetic suspension: analytical and experimental results. *Mechanical Systems and Signal Processing*, 22(6):1297–1303.

Ha, Q. P., Nguyen, Q. H., Rye, D. C., and Durrant-Whyte, H. F. (2001). Fuzzy sliding-mode controllers with applications. *IEEE Transactions on Industrial Electronics*, 48(1):38–46.

Hagiwara, M., Kawahara, T., Iijima, T., Yamanishi, Y., and Arai, F. (2012). High speed microrobot actuation in a microfluidic chip by levitated structure with riblet surface. In *Robotics and Automation (ICRA), 2012 IEEE International Conference on*, pages 2517–2522. IEEE.

Haisheng, G. and Jinkun, L. (2012). Sliding mode control for vtol aircraft based on high-gain observer. In *2012 Second International Conference on Instrumentation, Measurement, Computer, Communication and Control*, pages 305–309.

Halas, J. (2001). Development of a control circuit for a radial active magnetic bearing. *Periodica Polytechnica. Engineering. Mechanical Engineering*, 45(1):17.

Hassrizal, H. B. and Rossiter, J. A. (2016). A survey of control strategies for spacecraft attitude and orientation. In *2016 UKACC 11th International Conference on Control (CONTROL)*, pages 1–6.

Hedrick, J. and Girard, A. (2005). Control of nonlinear dynamic systems: Theory and applications. *Controllability and observability of Nonlinear Systems*, page 48.

Heredia, J. A. and Yu, W. (2000). A high-gain observer-based pd control for robot manipulator. In *Proceedings of the 2000 American Control Conference. ACC (IEEE Cat. No.00CH36334)*, volume 4, pages 2518–2522 vol.4.

Hong, S.-K. and Langari, R. (2000). Robust fuzzy control of a magnetic bearing system subject to harmonic disturbances. *IEEE Transactions on Control Systems Technology*, 8(2):366–371.

Hung, J. Y., Gao, W., and Hung, J. C. (1993). Variable structure control: a survey. *IEEE Transactions on Industrial Electronics*, 40(1):2–22.

Jang, S.-M., Park, Y.-S., Sung, S.-Y., Lee, K.-B., Cho, H.-W., and You, D.-J. (2011). Dynamic characteristics of a linear induction motor for predicting operating performance of magnetic levitation vehicles based on electromagnetic field theory. *Magnetics, IEEE Transactions on*, 47(10):3673–3676.

Kachroo, P. and Tomizuka, M. (1996). Chattering reduction and error convergence in the sliding-mode control of a class of nonlinear systems. *IEEE Transactions on Automatic Control*, 41(7):1063–1068.

Kalman, R. E., Falb, P. L., and Arbib, M. A. (1969). *Topics in mathematical system theory*, volume 1. McGraw-Hill New York.

Karimkashi, S. and Kishk, A. A. (2010). Invasive weed optimization and its features in electromagnetics. *IEEE Transactions on Antennas and Propagation*, 58(4):1269–1278.

Katayama, H. and Oshima, T. (2011). Stabilization of a magnetic levitation system by backstepping and high-gain observers. In *SICE Annual Conference 2011*, pages 754–759.

Kazadi, S., Koh, C.-H., Kim, K., Jung, K., Kim, B., and Wang, H. (2008). The e-axle and its application to a floating windmill. In *World Congress on Engineering and Computer Science 2008, WCECS'08. Advances in Electrical and Electronics Engineering-IAENG Special Edition of the*, pages 175–181. IEEE.

Keller, H. (1987). Non-linear observer design by transformation into a generalized observer canonical form. *International Journal of Control*, 46(6):1915–1930.

Khalil, H. K. (2008). High-gain observers in nonlinear feedback control. In *Control, Automation and Systems, 2008. ICCAS 2008. International Conference on*, pages xlvii–lvii. IEEE.

Khalil, H. K. (2015). High-gain observers in nonlinear feedback control.

Khalil, H. K. (2017). High-gain observers in feedback control: Application to permanent magnet synchronous motors. *IEEE Control Systems*, 37(3):25–41.

Khalil, H. K. and Praly, L. (2014). High-gain observers in nonlinear feedback control. *International Journal of Robust and Nonlinear Control*, 24(6):993–1015.

Knospe, C. R., Hope, R. W., Fedigan, S. J., and Williams, R. D. (1995). Experiments in the control of unbalance response using magnetic bearings. *Mechatronics*, 5(4):385–400.

Kou, S. R., Elliott, D. L., and Tarn, T. J. (1975). Exponential observers for nonlinear dynamic systems. *Information and control*, 29(3):204–216.

Kumar, N., Chatterjee, D., Gupta, A., and Mazumder, S. K. (2017). State observer design for a high frequency distributed power system. In *2017 IEEE Applied Power Electronics Conference and Exposition (APEC)*, pages 3541–3548.

Kumbernuss, J., Jian, C., Wang, J., Yang, H., and Fu, W. (2012). A novel magnetic levitated bearing system for vertical axis wind turbines (vawt). *Applied Energy*, 90(1):148–153.

Kwatny, H. and Siu, T. (1987). Chattering in variable structure feedback systems. In *Proceedings of the 10th World Congress of the International Federation on Automatic Control (IFAC)*, volume 8, pages 307–314.

Lahdhiri, T. and Alouani, A. (1995). Nonlinear stabilizing controller for a single machine infinite-bus power system. In *Control Applications, 1995., Proceedings of the 4th IEEE Conference on*, pages 1014–1019. IEEE.

Levant, A. (2003). Introduction to high-order sliding modes. *School of Mathematical Sciences, Israel*, 58(6):1.

Li, D. and Gutierrez, H. (2008). Observer-based sliding mode control of a 6-dof precision maglev positioning stage. In *2008 34th Annual Conference of IEEE Industrial Electronics*, pages 2562–2567.

Liebert, W. (1995). Performance evaluation of a fast digital fuzzy controller for an active magnetic bearing. In *Proceedings of the IEEE Applied Power Electronics Conference, Zurich, Switzerland*.

Liu, S., Li, D., and e Huang, C. (2012). Nonlinear robust control with high gain observer for governor of hydro-turbine generator sets. In *Proceedings of the 10th World Congress on Intelligent Control and Automation*, pages 2752–2757.

Mahmud, M., Pota, H., and Hossain, M. (2012). Full-order nonlinear observer-based excitation controller design for interconnected power systems via exact linearization approach. *International Journal of Electrical Power & Energy Systems*, 41(1):54–62.

Mehta, A. and Bandyopadhyay, B. (2015). Preliminaries of sliding mode control. In *Frequency-Shaped and Observer-Based Discrete-time Sliding Mode Control*, pages 9–25. Springer.

Mizuno, T., Araki, K., and Bleuler, H. (1996). Stability analysis of self-sensing magnetic bearing controllers. *IEEE transactions on control systems technology*, 4(5):572–579.

Munaro, C. et al. (2001). A design methodology of tracking controllers for magnetic levitation systems. In *Control Applications, 2001.(CCA'01). Proceedings of the 2001 IEEE International Conference on*, pages 47–51. IEEE.

Munaro, C. J., Borges, R., da Silva Munareto, S., da Costa, W., et al. (2002). Modeling and observer-based nonlinear control of a magnetic levitation system. In *Control Applications, 2002. Proceedings of the 2002 International Conference on*, volume 1, pages 162–167. IEEE.

Nasir, A. and Tokhi, M. (2015). An improved spiral dynamic optimization algorithm with engineering application. *Systems, Man, and Cybernetics: Systems, IEEE Transactions on*, PP(99).

Polinder, H., Van der Pijl, F. F., De Vilder, G.-J., and Tavner, P. J. (2006). Comparison of direct-drive and geared generator concepts for wind turbines. *IEEE Transactions on energy conversion*, 21(3):725–733.

Primbs, J. (1996). Survey of nonlinear observer design techniques. *Penn State Notes*, 1(1):1–18.

Romero Acero, A., Orozco Quiceno, J. A., Bulies, J., and Alberto, J. (2016). Modelling and simulation of lqr and lfsv controllers in the magnetic levitation system (mls). *Prospectiva*, 14(1):28–38.

Rosales, P., Cerezoa, J., Monteroa, G., and Lambertb, A. (2013). Comparative assessment of a horizontal small wind turbine with ball and magnetic bearings on the starting. *CHEMICAL ENGINEERING*, 34.

Saberi, A. and Sannuti, P. (1990). Observer design for loop transfer recovery and for uncertain dynamical systems. *IEEE Transactions on Automatic Control*, 35(8):878–897.

Shameli, E., Khamesee, M. B., and Huissoon, J. P. (2007). Nonlinear controller design for a magnetic levitation device. *Microsystem Technologies*, 13(8-10):831–835.

Shao, N., Li, H., Wu, X., and Li, G. (2015). Distributed containment control and state observer design for multi-agent robotic system. *International Journal of Modelling, Identification and Control*, 23(3):193–203.

Shi, J. and Lee, W. S. (2010). *Design and implementation of conventional and advanced controllers for magnetic bearing system stabilization*. INTECH Open Access Publisher.

Shrestha, G., Polinder, H., Bang, D., and Ferreira, J. (2017). Direct drive wind turbine generator with magnetic bearing. *Proceedings Offshore wind 2007*.

Shrestha, G., Polinder, H., Bang, D., Ferreira, J., and Mcdonald, A. (2008). A new concept for weight reduction of large direct drive machines. In *Electrical Machines, 2008. ICEM 2008. 18th International Conference on*, pages 1–6. IEEE.

Shrestha, G., Polinder, H., Bang, D.-J., and Ferreira, J. A. (2010). Structural flexibility: A solution for weight reduction of large direct-drive wind-turbine generators. *IEEE Transactions on Energy Conversion*, 25(3):732–740.

Shu, G. and Meisinger, R. (2011). State estimation and simulation of the magnetic levitation system of a high-speed maglev train. In *Proceedings of 2011 International Conference on Electronic Mechanical Engineering and Information Technology*, volume 2, pages 944–947.

Slotine, J.-J., Hedrick, J. K., and Misawa, E. (1986a). On sliding observers for nonlinear systems. In *American Control Conference, 1986*, pages 1794–1800. IEEE.

Slotine, J. J. E., Hedrick, J. K., and Misawa, E. A. (1986b). On sliding observers for nonlinear systems. In *1986 American Control Conference*, pages 1794–1800.

Slotine, J.-J. E., Li, W., et al. (1991). *Applied nonlinear control*, volume 199. Prentice-hall Englewood Cliffs, NJ.

Srivastava, Y. (2016). Seminar on magnetic levitation (maglev). Available online at `https://image.slidesharecdn.com/seminaronmagneticlevitationmaglav-161013095920/95/seminar-on-magnetic-levitation-maglav-8-638.jpg?cb=1476353076`, Last visited 2017-07-05.

Sun, Y., Li, W., and Qiang, H. (2016). The design and realization of magnetic suspension controller of low-speed maglev train. In *2016 IEEE/SICE International Symposium on System Integration (SII)*, pages 1–6.

Tamura, K. and Yasuda, K. (2011a). Primary study of spiral dynamics inspired optimization. *IEEJ Transactions on Electrical and Electronic Engineering*, 6(S1).

Tamura, K. and Yasuda, K. (2011b). Spiral dynamics inspired optimization. *Journal of Advanced Computational Intelligence and Intelligent Informatics*, 15(8):1116–1122.

Tamura, K. and Yasuda, K. (2012). Quantitative analysis based tuning law for convergence rate of spiral optimization. In *Systems, Man, and Cybernetics (SMC), 2012 IEEE International Conference on*, pages 767–772. IEEE.

Thau, F. (1973). Observing the state of non-linear dynamic systems. *International journal of control*, 17(3):471–479.

Uswarman, R., Cahyadi, A. I., and Wahyunggoro, O. (2014). Design and implementation of a magnetic levitation system controller using global sliding mode control. *Journal of Mechatronics, Electrical Power, and Vehicular Technology*, 5(1):17–26.

Utkin, V., Guldner, J., and Shi, J. (2009). *Sliding mode control in electro-mechanical systems*, volume 34. CRC press.

Werner, H. (1999). Fast output sampling regulators with integral action. In *Control Conference (ECC), 1999 European*, pages 527–532. IEEE.

Wu, H., Wang, Z., and Hu, Y. (2010). Study on magnetic levitation wind turbine for vertical type and low wind speed. In *Power and Energy Engineering Conference (APPEEC), 2010 Asia-Pacific*, pages 1–4.

Yang, Z. J., Hara, S., Kanae, S., and Wada, K. (2009). Robust output feedback control of a magnetic levitation system via high-gain observer. In *Proceedings of the 48h IEEE Conference on Decision and Control (CDC) held jointly with 2009 28th Chinese Control Conference*, pages 7575–7580.

Young, K. D. and Drakunov, S. V. (1992). Sliding mode control with chattering reduction. In *American Control Conference, 1992*, pages 1291–1292. IEEE.

Young, K.-K. (1977). Asymptotic stability of model reference systems with variable structure control. *IEEE Transactions on Automatic Control*, 22(2):279–281.

Young, K. K. D. (1978). Controller design for a manipulator using theory of variable structure systems. *IEEE Transactions on Systems, Man, and Cybernetics*, 8(2):101–109.

Yu, D., Liu, H., and Hu, Q. (2010). Fuzzy sliding mode control of maglev guiding system based on feedback linearization. In *Fuzzy Systems and Knowledge Discovery (FSKD), 2010 Seventh International Conference on*, volume 3, pages 1281–1285. IEEE.

Yu, W. and Li, X. (2014). A magnetic levitation system for advanced control education. *IFAC Proceedings Volumes*, 47(3):9032–9037.

Yu, W. J. and Qian, X. Y. (2012). Stability of wind power turbines magnetic bearing. In *Applied Mechanics and Materials*, volume 195, pages 47–51. Trans Tech Publ.

Zeitz, M. (1987). The extended luenberger observer for nonlinear systems. *Systems & Control Letters*, 9(2):149–156.

Zhang, G., Mei, L., and Yuan, Y. (2012a). Variable universe fuzzy pid control strategy of permanent magnet biased axial magnetic bearing used in magnetic suspension wind power generator. *Intelligent Robotics and Applications*, pages 34–43.

Zhang, X. D., Wu, G. Q., Mao, J. F., and Yang, K. (2012b). Self adaptive integral-type sliding mode control for supporting structure of a magnetic vertical axis wind turbine. In *Applied Mechanics and Materials*, volume 150, pages 90–94. Trans Tech Publ.